1-1-1988

Physical properties of poly(ether ether ketone)/

Youngchul Lee
University of Massachusetts Amherst

PHYSICAL PROPERTIES OF POLY(ETHER ETHER KETONE)

A Dissertation Presented

By

YOUNGCHUL LEE

Submitted to the Graduate School of the
University of Massachusetts in partial fulfilment
of the requirements for the degree of

DOCTOR OF PHILOSOPHY

May 1988

Polymer Science and Engineering

PHYSICAL PROPERTIES OF POLY(ETHER ETHER KETONE)

A Dissertation Presented

By

YOUNGCHUL LEE

Approved as to style and content by:

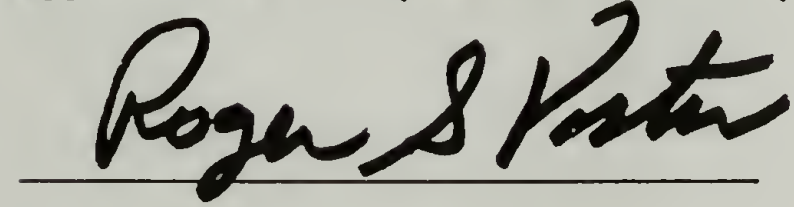

Roger S. Porter, Chairman

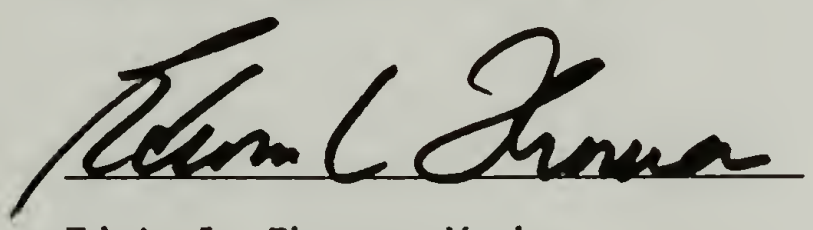

Edwin L. Thomas, Member

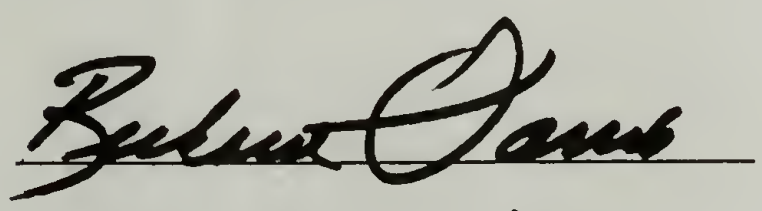

Richard J. Farris, Member

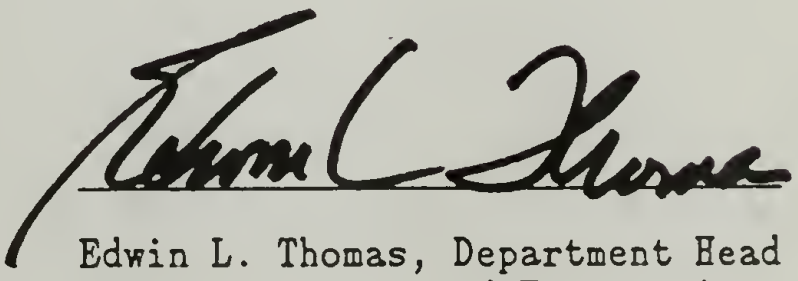

Edwin L. Thomas, Department Head
Polymer Science and Engineering

DEDICATION

To my parents, my wife, Meekyung
and daughter, Minjung
with gratitude for their love.

ACKNOWLEDGEMENTS

I wish to thank my advisor, Professor Roger S. Porter, for his enthusiastic support, guidance, and advice throughout the research and the writing of the dissertation. I also wish to thank Professor Edwin L. Thomas and Professor Richard J. Farris for their help and advice.

I would like to acknowledge the helpful suggestions of Dr. J.S. Lin of Oak Ridge National Laboratory and Dr. Jean-Marc Lefebvre.

I especially thank Matt Muir for our interesting discussion and for his friendship over the last five years. Kevin Schell, Rick Brady, Bob Karcha, and Matt Muir critically read my dissertation and made many good suggestions. I really appreciate their help.

I would like to thank my class mates and Professor Porter's group including: Jerry Palmer, Eric Beckman, Gary Adams, David Gagnon, Jim Jonza, Steve DeTeresa, Ravi Saraf, and Jiayu Guan. I appreciate the help of Lou Raboin, Jay Conway, Will McCarthy, Eleanor Thorpe, and Mareile Fenner.

Finally, I wish to thank all my teachers, including Professor I. Cho and Dr. H.J. Pyun, who have inspired me to pursue science.

ABSTRACT

Physical Properties of Poly(ether ether ketone)

May, 1988

Youngchul Lee, B.S., Seoul National University

M.S., Korea Advanced Institute of Science & Technology

Ph.D., University of Massachusetts

Directed by: Professor Roger S. Porter

This dissertation discusses studies on the physical properties of poly(ether ether ketone) (PEEK). Several investigations involving the crystallization and melting behavior of PEEK, crystallization of PEEK on carbon fibers, and uniaxial draw of PEEK are presented.

The double-melting behavior of isothermally crystallized PEEK was investigated using differential scanning calorimetry (DSC) and wide and small-angle X-ray scattering. The double-melting was found to be due to a crystal reorganization on heating. The low and high-melting endotherms are the sum of four contributions: Melting of the original crystals, their recrystallization, remelting of recrystallized crystals and melting of core crystals. Material parameters such as the thermodynamic melting point (384, 389°C) and surface free energy (39 erg/cm^{2}) of the PEEK crystal were measured.

The isothermal and non-isothermal crystallization of PEEK was found to depend on the previous thermal history. This was explained

by a persistence of small residual crystalline regions up to the thermodynamic melting point, at which the infinitely large and perfect crystals melt.

The crystallization of PEEK on carbon fibers was studied by DSC, electron and optical microscopy. The control, characterization, and effect of the crystalline interface between PEEK and carbon fiber were investigated. The carbon fiber surface was found to compete with nuclei in the PEEK matrix for crystallization growth. Reducing the number of nuclei in the matrix by long preheating favored PEEK crystallization on the carbon fiber, resulting in about 2 times stronger interfacial bond as indicated by transverse tensile tests.

PEEK films and rods were solid-state extruded at 154 and 310°C. The tensile mechanical properties were improved by drawing. The modulus and strength were increased up to 6.5 GPa and 600 MPa, respectively. The structural evolution of PEEK on drawing was studied using wide-angle X-ray diffraction and birefringence. The c axis crystal orientation function (up to 0.67) and birefringence (up to 0.30) were increased with draw ratio.

TABLE OF CONTENTS

LIST OF TABLES

LIST OF FIGURES

Figure

C H A P T E R I

INTRODUCTION

1.1 Background

The synthesis of poly(ether ether ketone) (PEEK) was first reported in 1967 [1-4]. Due to the crystallization of PEEK chains the polymer precipitated from the polymerization medium, resulting in low molecular weight. It was not until phenyl sulphone was used as the solvent at temperatures up to 335°C that a high molecular weight of PEEK was obtained [2]. The condensation polymerization method in Fig. 1.1 is used to to produce commercial PEEK [5]. The IUPAC name of PEEK is poly(oxy-1,4-phenyleneoxy-1,4-phenylenecarbonyl-1,4-phenylene). It generally shows a glass transition (T_g) and melting temperature (T_m) at around 145 and 335°C, respectively.

PEEK has been specified for injection molded parts for use at high temperature in aggresive environments, for coating high perfomance wires and cables, for chemically resistant surface coatings, in monofilaments for industrial belts and filters and the matrix in carbon fiber composites for structural aerospace components [2]. Potential advantages of thermoplastic matrices over thermoset ones are

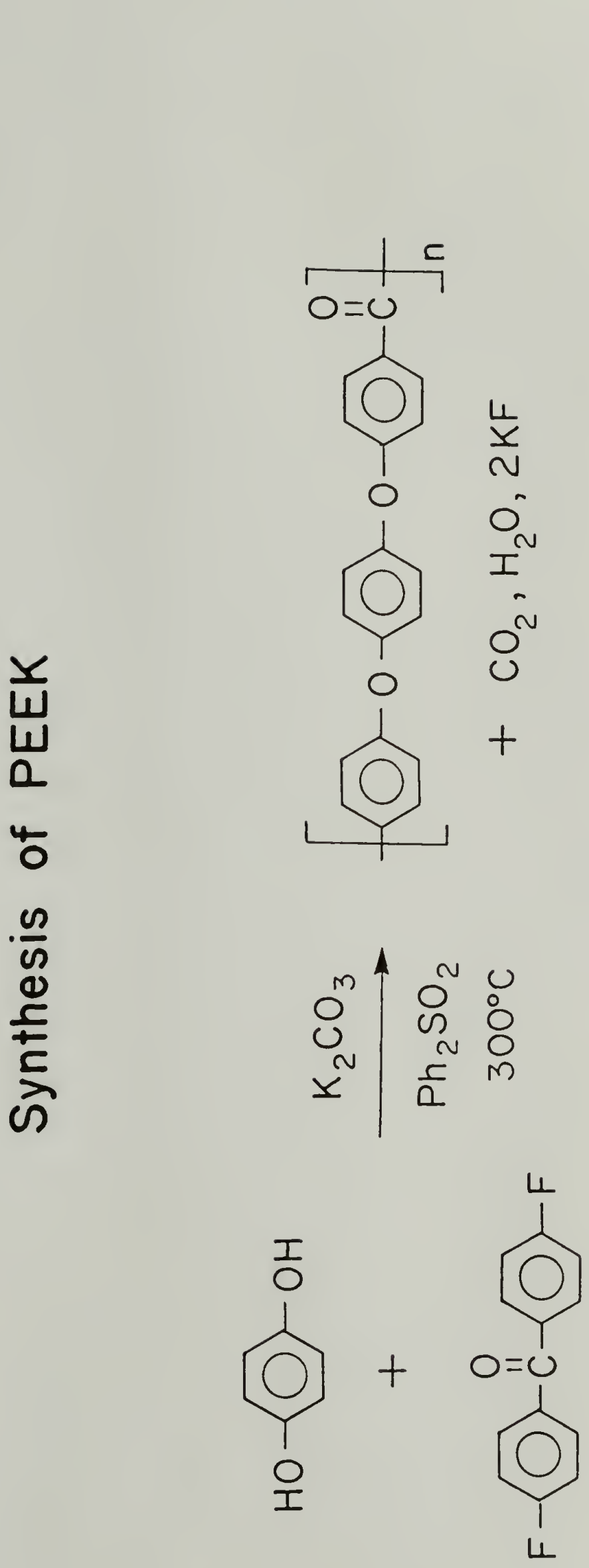

Figure 1.1. Condensation polymerization of PEEK.

long shelf-life, toughness, and rapidity of fabrication [6]. PEEK seems to be one of the first thermoplastics which show high stiffness at elevated temperature and sufficient resistance to chemical attack [6,7]. Typical properties of PEEK are listed in Table 1.1 [7].

1.2 Overview of Dissertation

Since 1981 when PEEK became commercialized, considerable attention has been given to this material as a high performance thermoplastic as well as a matrix for advanced composites. The crystallinity of PEEK (< 48%) confers good mechanical properties, great resistance to high temperature and solvent, and the ability to form oriented fibers.

Chapter II describes the melting behavior of isothermally crystallized PEEK. Differential scanning calorimetry (DSC) traces of the PEEK usually show two melting endotherms. No detailed study on the mechanism for the two melting endotherms of PEEK has been previously reported. A mechanism is proposed from the results of DSC at various heating rates and from wide-angle X-ray diffraction (WAXD) studies. The true melting point representing the complete melting of the original crystals without reorganization is discussed. Comparable thermodynamic melting points of PEEK were measured using a Hoffman-Weeks plot and Thomson-Gibbs equation. The lamellar thickening factor and folding-surface free energy were also measured and reported in Chapter II.

Table 1.1 Physical properties of poly(ether ether ketone) [7].

Melting point	~ 335°C
Glass transition temperature	~ 145°C
Number average molecular weight	~ 15000 g/mole
Weight average molecular weight	~ 40000 g/mole
Maximum crystallinity	48 %
Water absorption after 24h @ 40% RH	0.15 %
Melt viscosity, 400°C, 1000 sec^{-1}	4000-5000 Poise
Processing temperature	371-399°C
Thermal stability at 400°C	> 1 hr
Tensile strength	100 MPa
Flexural modulus	3.8 GPa
Heat distortion temperature	165°C
Volume resistivity	> 10^{16} Ohm cm
Dielectric strength	480 KV/in

Chapter III reports isothermal and nonisothermal crystallization of PEEK as a function of the previous melt temperature and holding time. Isothermal crystallization has been analyzed using the Avrami equation. The dependence of crystallization on the thermal history has been attributed to a persistence of small residual crystalline regions in the bulk. It is proposed that these residual crystalline regions only persist up to the thermodynamic melting point, which is also supported by several other polymers. The thermal stability of PEEK has been assessed by thermo-gravimetric analysis and by solution viscosity.

Chapter IV evaluates the tendency of carbon fibers to nucleate the crystallization of PEEK. A cyclic DSC experiment consisting of melting and crystallization was found effective to measure the nucleation density. Given equivalent thermal histories, PEEK with carbon fibers has been found to have a higher nucleation density than PEEK itself. In Chapter III, it is shown that nucleation density depends on the prior thermal history. This characteristic has been utilized to investigate the effects of crystallization on the carbon fiber surface.

Chapter V investigates the structural evolution of PEEK upon drawing. In quest of improved mechanical properties, PEEK has been solid-state extruded using a capillary rheometer. Orientation of crystals on drawing has been measured using WAXD. Changes on draw in physical properties such as tensile modulus and strength, density, thermal behavior, and birefringence are discussed.

Chapter VI suggests future research projects based on the studies described above.

C H A P T E R II

DOUBLE-MELTING BEHAVIOR OF POLY(ETHER ETHER KETONE)

2.1 Introduction

The observation of two distinct melting endotherms for PEEK during differential thermal analysis is of interest as a parallel to the double-melting found for several other polymers. The double-melting behavior of PEEK was mentioned and considered comparable to poly(ethylene terephthalate) (PET) [8]. It was believed that the low-temperature endotherm was due to melting of the original crystals which existed in the sample prior to heating and the high-temperature endotherm was due to melting of the crystals which had been continuously reorganized on heating [8]. Therefore, the peak temperature of the low-temperature endotherm (T_m1) was used as the melting temperature of PEEK in the calculation of the thermodynamic melting point (T_m^o) and surface free energy of PEEK crystals [8]. This point of view is critically discussed and a new mechanism of the double-melting behavior is proposed in this chapter. The true melting point at which the original crystals melt completely without reorganization is also discussed. Measurement of the thermodynamic

melting point, surface energy, and heat of fusion of PEEK crystal is reported.

2.1.1 Origin of Multiple-Melting Endotherms

Since double-melting endotherms of drawn nylon 6,6 were first observed in differential thermal anaysis traces [9] multiple-melting endotherms of many polymers have been investigated [10-27]. For the drawn nylon 6,6, the low and high-temperature melting endotherms were erroneously attributed to disorientation of the oriented crystals and melting of the crystalline regions, respectively [9]. Though it was renounced later, melting of folded-chain crystals and partially extended-chain crystals had been suggested for the double-melting endotherms of drawn nylon 6,6 and poly(ethylene terephthalate) (PET) [10-14].

Simultaneous melting and recrystallization has been verified as the origin of double-melting of several polymers, including PET [13-16], isotactic polystyrene [17,18] polyethylene [19,20], and polyoxymethylene [21]. Different crystal structures have been found to cause the multi-melting peaks for trans-1,4-polyisoprene [22], isotactic polypropylene [23] and poly(vinylidene fluoride) [24]. Different morphological species of different lamellar thickness have been found for cis-1,4-polyisoprene [25]. Double-melting endotherms of a copolyether-ester have been attributed to two crystalline populations with different size and/or perfection [26]. Sometimes

more than one reason is responsible for multiple-melting endotherms [22,27].

2.1.2 Measurement of Crystallinity

The crystallinty of neat PEEK and PEEK in carbon fiber composites depends on thermal history and significantly influences mechanical properties [28]. The crystallinity of PEEK has been measured using several different methods, such as density [8], wide-angle X-ray diffraction (WAXD) [8,29,30], and heat of fusion [31,32]. Crystallinity from WAXD curves was obtained by drawing a straight base line between $2\theta = 10^{\circ}$ and 36°, and then fitting a scaled amorphous curve under the diffraction peaks [8]. The ratio of the areas of the crystalline peaks to the total area was taken as a measure of the degree of crystallinity. This X-ray crystallinity showed a linear relationship with density. The densities of 100% crystalline and 100% amorphous PEEK were extrapolated to be 1.401 and 1.260 g/cm^3, respectively, which are consistent with the densities of the calculated unit cell and the observed density of amorphous PEEK [8]. This consistency indicates that a two-phase system, consisting of crystalline and amorphous regions, is a good model for semicrystalline PEEK.

Using the heat of fusion for the PEEK crystal, the crystallinity can also be measured from the melting trace of differential scanning calorimetry (DSC). The heat of fusion has been deduced to be 31.1 cal/g at the melting point by correlating with densities and X-ray

crystallinity [8]. Also the heat of fusion of 39.5 cal/g has been obtained, as will be discussed in Section 2.3.5. The crystallinity of PEEK measured by Fourier Transform Infrared (FTIR) [32], Raman spectroscopy [33], and Nuclear Magnetic Resonance (NMR) [34] has also been reported.

2.2 Experimental

2.2.1 Materials and Sample Preparation

PEEK powder was obtained from Imperial Chemical Industries (ICI), Wilton, U.K. The reported $\bar{M}_n$ and $\bar{M}_w$ are 14,100 and 38,600, respectively. Fully amorphous PEEK, in 0.1 or 0.3 mm-thick films, was made by compression molding at 400°C for 10 min, then quenching into cold water. DSC traces of the PEEK powder and amorphous PEEK film are shown in Fig. 2.1.

Amorphous PEEK films were isothermally cold-crystallized either within the sample cell of a Perkin-Elmer DSC-2 or between preheated hot plates and quenched (cold-crystallized). A heating rate of 320°C/min was used to avoid nonisothermal crystallization before thermal equilibration. Though the fastest heating rate (320°C/min) of the DSC was used, a temperature of 210°C was the highest isothermal crystallization temperature attained without any crystallization before thermal equilibration. Amorphous films were also annealed after nonisothermal crystallization (annealed). With a Perkin-Elmer

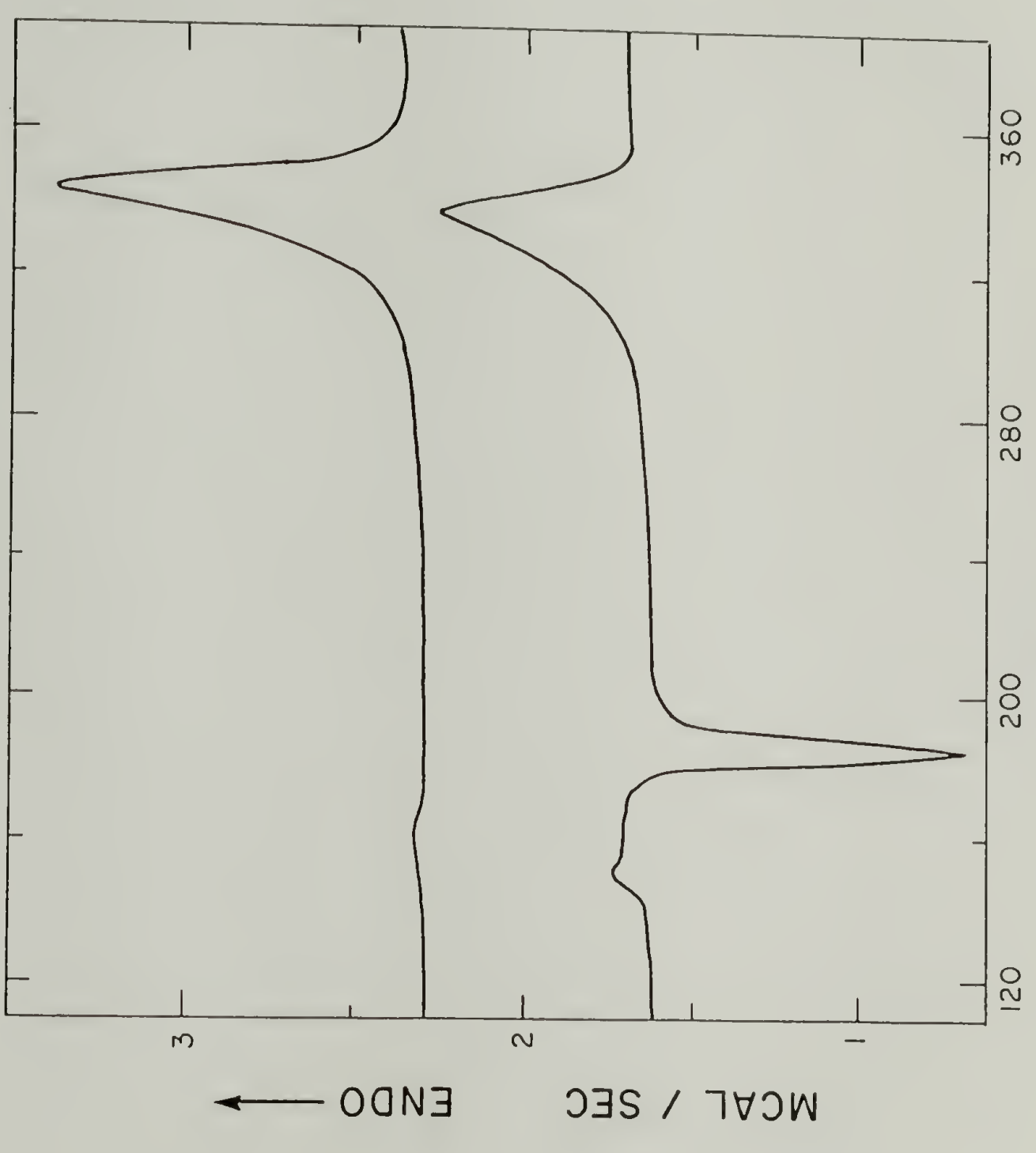

Figure 2.1. DSC traces of reactor powder (top) and amorphous (bottom) PEEK. Heating rate was 80°C/min. Normalized to 1 mg of sample.

DSC-4, the samples were heated to the annealing temperature at 80°C/min. At this heating rate, a cold-crystallization exotherm occurred as a peak at 185°C as shown in Fig. 2.1. Most of the crystallization is completed by 200°C. Melt-crystallization was conducted in a DSC-4 by rapid cooling (-200°C/min) from the melt (400°C for 10 min). After isothermal crystallization, the samples were cooled rapidly
(-200°C/min) to room temperature. A schematic representation of crystallization methods is shown in Fig. 2.2.

Amorphous poly(ethylene terephthalate) (PET) film (Intrinsic viscosity, 0.83 dl/g) was annealed in an oven, under nitrogen atmosphere at 190°C for 2 or 20h.

All the experiments with DSC were performed under dry nitrogen atmosphere. After examination, samples of 0.1-5 mg were used in order to avoid saturation or broadness of heat flow due to a large sample size or low thermal conductivity [35]. DSC traces were normalized to 1 mg of sample and shown in the figures. The heat flow of DSC traces at different heating rates were also normalized to the heat flow at 20°C/min.

2.2.2 Temperature Calibration

Indium, tin, lead, and zinc were used for calibrations of temperature and heat of transition at each heating rate. It has been shown that the observed temperature by DSC is dependent on scanning rate [36].

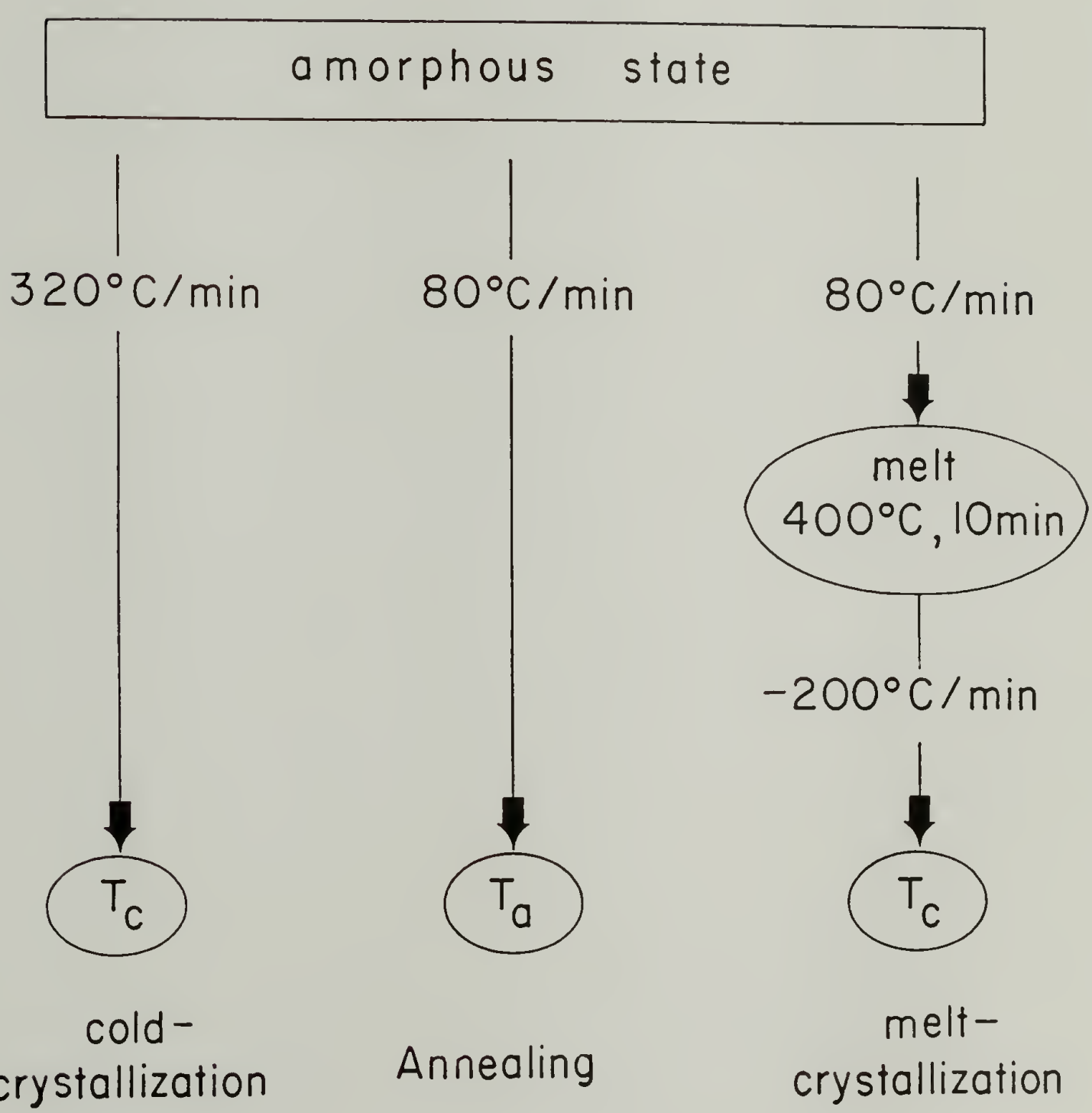

Figure 2.2. Schematic diagram of crystallization of PEEK.

$$T_{true} = T_{obs.} - C\ dT/dt + D \qquad (2.1)$$

where T_{true} is actual temperature, $T_{obs.}$ observed temperature, and dT/dt scanning rate in degrees per minute. C and D are constants with C typically equal to 0.085 min. The constant C has been obtained for DSC-4 to be 0.05-0.074 min, depending on standards. Isothermal crystallization and annealing temperatures were calibrated with extrapolated melting points of the standards to zero heating rate.

2.2.3 Density Measurement

The densities of the PEEK films crystallized at various temperatures were measured in a density column made from aqueous solutions of calcium nitrate at 23°C [37]. The sensitivity of the column was about 0.0001 $g/cm^3 mm$; thus the accuracy of the density measurement was 0.05% or better. The amorphous PEEK films used in this study exhibited a density of 1.2631±0.0005, in agreement with a reported value [8].

2.2.4 Wide and Small-Angle X-ray Scattering

A Siemens D-500 X-ray diffractometer equipped with a pulse-height scintillation counter was used to examine the diffraction pattern. Wide-angle X-ray diffraction experiments were conducted in transmission mode with Ni-filtered Cu-K_α radiation at 30 mA and 40 kV. The intensity was corrected for background.

The long period of the PEEK film was measured with the small-angle X-ray scattering (SAXS) facility at the National Center for Small Angle Scattering Research (NCSASR) at Oak Ridge National Laboratories, Oak Ridge, Tennessee. It consists of a pinhole-collimated Cu-K_α X-ray source and a two-dimensional position sensitive detector. Intensity was corrected for detector sensitivity, sample absorption, background and dark current. The intensity was also Lorentz corrected. The long period is measured from the peak position of the intensity maximum using Bragg's equation.

2.3 Results and Discussion

Poly(ether ether ketone) (PEEK) can be quenched from the melt to produce an amorphous, glassy state at room temperature. PEEK can be crystallized either by cooling from the melt (melt-crystallized) or by heating from the amorphous state (cold-crystallized, annealed), as shown in Fig. 2.2. When amorphous PEEK is heated from room temperature at 80°C/min in a differential scanning calorimeter (DSC), a cold-crystallization exotherm occurs about 40°C higher than its glass transition temperature (145°C) as shown in Fig. 2.1. Fig. 2.1 also shows a DSC trace of the original PEEK reactor powder showing larger melting endotherm and higher melting temperature than amorphous PEEK. Cold and melt-crystallization methods were used for PEEK crystallized at higher and lower supercoolings, respectively.

The DSC traces of PEEK show two melting endotherms after isothermal crysyallization or annealing. Fig. 2.3 shows DSC traces of annealed and melt-crystallized PEEK. As the annealing or crystallization time is increased, the low-temperature melting endotherm shifts to higher temperature; however, the high temperature endotherm does not change. This suggests that the reason for the double-melting of PEEK is not associated with populations of different crystal size and/or perfection. With crystallization time, the low and high-temperature melting endotherms of a random block copolymer of poly(butylene terephthalate) and poly(tetramethylene ether glycol) have been found to shrink and grow, respectively [26]. Isothermally cold-crystallized samples of PEEK show the same behavior, and the peak temperatures are listed in Table 2.1.

The effect of annealing time was examined. A sample showing two melting endotherms had been annealed at the peak temperature of the low-temperature melting endotherm for various time. As shown in Fig. 2.4, the low-temperature melting endotherm grows, but little change of the high-temperature melting endotherm is observed with increased annealing time. The areas under DSC peaks or heats of fusion are shown in Fig. 2.5. As the annealing time was increased, the heat of fusion for the low-temperature melting endotherm increased but that of the high-temperature melting endotherm did not change.

The effect of cooling rate was also investigated. Amorphous PEEK films were held in the melt (400^{o}C, 5 min) then cooled at various cooling rates in a DSC. The heating scans of the samples at 20^{o}C/min

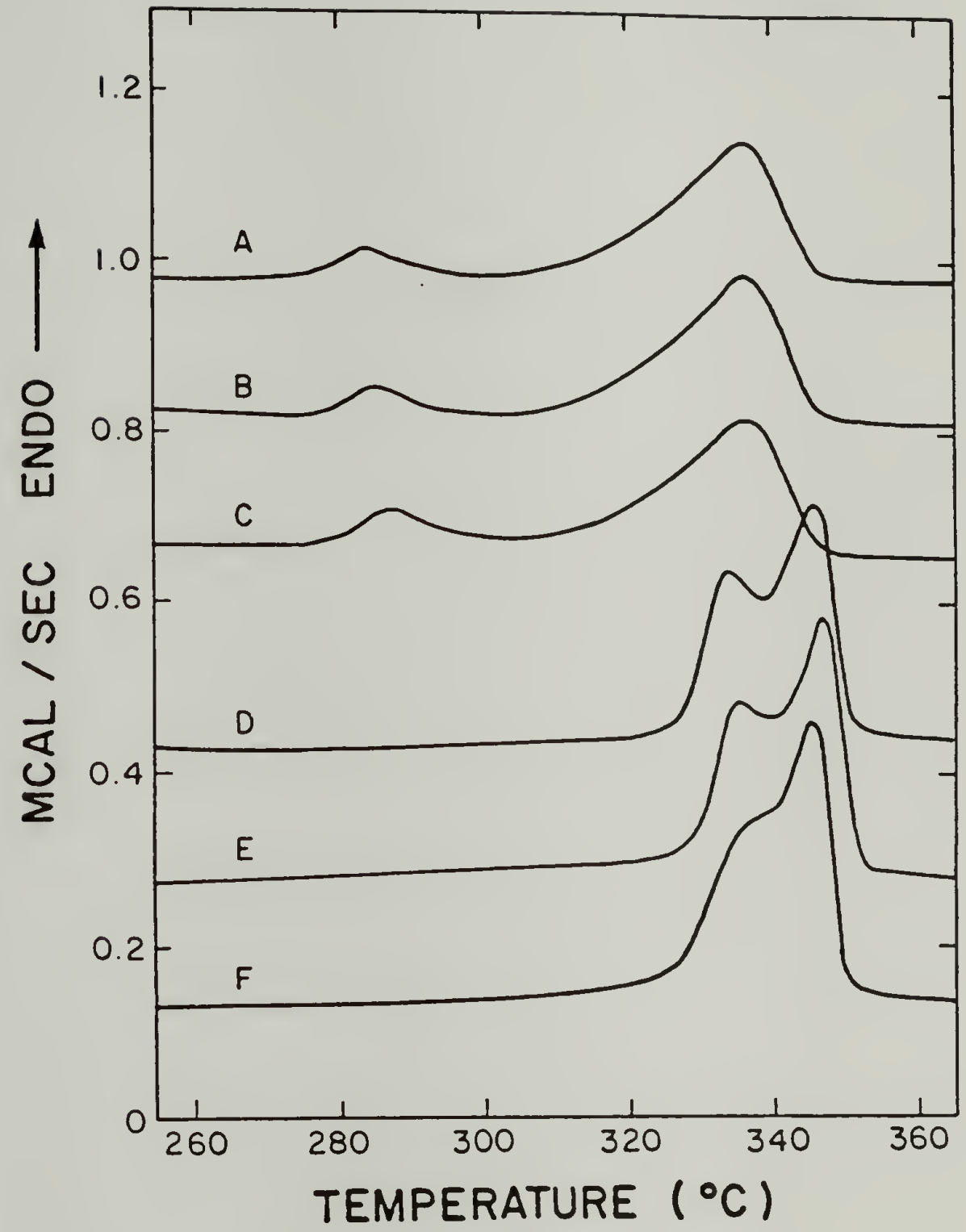

Figure 2.3. DSC traces for isothermally crystallized PEEK (heating rate 20°C/min): A, B and C, crystallized at 269.3°C from the glassy state for 2, 4 and 10.2h, respectively; D, E and F, crystallized at 319.6°C from the melt (400°C, 10min) for 14, 22.5 and 35h, respectively.

Table 2.1. Peak temperatures of the low and high-temperature melting endotherms (T_m1 and T_m2, respectively) and densities for isothermally crystallized and annealed PEEK.

	T_c or T_a (°C)	Time (h)	T_m1[a] (°C)	T_m2[a] (°C)	Density (g/cm^3)
Cold-Crystallized	200.0	1.0	220.8	337.4	1.293
	200.0	4.0	224.1	336.6	1.293
	200.0	18.5	227.2	337.0	1.294
	200.0	42.5	229.6	337.4	1.294
Annealed	200.0	1.0	219.2	337.7	1.2925
	250.0	1.0	267.9	337.0	1.2974
	269.3	1.0	284.2	336.6	1.2991
	269.3	2.0	284.5	336.6	1.2993
	269.3	4.0	286.0	336.7	1.2999
	269.3	10.2	287.7	336.6	1.3004
	290.0	1.0	303.3	336.5	1.3011
	320.0	1.0	330.4	336.9	1.3045
	320.0	21.5	335.8[b]		1.3064
Melt-Crystallized	314.3	5.6	328.7	344.7	1.3063
	316.0	14.5	331.3	345.8	1.3091
	318.6	14.0	334.9	347.7	--
	319.6	14.0	334.8	347.6	1.3087
	319.6	22.5	335.5	347.4	1.3092
	319.6	35.0	338.8	347.4	1.3096
	322.8	20.0	339.1	350.5	1.3060
	323.6	25.0	339.8	349.6	1.3052
	328.6	34.0	344.3	352.8	1.3069

a. measured by DSC at a heating rate 20°C/min.
b. shows only one peak.

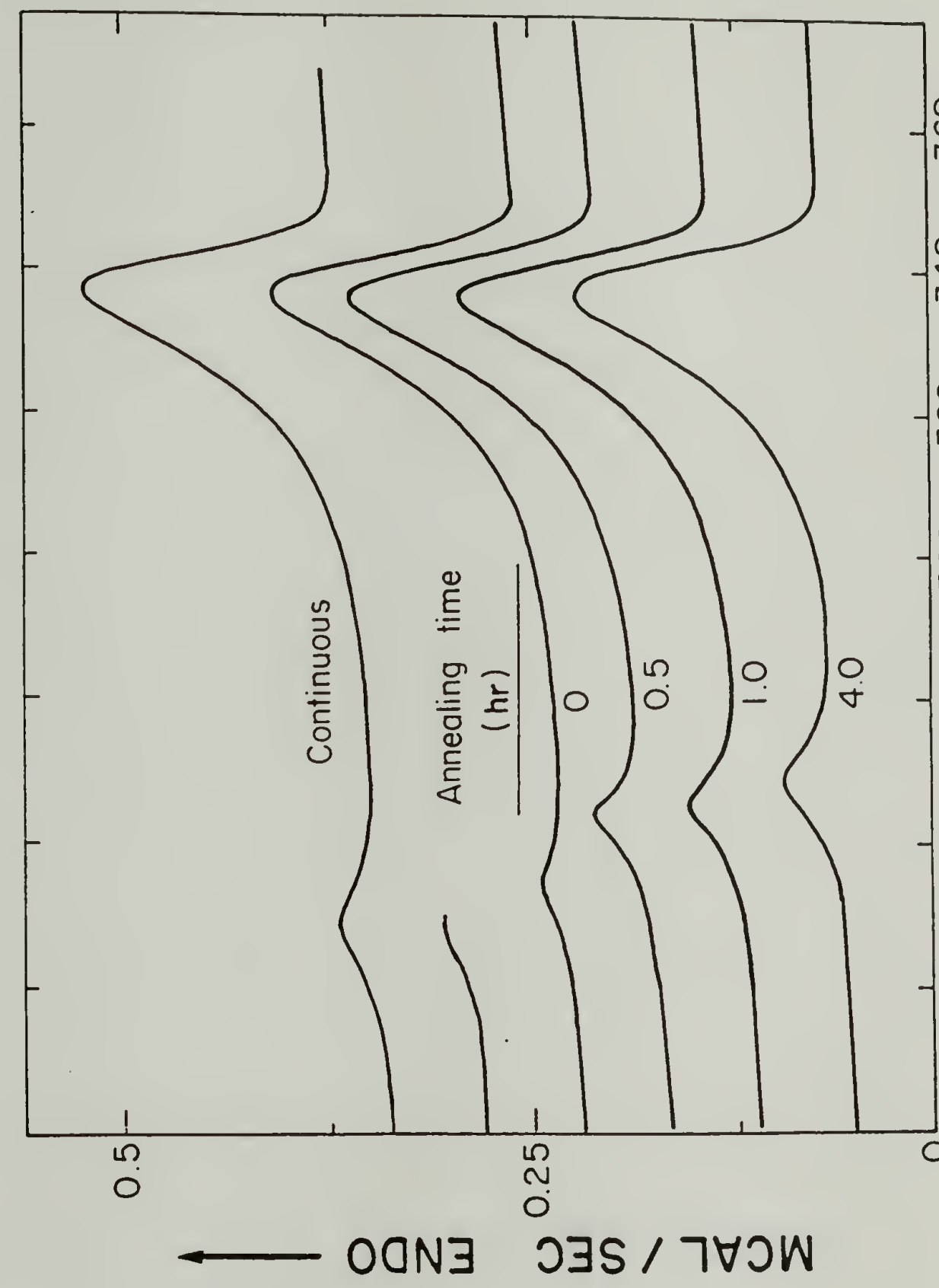

Figure 2.4. DSC traces of PEEK annealed at 248°C for various time. The original sample were cold-crystallized at 220°C for 75h prior to annealing. Heating rate was 20°C/min.

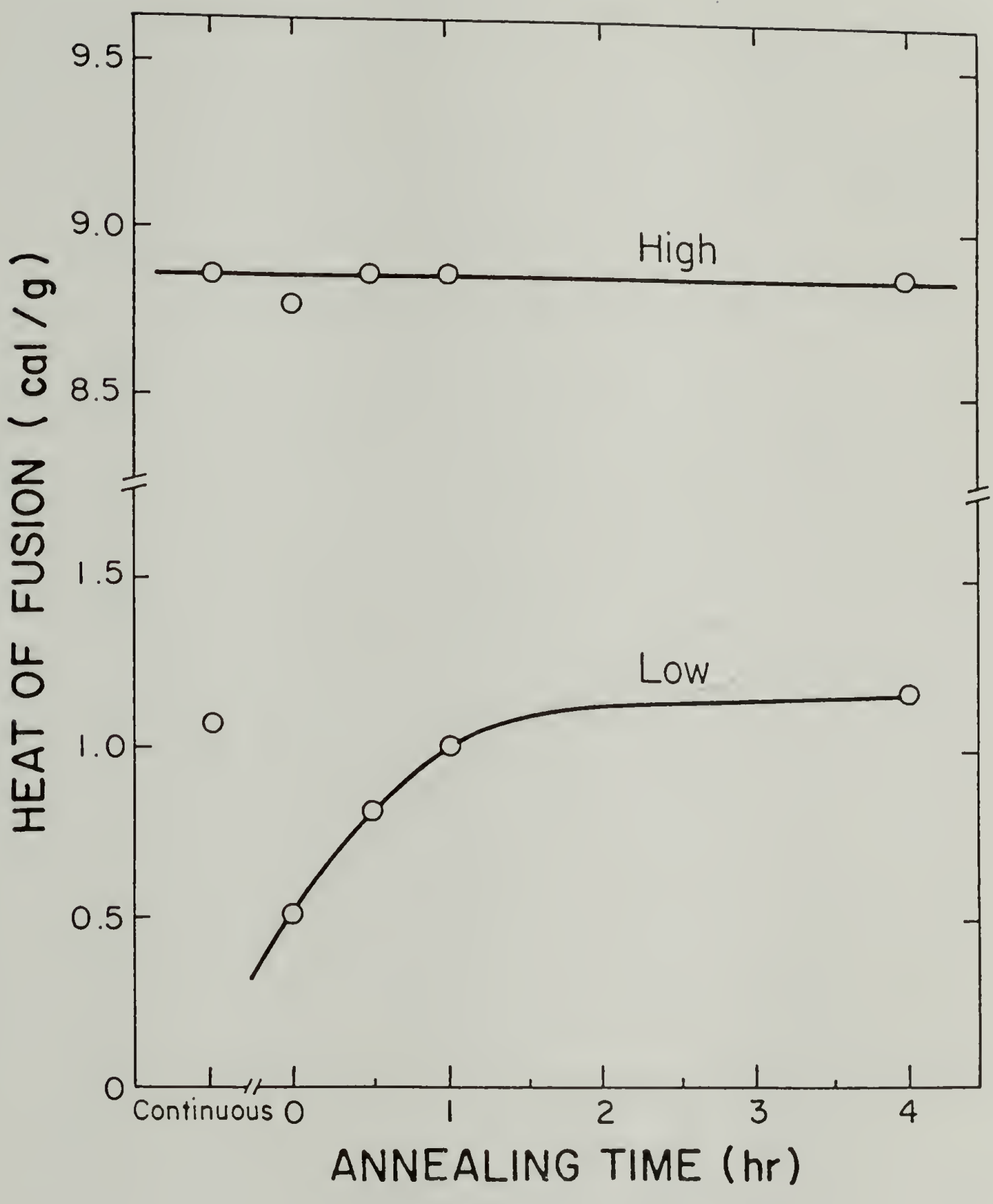

Figure 2.5. Heat of fusion for low and high-temperature melting endotherms vs. annealing time at 248°C.

are shown in Fig. 2.6. As the cooling rate was increased the low-temperature melting endotherm became smaller and shifted to low temperature due to lower crystallization temperature. PEEK cooled at - 90°C/min or higher cooling rate did not show low-temperature melting endotherm.

2.3.1 Heating Rate Study

PEEK films, which had been isothermally crystallized at 220°C for 75h from the quenched glassy state, were scanned at different heating rates. The heats of fusion and peak temperatures of the low and high-temperature melting endotherms are plotted vs. heating rate in Fig. 2.7 and 2.8, respectively. As the heating rate was increased, the heat of fusion of the low-temperature endotherm increased but that of the high-temperature endotherm decreased. For the case of annealed PET or drawn nylon 6,6 [12,13], two melting endotherms also usually appear in the DSC heating scan and show behavior comparable to Fig. 2.7 and 2.8. For those cases, it has been concluded that the low-temperature endotherm is the melting of crystals which exist prior to the heating scan and the high-temperature endotherm is the result of melting of crystals formed by simultaneous melting and recrystallization (reorganization) during the DSC heating scan. As the heating rate was increased, the amount of the crystalline region which has time to recrystallize decreased; this resulted in a smaller high-temperature melting endotherm and a larger low-temperature melting endotherm in Fig. 2.7. The total heat of fusion for both

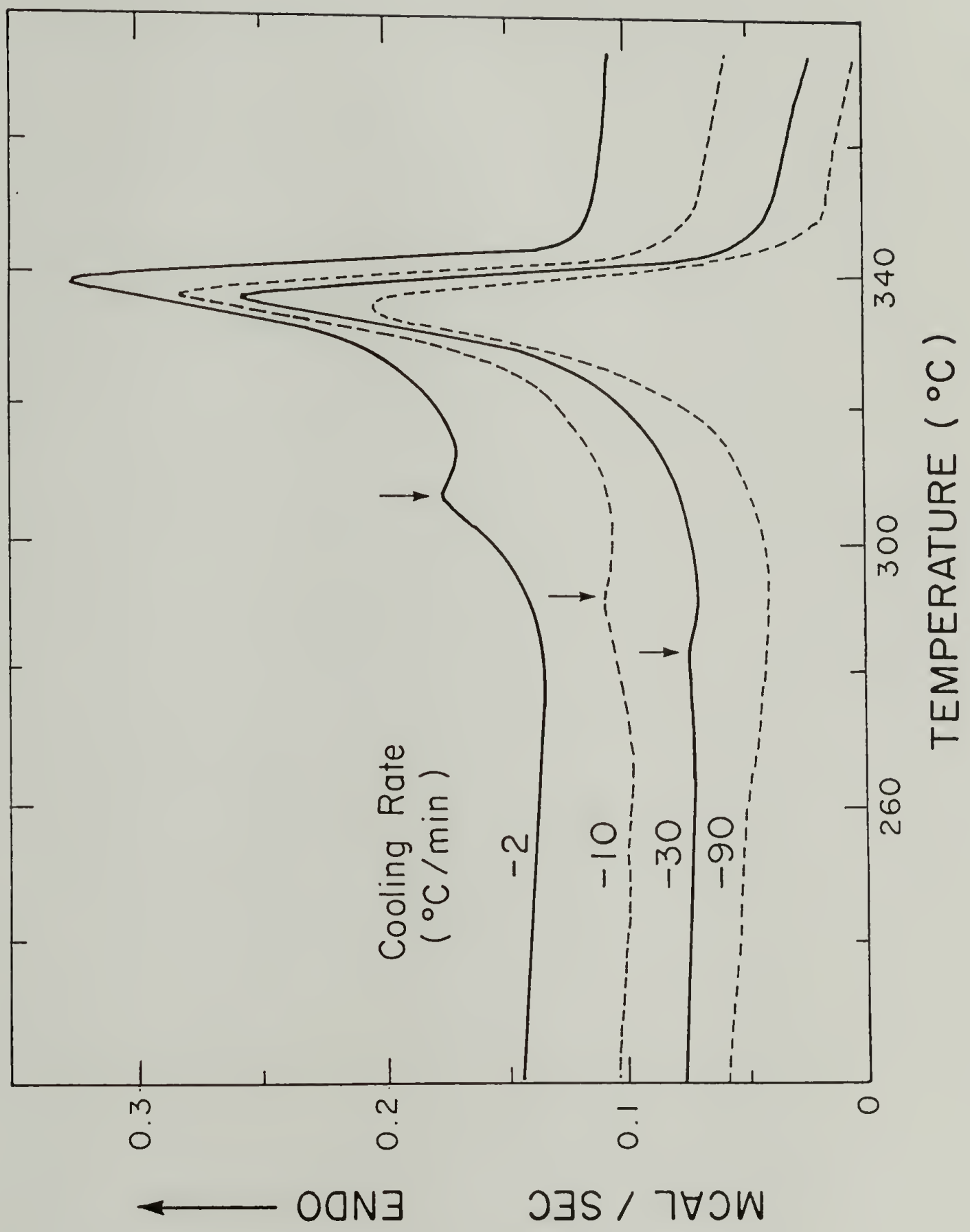

Figure 2.6. DSC traces of PEEK cooled at various rates from the melt (400°C, 5 min). Heating rate was 20°C/min.

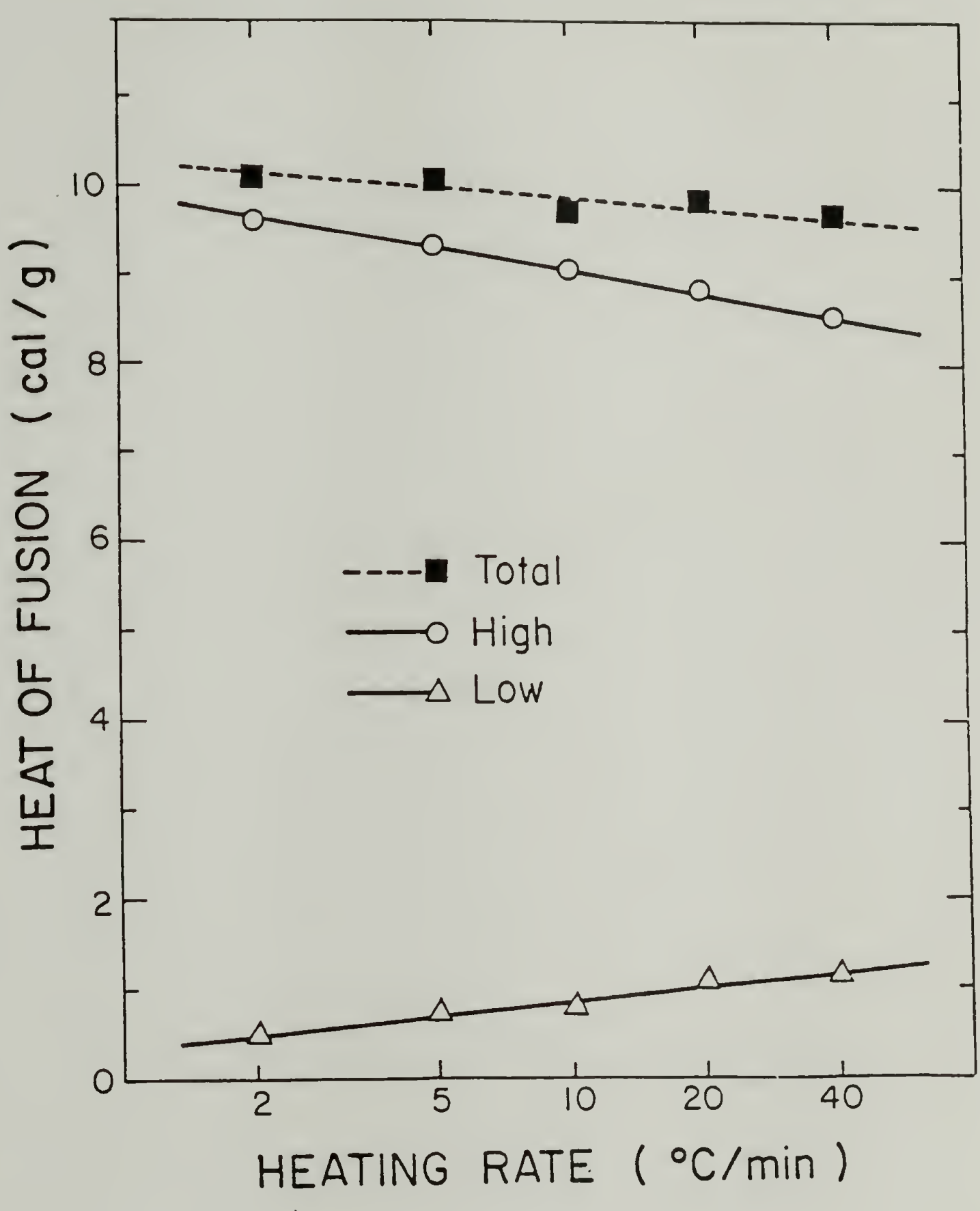

Figure 2.7. Heats of fusion of the high and low-temperature melting endotherms vs. heating rate. The PEEK samples were cold-crystallized at 220°C for 75h.

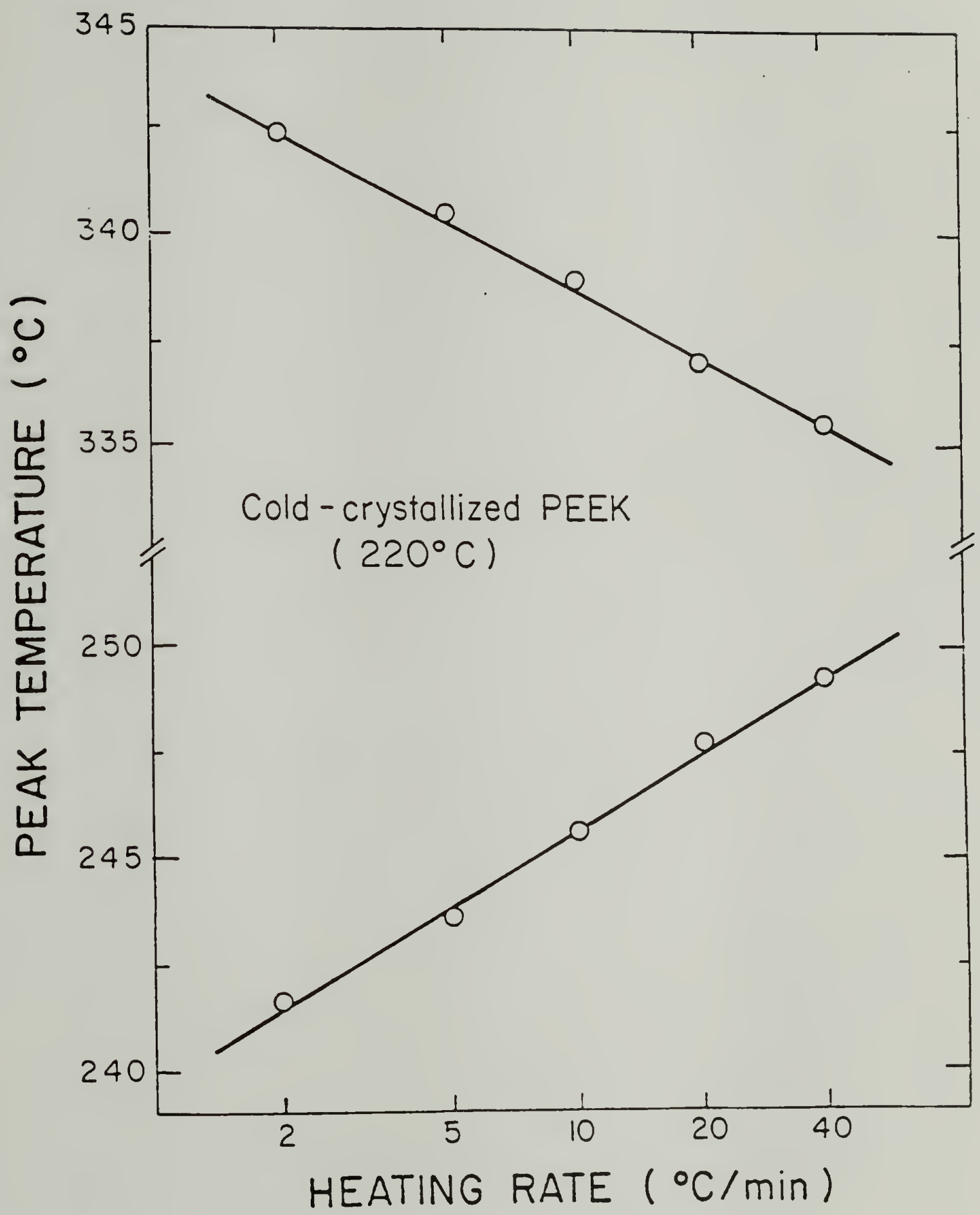

Figure 2.8. The two melting peak temperatures vs. heating rate. The PEEK samples were cold-crystallized at 220°C for 75h.

endotherms decreased slightly with increasing heating rate, due to restricted annealing on heating.

Fig. 2.8 shows that the peak temperature of the high-temperature endotherm (T_m2) is decreased, but the peak temperature of the low-temperature endotherm (T_m1) is increased, at increased heating rate. The decrease in T_m2 with heating rate may be explained in terms of the shorter reorganization times; the size and perfection of the recrystallized PEEK decreases with increasing heating rate. These results are consistent with the studies on the several polymers showing double-melting peaks due to the reorganization process [4,12-15,17,22]. Recrystallization or reorganization of cold-crystallized PEEK has been found in an analysis using solid and liquid heat capacity [38].

Examples for the superheating of macromolecules and their explanations have been reported [39]. The superheating of relatively large and perfect macromolecular crystals of extended-chain conformation has been explained to be due to the intrinsic slowness of crystal melting or due to an initial reduction of the entropy on melting. The small nonequilibrated crystals may superheat due to strained amorphous tie molecules or due to anomalous molecular conformations at the crystal surface showing a reduced entropy of fusion on melting. From the following X-ray scattering experiments, it is considered that the two melting endotherms of PEEK do not represent two morphologically different crystal or lamellar species;

therefore, the superheating of the low-temperature melting peak should be explained in connection with the high-temperature melting peak.

2.3.2 Wide-Angle X-ray Diffraction

Wide-angle X-ray Diffraction (WAXD) patterns of PEEK samples which show one or two melting peaks in DSC traces are the same in terms of diffraction peaks. This indicates that only one crystal structure exists in PEEK regardless of its melting behavior. The reflections are in agreement with those reported for an orthorhombic unit cell [40]. Fig. 2.9 shows WAXD patterns of annealed PEEK where diffraction peaks become sharper as annealing time or temperature is increased, indicating improvement of crystalline order. For PET, the same behavior has been found and ascribed to an increase in the size of the mosaic blocks building up the lamellae [41,42]. No evidence for two different lamellar thicknesses for either melt or cold-crystallized PEEK has been found using small-angle X-ray scattering.

2.3.3 Mechanisms for Double-Melting Behavior

Rim and Runt have considered the double melting of poly(ϵ-caprolactone) as a combination of the three peaks due to the melting of original crystals, recrystallization and melting of the recrystallized material, as shown in Fig. 2.10A [43]. The areas of the recrystallization exotherm and the melting endotherm of the recrystallized material are the same. At a low heating rate, there will be a large recrystallization exotherm superimposed on the melting

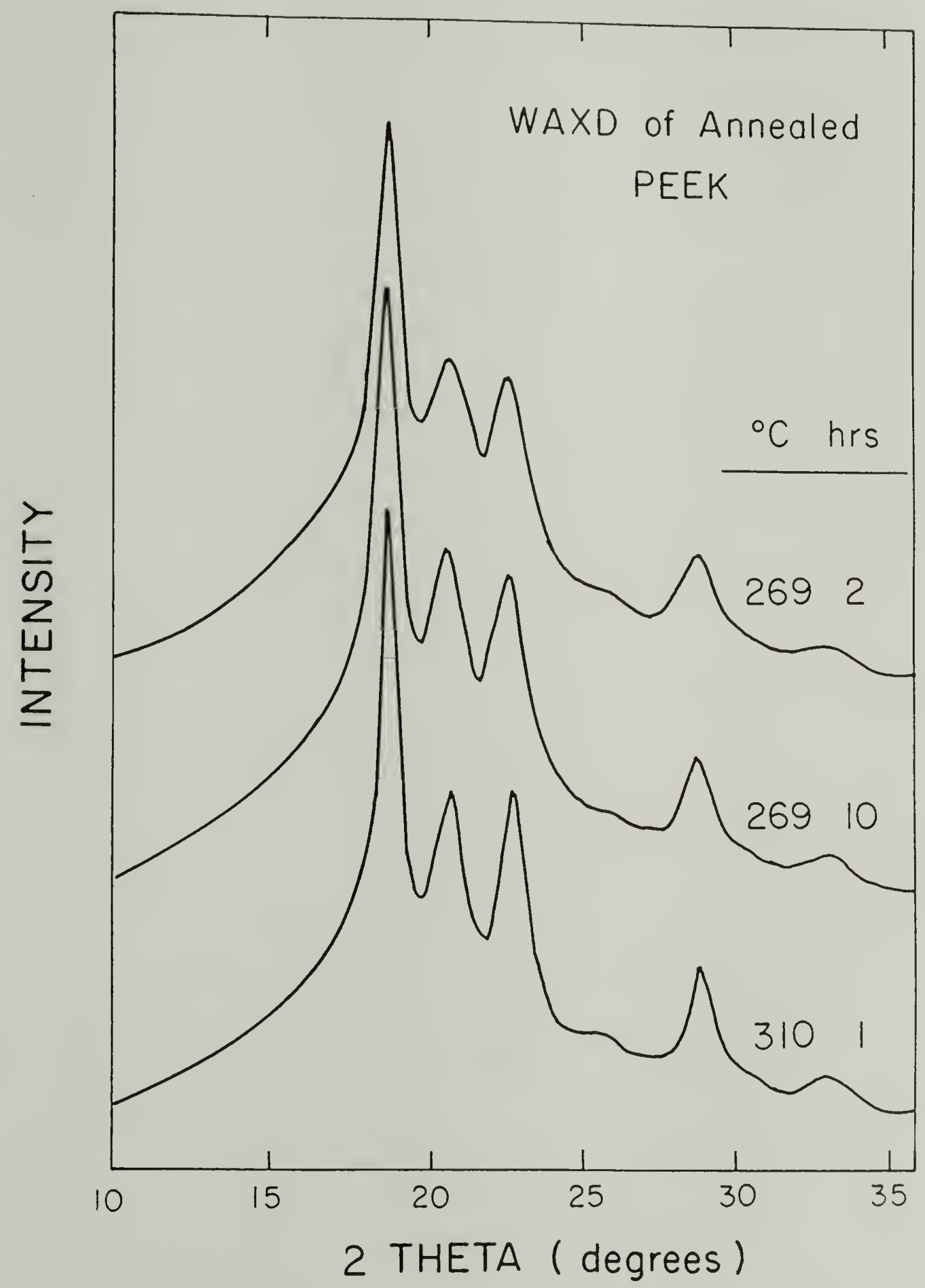

Figure 2.9. Wide-angle X-ray diffraction of annealed PEEK films.

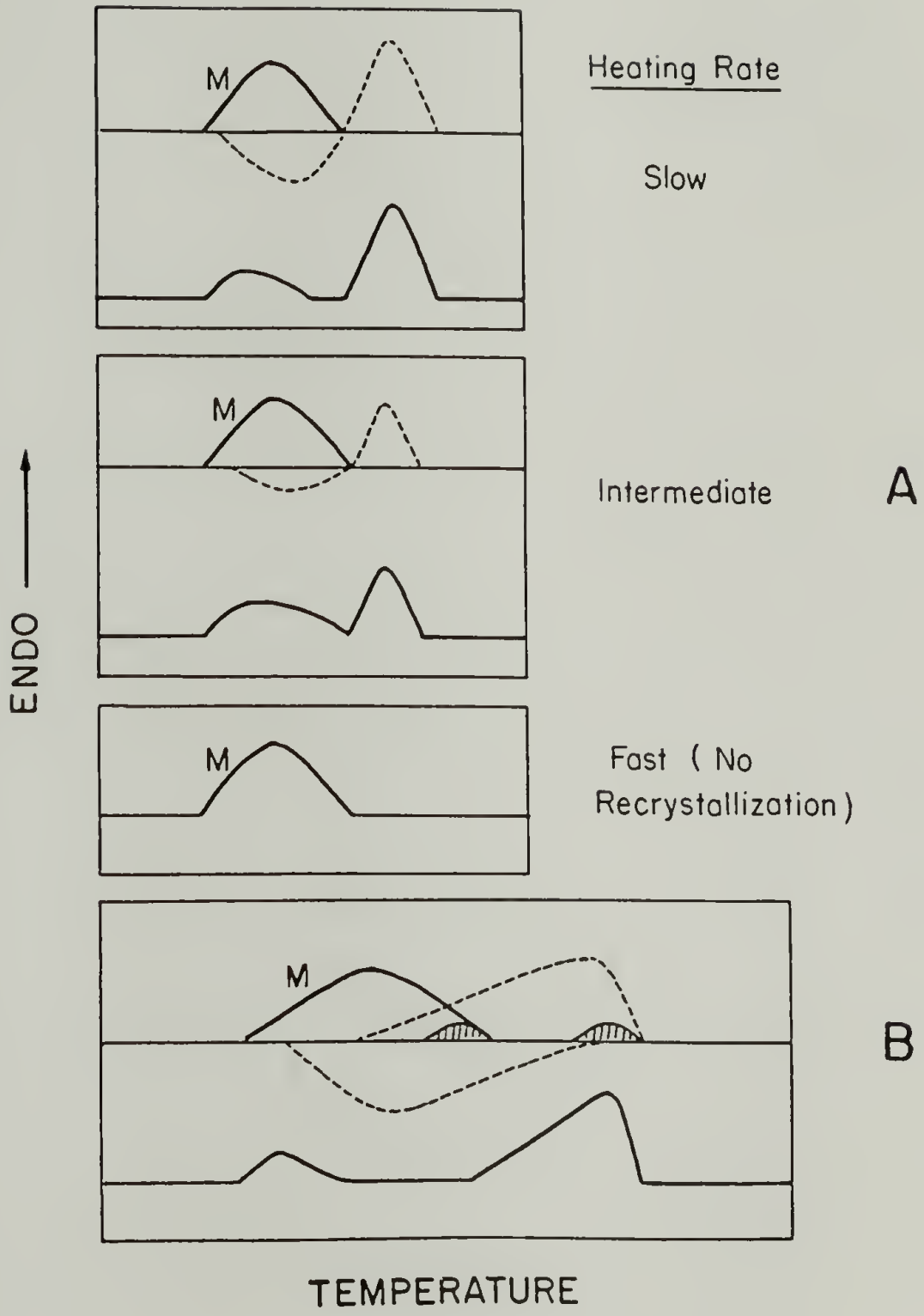

Figure 2.10. A; Schematic representaion of melting mechanism proposed for poly(caprolactone) [43] B; proposed for PEEK. M represents the melting endotherm of the original crystals. Dotted lines represent the recrystallization exotherm and the melting endotherm of the recrystallized materials. Shaded area in B represents melting endotherms of core crystalline region.

endotherm of original crystals and another melting endotherm of the recrystallized material (remelting peak) at high temperature. As the heating rate is increased, the crystals will have less time to reorganize; thus the recrystallization exotherm, and consequently the remelting endotherm, will decrease in magnitude. At a high heating rate, however, recrystallization is restricted so that the melting of original crystals will be observed directly. When the heating rate is high the effect of thermal conductivity will be considerable; therefore, superheating due to the low thermal conductivity of polymers will be observed [35,39].

The superheating of T_m1 in Fig. 2.8 can be explained by the sums of the three peaks for different heating rates as shown in Fig. 2.10A. It is important to note that there is little resemblance between the melting endotherm of the original crystals and the low-temperature endotherm. The low-temperature melting endotherm observed in a heating scan is determined by the sum of the recrystallization exotherm and the melting endotherm of original crystals.

The shape of the recrystallization exotherm cannot be measured directly by DSC, since only the net sum of two opposing contributions is detected. However, the following experiments can give an idea of the shape of the recrystallization exotherm. Heating scans were stopped at the peak temperatures of the low and high-temperature endotherms and in the middle of two melting peaks, whereafter the samples were immediately cooled (-150°C/min) and rescanned. Fig. 2.11 shows the first and three of the second scans for cold and melt-

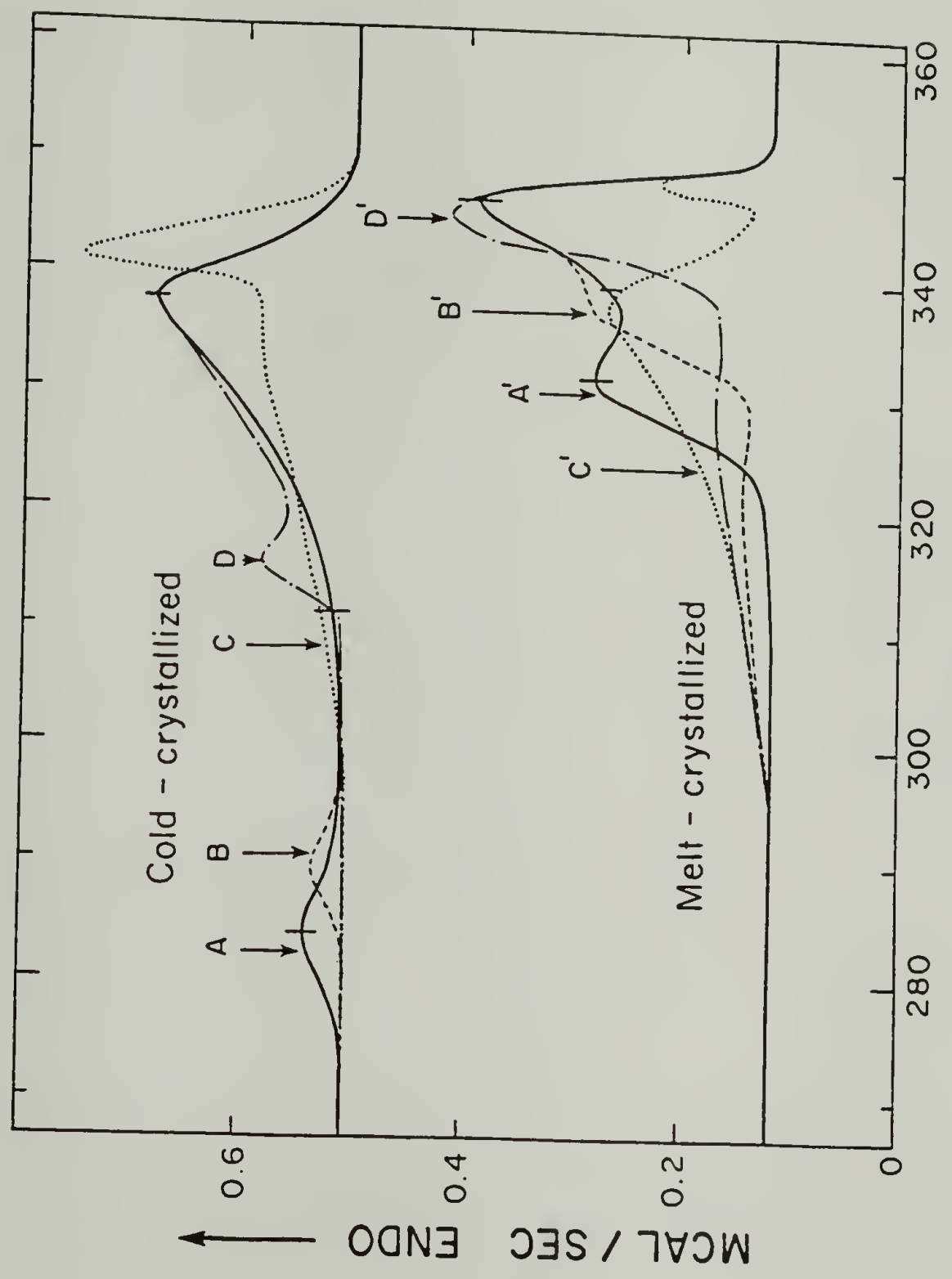

Figure 2.11. DSC traces (20°C/min) of cold-crystallized PEEK at 269.3°C for 2h (A) and melt-crystallized PEEK at 316°C for 14.5h (A'). The heating scan was stopped at the low-temperature melting peak (T_m1) for B and B'; at the high-temperature melting peak (T_m2) for C and C'; and in the middle of T_m1 and T_m2 for D and D'; when the scan was stopped, each sample was immediately cooled, and a second scan (20°C/min) begun. The stopping temperatures (T_s) indicated on the curve A are 285, 312 and 338°C; on the curve A', 332, 339 and 346°C.

crystallized PEEK. For all, the second scan shows a new melting endotherm at a temperature greater than the stopping temperature (T_s), due to the melting of material recrystallized up to T_s. A new, large endotherm above T_s in the curve C indicates that the recrystallization still occurs at T_m2 for cold-crystallized PEEK. This suggests that the recrystallization exotherm and remelting endotherm of PEEK overlap (see Fig. 2.10). The broad melting endotherm at a temperature below T_s is evidence of the crystalline region which has failed to recrystallize in the first scan and crystallized on cooling. As T_s is increased, a broader melting endotherm below T_s is observed. Curve C' for melt-crystallized PEEK shows a large broad endotherm below T_s, indicating that most crystals have melted without recrystallization up to T_s. Less endotherms are observed below T_s than the amount of melting endotherm up to T_s in the first scan. This effect is more pronounced in the cold-crystallized PEEK than in the melt-crystallized sample.

This result is in accord with the suggestion that the reorganization process involves more recrystallization for PEEK crystallized at higher supercooling [38]. If the low-temperature melting endotherm were due to the melting of another different crystalline species or the entire melting of the original crystals, the endotherms below T_s would be equal amount for both the first and second scan. This result supports the explanation that the low-temperature endotherm represents only a portion of the melting of the original crystals which exist in the sample prior to the heating scan

(see Fig. 2.10). Therefore, using T_m1 as the melting peak temperature of the original crystals is considered to be groundless [8]. Moreover, as shown in Fig. 2.8, the measured T_m1 varies by about 8°C depending on the heating rate, which presents difficulties in determining the melting peak temperature of the original crystals for use in the Thomson-Gibbs equation (Eq. 2.2) [39].

$$T_m = T_m^{\circ}\{ 1 - 2\sigma_e/(\Delta h_f \ell_c) \} \qquad (2.2)$$

Table 2.1 shows the two melting temperatures and densities for isothermally crystallized and annealed PEEK. With increasing T_a, the sample density is increased more sensitively than with annealing time. In contrast to the annealed or cold-crystallized samples, the melt-crystallized PEEK shows an increase in T_m2 with increasing T_c. The samples cold-crystallized at 200°C or melt-crystallized at 319.6°C show that T_m2 is constant but T_m1 and density increase with increasing crystallization time. Samples annealed at 269.3°C also show this same behavior. Since T_m1 increases more sensitively than density, some other reasons besides an increase in crystallinity are needed. For PET, it has been concluded that smoothing of the crystal folding surfaces occurs during isothermal crystallization, resulting in an increase in T_m1 [15]. According to the Thomson-Gibbs equation (Eq. 2.2), increased regularity in the chain conformation at the crystal surface reduces the surface energy (σ_e) and increases the melting temperature of original crystals. The high-temperature-shifted

melting endotherm of original crystals is subtracted by the recrystallization exotherm to produce a high-temperature-shifted low-temperature endotherm (Fig. 2.10A). Besides smoothing of the folding surfaces, regularization of lateral surfaces and rejection of defects have been suggested as responsible for the increase in T_m1 as annealing time of PET is increased [16].

As discussed previously, the high-temperature endotherm is the melting of the recrystallized PEEK resulting from a reorganization. Crystal surfaces are metastable due to the existence of chain folds, loops, cilia and tie molecules. Zachmann and Peterlin have suggested that melting or crystallization can occur at the crystal surface, even when the overall crystal is stable [44]. Arakawa et al. have shown that the reorganization is inhibited by chemical reaction on the crystal surfaces and in the amorphous region [45]. After methoxymethylation, the double-melting peaks of nylon 6 were coalesced into a single peak which did not depend on heating rate. The surface melting before core melting has been observed for polyethylene using SAXS [46]. Therefore, the reorganization process is considered as a partial melting followed by simultaneous recrystallization at the crystal surface. This reorganization process, occurring at the crystal surfaces, may prevent some core crystalline portion from melting. The model shown in Fig. 2.10A has been modified to accomodate the above observations for PEEK. The major points of this model, shown in Fig. 2.10B, are outlined as follows.

* The magnitude of the recrystallization exotherm at a temperature depends on the amount of crystals which have melted and decreases with increasing temperature due to a lower degree of supercooling.
* Recrystallization ends below T_m2 in PEEK melt-crystallized at low supercooling and above T_m2 in cold-crystallized samples.
* Recrystallized material melts at several degrees higher than its recrystallization temperature.
* A core portion of the original crystals melts at the temperature where the reorganization process ends.

This new model can explain the superheating of T_m1 similarly to the one in Fig. 2.10A.

2.3.4 Hoffman-Weeks Plot

Fig. 2.12 shows the two peak temperatures for isothermally crystallized and annealed PEEK from the amorphous state. The isothermal data of ref. 8 and 38 are also included. T_m1 and T_m2 of samples annealed after nonisothermal crystatallization (peak at 185°C) are very close to those of isothermally crystallized PEEK; T_m1 is 10-20 degrees higher than the crystallization temperature (T_c) or annealing temperature (T_a), and T_m2 is almost constant regardless of T_c or T_a. This may be due to imperfect, small crystals that are readily melted and recrystallized since they were produced at low temperature (around 185°C). It has been shown by successive heating

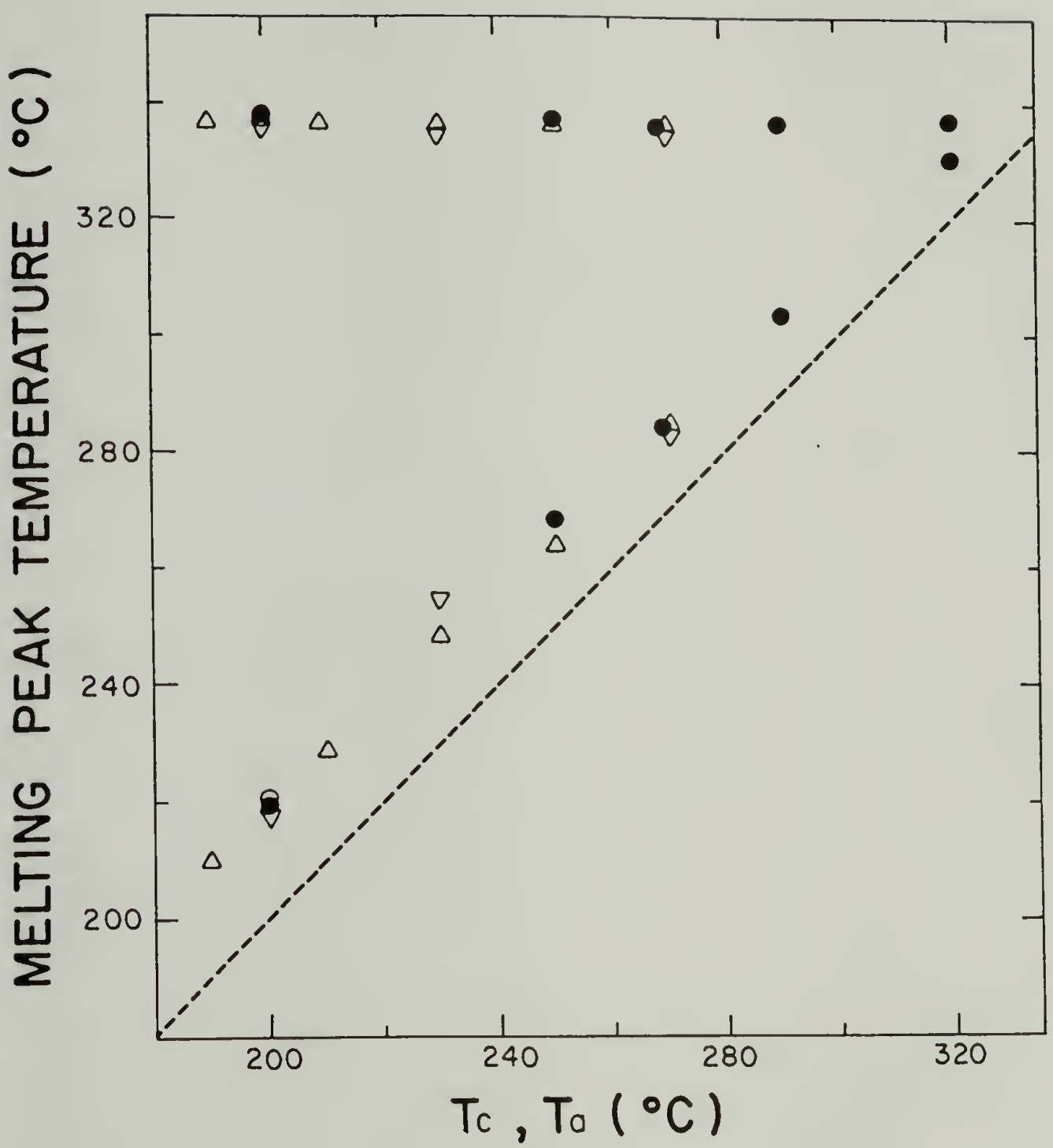

Figure 2.12. The two melting peak temperatures of isothermally cold-crystallized (△,▽,○) and annealed (●) PEEK vs. crystallization (T_c) or annealing temperature (T_a). Crystallization or annealing time was 1h and DSC heating rate was 20°C/min except for (△). (△) Data of ref. 38. Crystallization time is 2h and DSC heating rate was 10°C/min. (▽) Data of ref. 8. The dashed line is for $T_m = T_c$.

scans that such imperfect crystals melt just above their formation temperature and reorganize into more perfect crystals [47].

PEEK films melt-crystallized at a lower degree of supercooling were scanned at different heating rates (Fig. 2.13). The measured T_m1 and T_m2 are shown in Fig. 2.14. In contrast to PEEK cold-crystallized at high supercooling, T_m2 does not change with heating rate (2-40°C/min). The difference in melting behavior of the two PEEK samples may be related to the crystalline morphology which was produced at different degree of supercooling. Also in comparison to melt-crystallized PEEK, cold-crystallized PEEK has been found to contain spherulites, smaller by an order of magnitude and thinner lamellae due to higher nucleation density [48]. Owing to slow crystallization, the chain conformations at the crystal surfaces are more perfect in the PEEK crystals which were melt-crystallized at low supercooling than those in samples cold-crystallized at high supercooling. The temperature range of reorganization for the melt-crystallized PEEK is small, as shown in Fig. 2.3. Therefore, the reorganization process of a melt-crystallized PEEK occurs easily and within the heating rates. Also the same size and perfection of crystals is produced through the fast reorganization process regardless of heating rate. DSC traces for melt-crystallized PEEK may be represented by close-overlap of the four peaks in Fig. 2.10B. The area ratio of the low and high-temperature endotherms in Fig. 2.3 suggests that a smaller recrystallization exotherm is involved in the heating scan of melt-crystallized PEEK than in that of annealed PEEK. The curve C' of

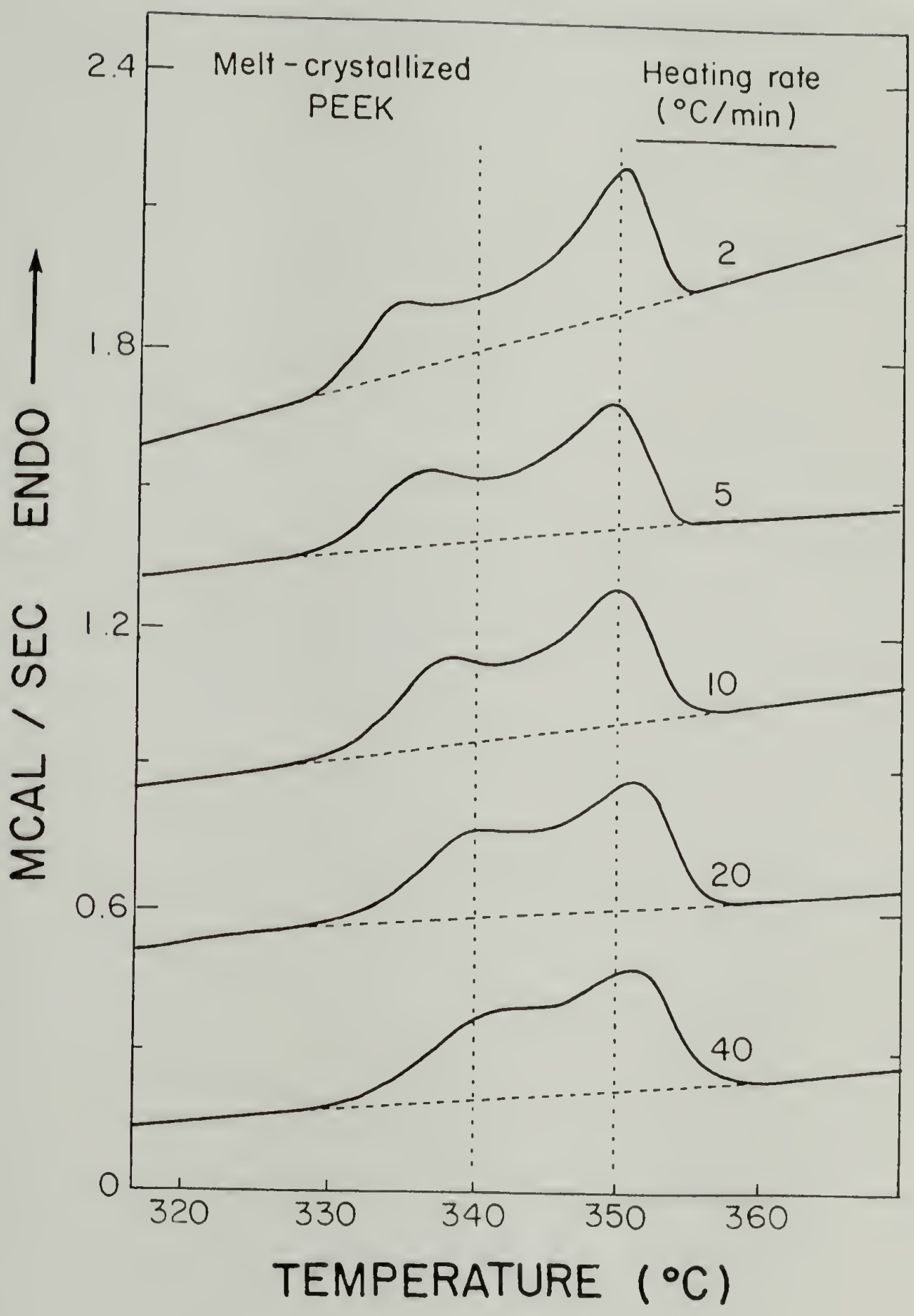

Figure 2.13. DSC traces of PEEK melt-crystallized at 322.8°C for 20h at various heating rates.

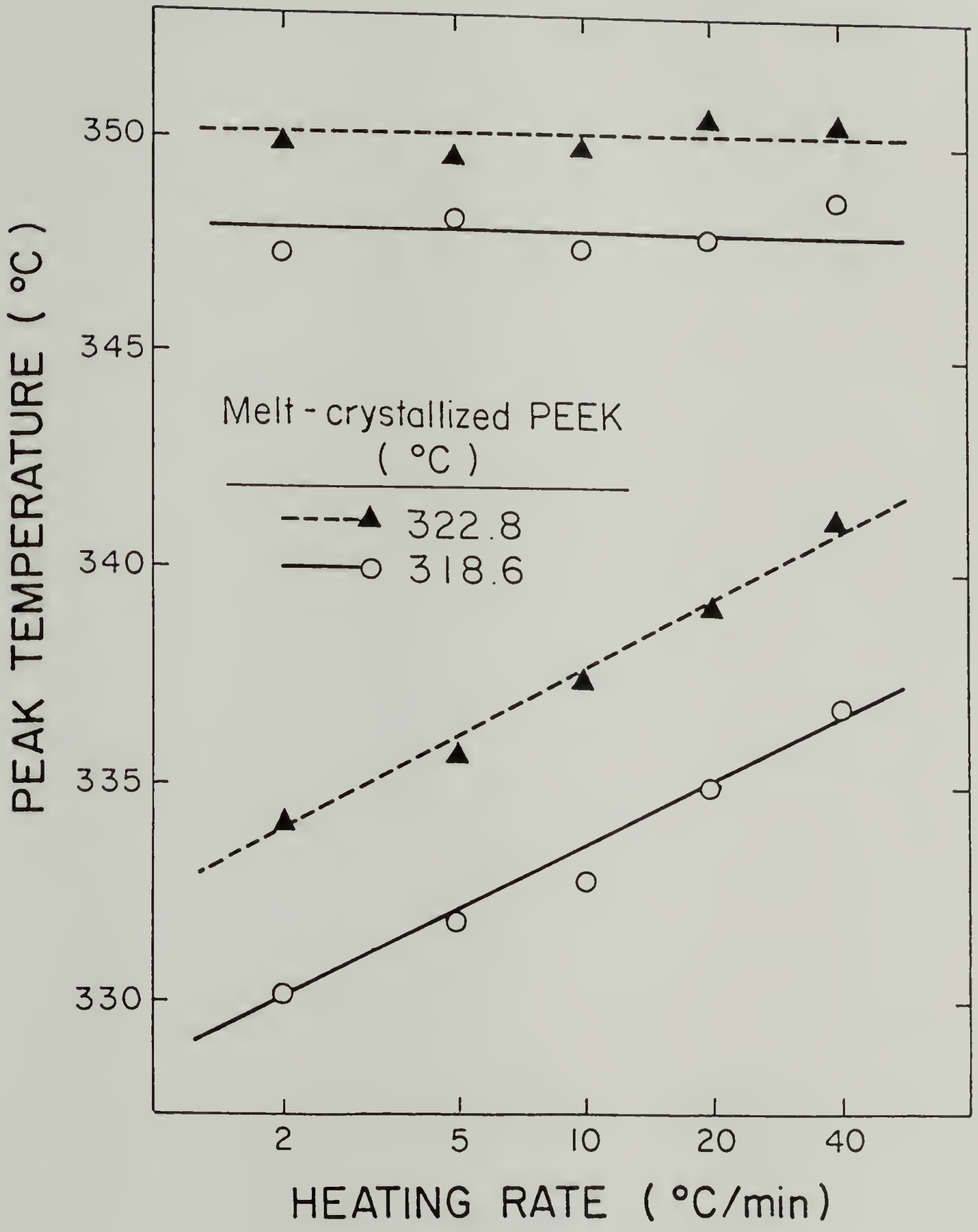

Figure 2.14. The two melting peak temperatures vs. heating rate for PEEK melt-crystallized at 322.8°C for 20h and at 318.6°C for 14h.

melt-crystallized PEEK in Fig. 2.11 shows a new melting endotherm above T_s with the same magnitude as that in the first scan. This indicates that the recrystallization of melt-crystallized PEEK ends below T_m2. Superheating of T_m1 is also observed and can be explained in the same way as that in cold-crystallized PEEK.

In Fig. 2.15, T_m1 and T_m2 are plotted schematically with T_c for melt and cold-crystallized PEEK. T_m1 from both crystallization methods exhibit a range essentially parallel to the $T_m = T_c$ line. Recall that T_m1 increases as the crystallization time increases (Fig. 2.3 and Table 2.1). T_m2 of cold-crystallized PEEK shows almost constant temperature (about 337°C) regardless of crystallization temperature and time. In contrast, T_m2 of melt-crystallized PEEK (T_c > 310°C) falls on a line with a slope of 0.60.

In case of laterally large lamellae, only the top and bottom surfaces contribute significantly to the free energy of the crystal, so that the Thomson-Gibbs equation can be simplified to Eq. 2.2 [39].

$$T_m = T_m^{\circ}\{ 1 - 2\sigma_e/(\Delta h_f \ell_c) \} \qquad (2.2)$$

where T_m° is the thermodynamic melting temperature, σ_e the top and bottom surface free energy, Δh_f the heat of fusion, and ℓ_c the crystal thickness. When it is assumed that the lamellar thickness achieves a final value on the average at the end of a crystallization experiment or a lamellar thickening process, the final lamellar thickness (ℓ) will be γ times larger than the initial thickness (ℓ_g^*).

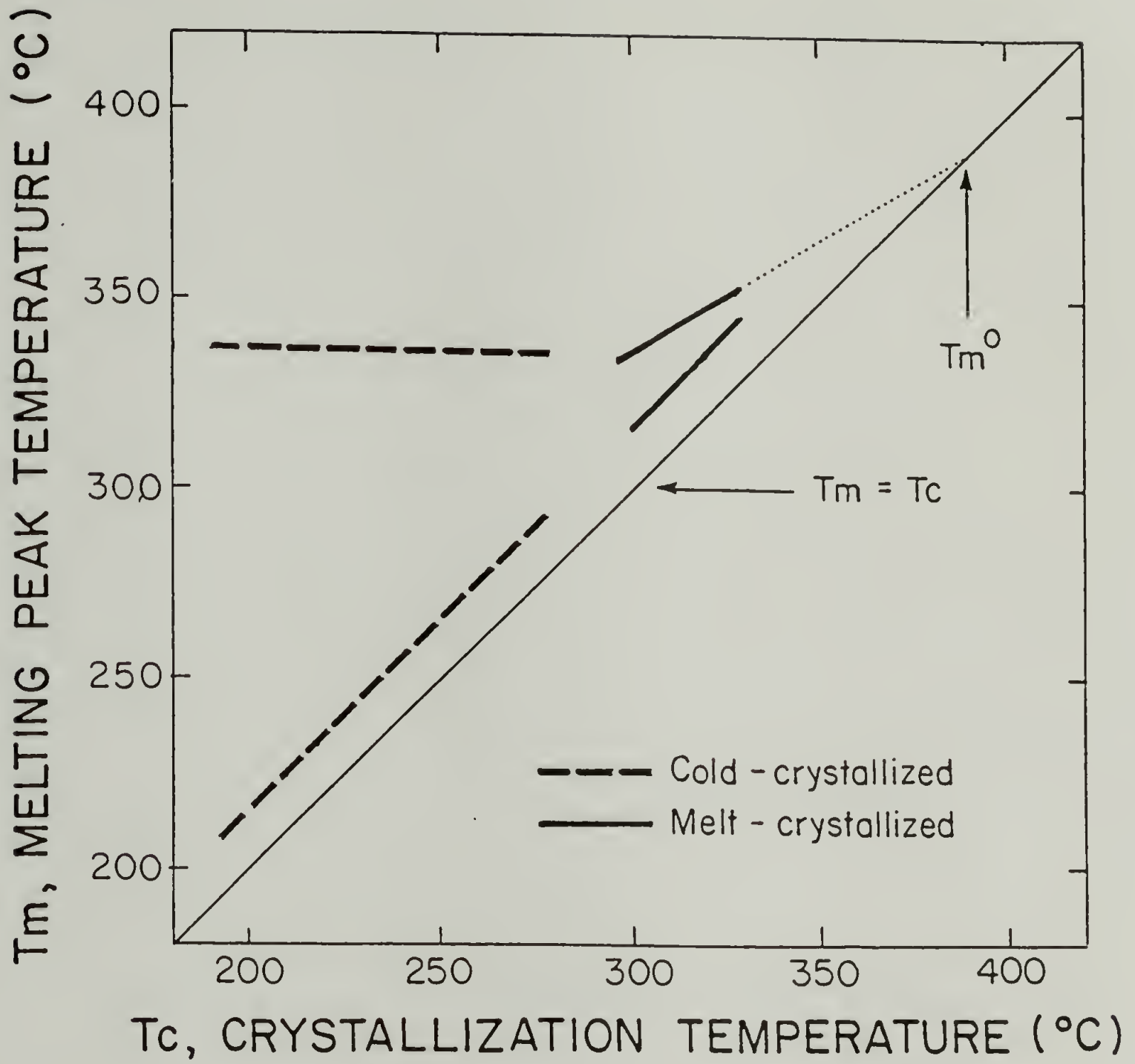

Figure 2.15. The two melting peak temperatures (at 20°C/min) vs. crystallization temperatures for cold and melt-crystallized PEEK.

$$\ell = \gamma \ell_g^* \qquad (2.3)$$

According to the kinetic theory of Lauritzen and Hoffman [49,50], the initial thickness (ℓ_g^*) of a chain-folded lamella, which is kinetically determined, is expressed by

$$\ell_g^* = (2\sigma_e/\Delta f) + \delta\ell = [2\sigma_e T_m^\circ/(\Delta h_f \Delta T)] + \delta\ell \qquad (2.4)$$

where Δf is the free energy per unit volume of crystal, ΔT the supercooling ($T_m^\circ - T_c$) and $\delta\ell$ a small positive quantity that is only a weak function of the supercooling. Since $2\sigma_e/\Delta f >> \delta\ell$ is a fair approximation for the crystal formed at low supercooling the following equation is derived by inserting Eq. 2.3 and 2.4 into Eq. 2.2.

$$T_m = T_m^\circ(1 - 1/\gamma) + (1/\gamma)T_c \qquad (2.5)$$

Eq. 2.5 shows that T_m° and the lamellar thickening factor (γ) are determined from the intersection with the $T_m = T_c$ line and the slope, respectively, in a Hoffman-Weeks plot of T_m vs. T_c [51]. Since recrystallization can more rapidly produce crystalline material than ordinary isothermal crystallization at the same temperature, concerns about the effects of recrystallization on observed melting temperature have been discussed [51,52]. When $T_m 2$ is considered to be the melting temperature in Eq. 2.5, the T_m° of PEEK is extrapolated to be 389±4°C, about 6°C lower than the previously reported value [8]. As discussed,

the reorganization process involves partial melting and recrystallization at the crystal surfaces and the reorganized crystals may be larger than the original crystals. T_m2 of melt-crystallized PEEK at a low supercooling ($T_c > 310^oC$) shows a linear relationship with T_c but no dependence on the crystallization time and heating rate. These results suggest that the reorganization process increases the crystal dimensions rapidly up to a limit, determined only by T_c. Therefore T_m2, the melting peak temperature of reorganized crystals, may be treated as the melting temperature of thickened crystals at the end of a crystallization.

T_m1 and T_m2 of the melt-crystallized PEEK are shown in Fig. 2.16. The crystallization times are listed in Table 2.1 or are similar to the listed values. Recall that T_m2 is not sensitive to crystallization time. From the slope of the line in Fig. 2.16 and Eq. 2.5, γ is calculated to be 1.7. During the crystallization the initial PEEK lamellae may be thickened and these lamellae are further increased in size during the heating scan in DSC. The final PEEK lamellar thickness, after reorganization, reaches 1.7 times the initial thickness. Lamellar thickening factors during isothermal crystallization have been found to be 2-2.5 for polyethylene [50,53], 2 for isotactic polystyrene [18] and 3.4 for poly(chlorotrifluoro-ethylene) [49,51]. T_m2 of melt-crystallized PEEK below 310^oC does not show the linear relationship with T_c and approaches T_m2 of cold-crystallized PEEK as T_c is decreased.

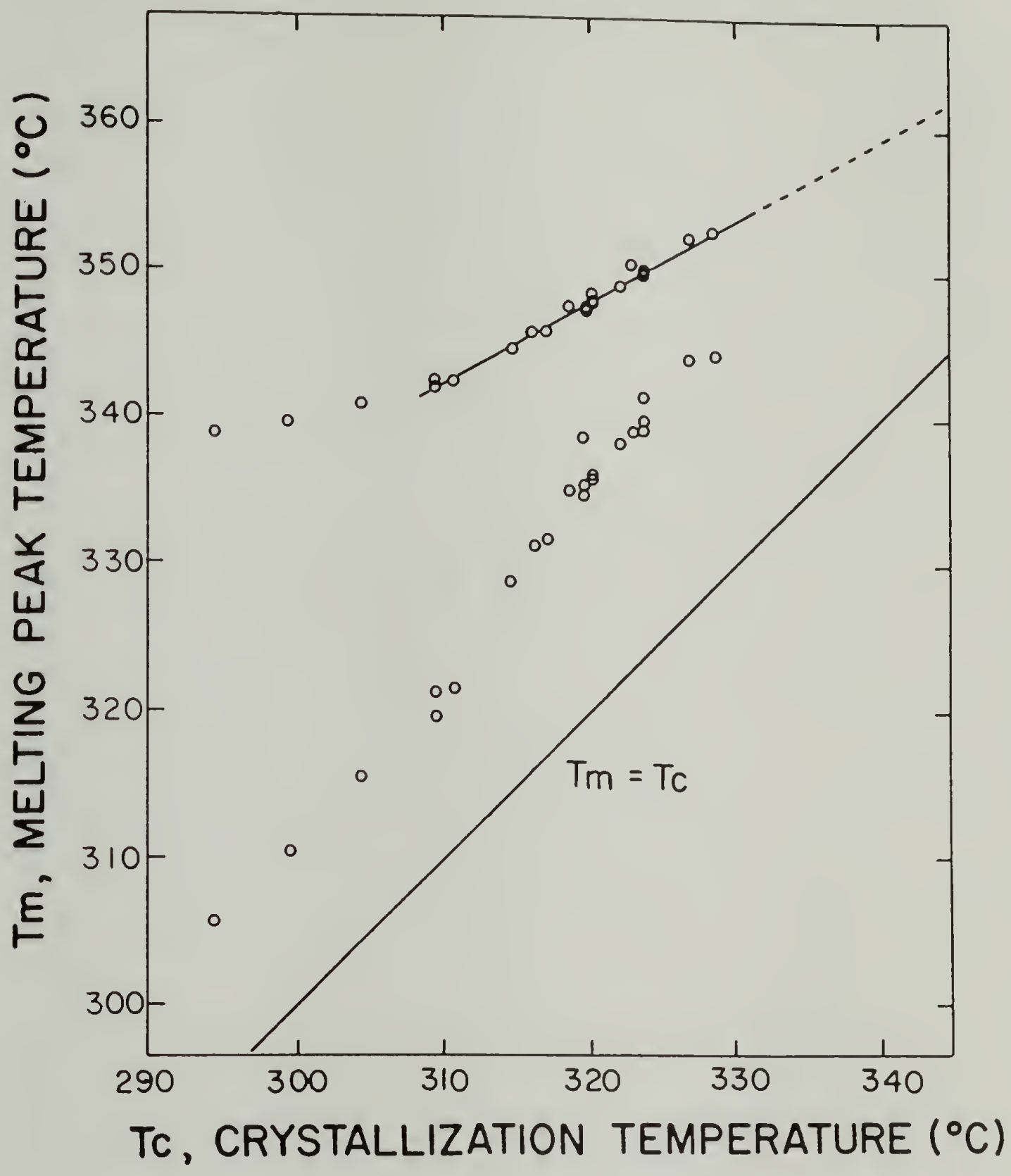

Figure 2.16. The two melting peak temperatures (at 20°C/min) of melt-crystallized PEEK vs. crystallization temperature.

2.3.5 The Heat of Fusion for PEEK Crystal

Densities and heats of fusion for PEEK samples have been measured and plotted in Fig. 2.17. Heats of fusion were measured using the net peak area method since it had been found to be better than the total enthalpy method for PET [8,54,55]. Heats of fusion show a linear relationship with densities. The crystallization conditions of PEEK are listed in either Table 2.1 or Table 2.2. Reproducible heat of fusion was not measured for PEEK crystallized at a low temperature, due to the curvature in instrument base line. A range of PEEK crystal densities, calculated from the unit cell dimensions measured with wide-angle X-ray diffraction (WAXD), has been reported [29,30,40,56-58]. It was found that diffraction patterns of PEEK drawn in our laboratory are consistent with the unit cell dimensions reported by Rueda et al. [40]. Therefore their crystal density (1.415 g/cm^3) was used to calculate the heat of fusion for fully crystalline PEEK. The line in Fig. 2.17 is extrapolated to yield 39.5 cal/g for fully crystalline PEEK at its melting temperature. Blundell and Osborn have measured the heat of fusion to be 31.1 cal/g using 1.401 g/cm^3 as the density of PEEK crystal [8].

2.3.6 True Melting Point

Fig. 2.18 shows DSC traces at various heating rates for PEEK annealed at 320°C. As the heating rate was increased, the low-temperature melting endotherm increased in size and peak temperature while the high-temperature endotherm decreased in size and peak

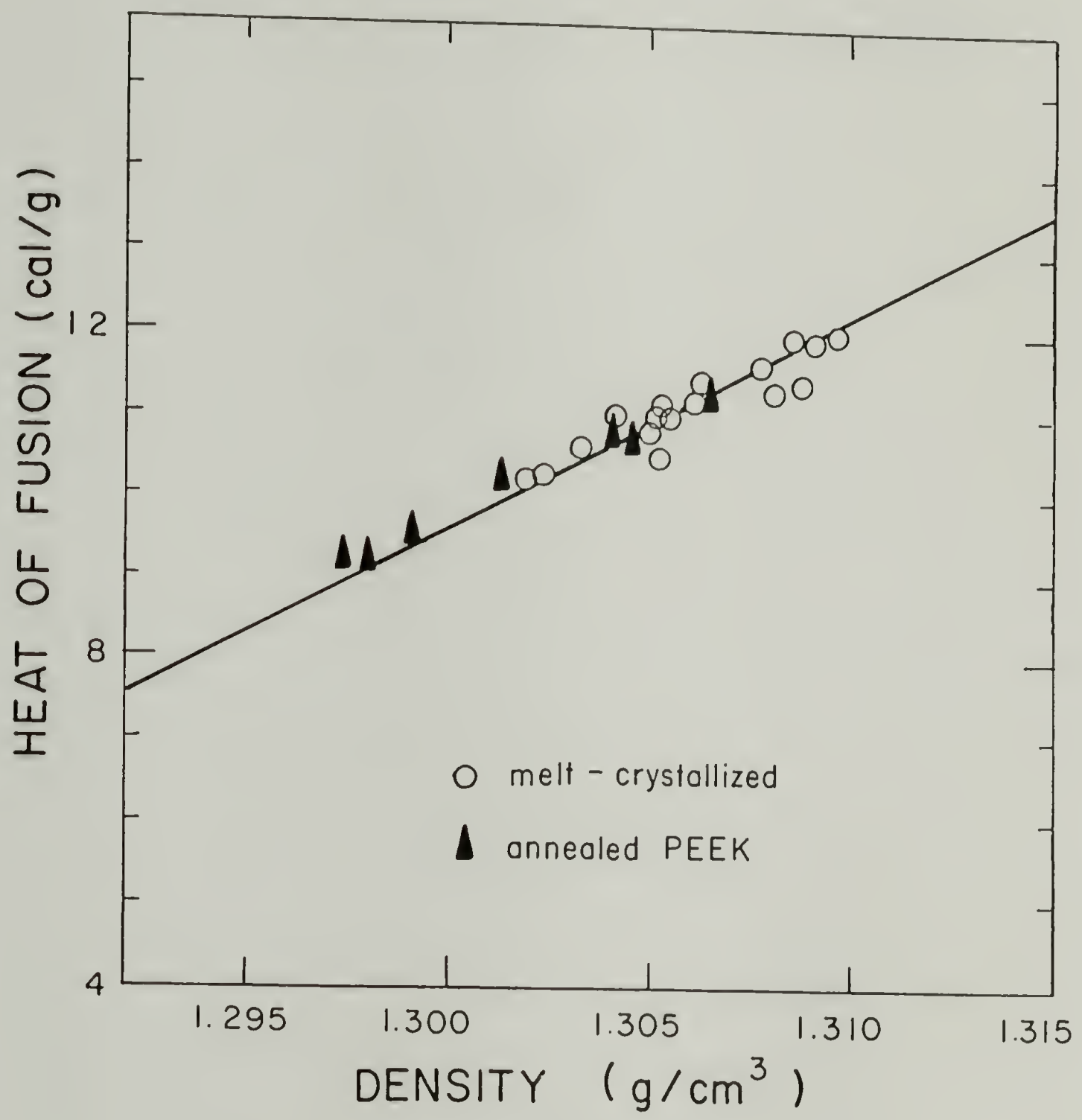

Figure 2.17. Heats of fusion for melt-crystallized and annealed PEEK. DSC heating rate was 20°C/min.

Table 2.2. Crystallization temperature, peak temperatures of low and high-temperature endotherms, average melting temperature, density, crystallinity from density, long period and crystal thickness for isothermally crystallized and annealed PEEK from amorphous state. Crystallization time is 1h except for the last sample.

T_c (^oC)	T_m1 (^oC)	T_m2 (^oC)	$\bar{T}_m$[a] (^oC)	ρ (g/cm^3)	χ_ρ[b] (%)	ℓ (Å)	ℓ_c (Å)
			Cold-crystallized PEEK				
180	195.1	337.9	266.5	1.2898	17.6	101	17.8
190	207.8	337.7	272.8	1.2905	18.1	104	18.8
200	220.8	337.4	279.1	1.2929	19.7	104	20.5
200	220.2	337.9	279.0	1.2926	19.5	104	20.3
210	230.2	336.8	283.5	1.2923	19.3	106	20.5
			Annealed PEEK				
200	219.2	337.7	278.5	1.2925	19.4	106	20.6
215	235.2	334.7	285.0	1.2936	20.1	115	23.1
230	251.5	335.3	293.4	1.2952	21.2	115	24.4
250	267.9	337.0	302.5	1.2974	22.6	119	26.9
269	284.2	336.6	310.4	1.2991	23.8	130	30.9
290	303.3	336.5	319.9	1.3011	25.1	137	34.4
310	323.6	337.7	330.7	1.3042	27.1	148	40.1
320	330.4	336.9	333.7	1.3045	27.3	157	42.9
320[c]	335.8	335.8	335.8	1.3064	28.6	157	44.9

a. $\bar{T}_m = (T_m1 + T_m2)/2$.

b. using 1.415 and 1.263 g/cm^3 as crystal and amorphous densities, respectively.

c. annealing time was 21.5h.

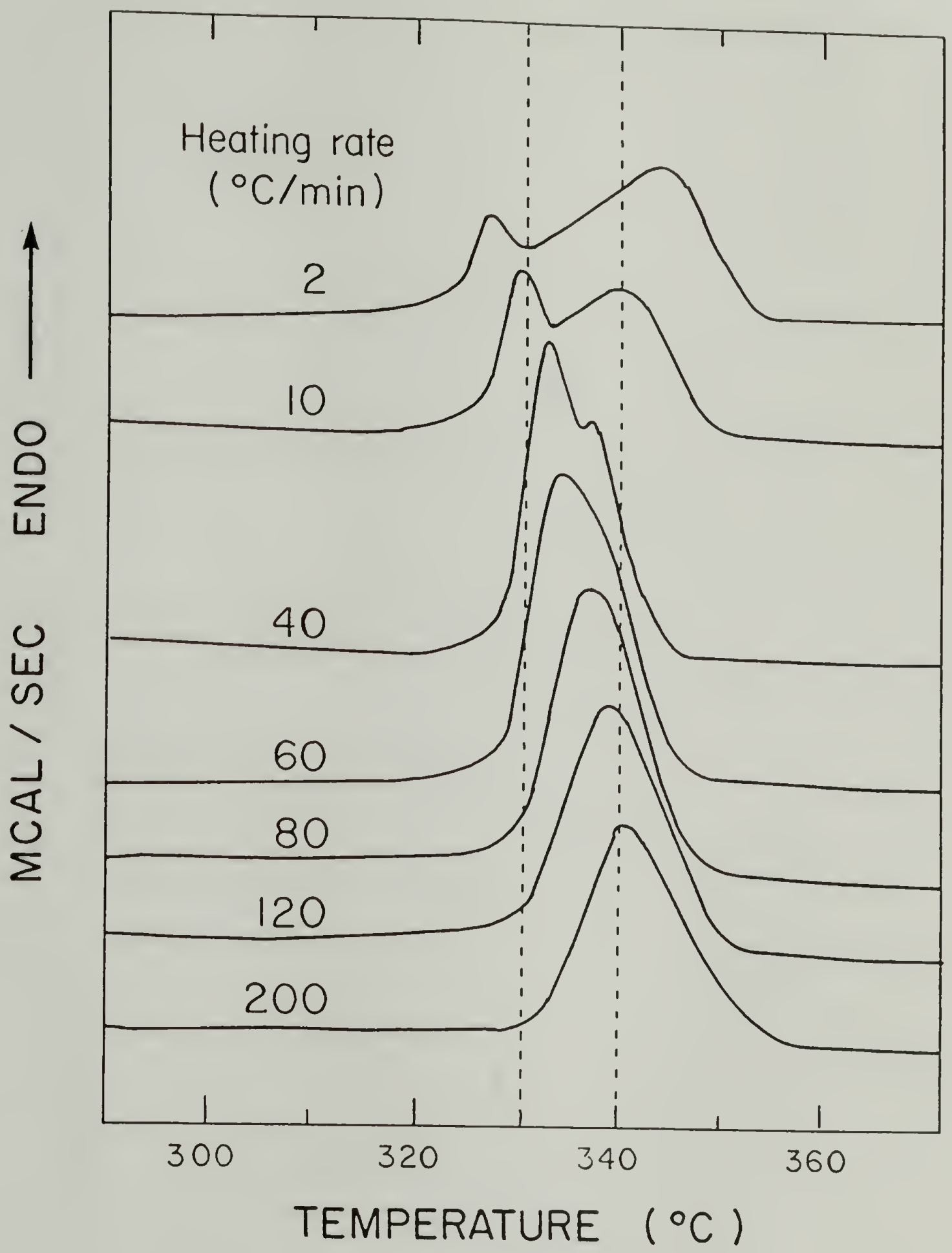

Figure 2.18. DSC traces of PEEK annealed at 320°C for 1h at various heating rates.

temperature. The same behavior was found for PEEK crystallized at 220°C, as shown in Fig. 2.7 and 2.8. The two distinct melting endotherms finally coalesced into a single peak at 60°C/min. For this particular sample, 60°C/min appears to be fast enough to minimize the reorganization. The peak temperature of the single endotherm increases with increased heating rate above 60°C/min. This is considered to be due to the low thermal conductivity of polymers; the same behavior was reported for poly(ϵ-caprolactone) [43]. The peak temperatures of the PEEK sample in Fig. 2.18 and PEEK annealed at 310°C are plotted vs. heating rate in Fig. 2.19. At high heating rate, the two endotherms coalesced into one. The coalescent endotherm is located nearly in the middle of two former endotherms.

The true melting temperature of a polymer is difficult to measure due to annealing on heating [39]. At a faster rate, the observed melting peak is closer to the true melting temperature. However, superheating due to the low heat conduction of a polymer arises at a high heating rate. The single melting endotherm without being superheated might represent the true melting of original PEEK crystals which exist in the sample prior to heating. Therefore, the true melting temperatures of PEEK crystals annealed at 320 and 310°C are considered to be 334.4 and 332.1°C, respectively (Fig. 2.19). It is interesting to note that these two true melting temperatures are nearly (within 2 degrees) in the middle of the two melting peak temperatures at low heating rates.

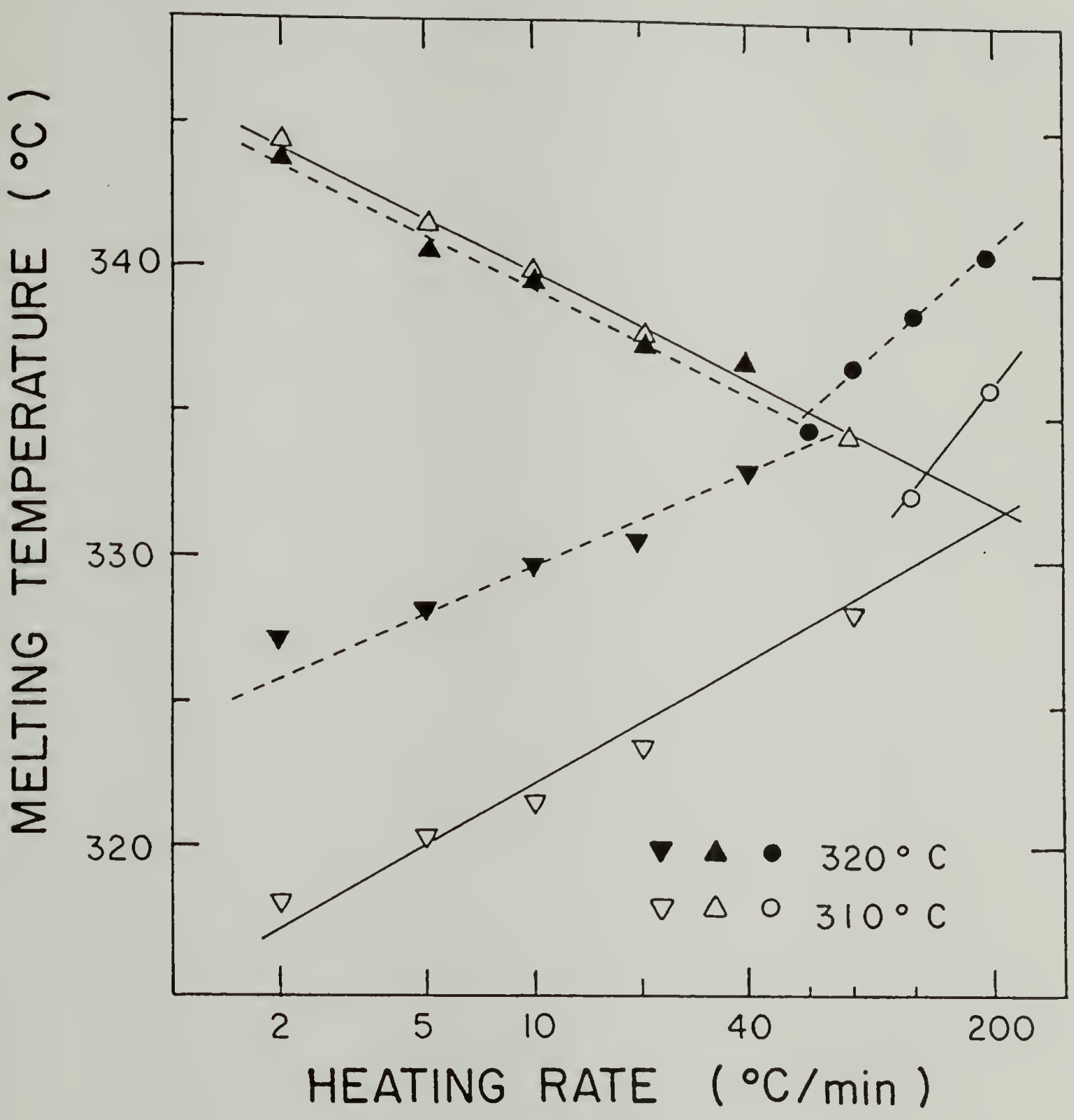

Figure 2.19. The two melting peak temperatures vs. heating rate for PEEK melt-crystallized at 310°C for 1h and at 320°C for 1h.

Isothermally crystallized or annealed poly(ethylene terephthalate) (PET) has also known to show two melting endotherms in DSC due to reorganization [13-16]. PET annealed at 190°C for 2 and 20h were scanned at various heating rates and the two peak temperatures were plotted vs. heating rate in Fig. 2.20. The two peak temperatures show the same behavior as those of PEEK in Fig. 2.19; T_m1 increases while T_m2 decreases with increased heating rate. Two melting endotherms coalesced into one endotherm whose peak temperature is nearly in the middle of T_m1 and T_m2. DSC traces of annealed PET at various heating rate have been reported to be comparable with Fig. 2.20 [14,15]. The DSC traces of Groeninckx et al. (20mg, 4-32°C/min) are not consistent with Fig. 2.19 or with the data in ref. 14 and 15, probably due to different temperature calibration for different heating rates or different size of samples [59]. It has been shown that the endotherms of large samples become less resolved as heating rate is increased [35].

Blundell and Osborn measured the thermodynamic melting point (T_m^o) of PEEK to be 395°C using the Thomson-Gibbs equation (Eq. 2.2) [8]. They believed that the low-temperature melting peak is the melting of crystals which exist in the sample prior to heating. Therefore, they used the peak temperature of the low-temperature endotherm (T_m1) in Eq. 2.2. However, it was pointed out that only about 10% of the total melting occurs at the low-temperature melting endotherm [47]. As shown in Fig. 2.8 and 2.19, T_m1 strongly depends on heating rate; T_m1 increases by 6-8 degrees when heating rate is changed from 2 to

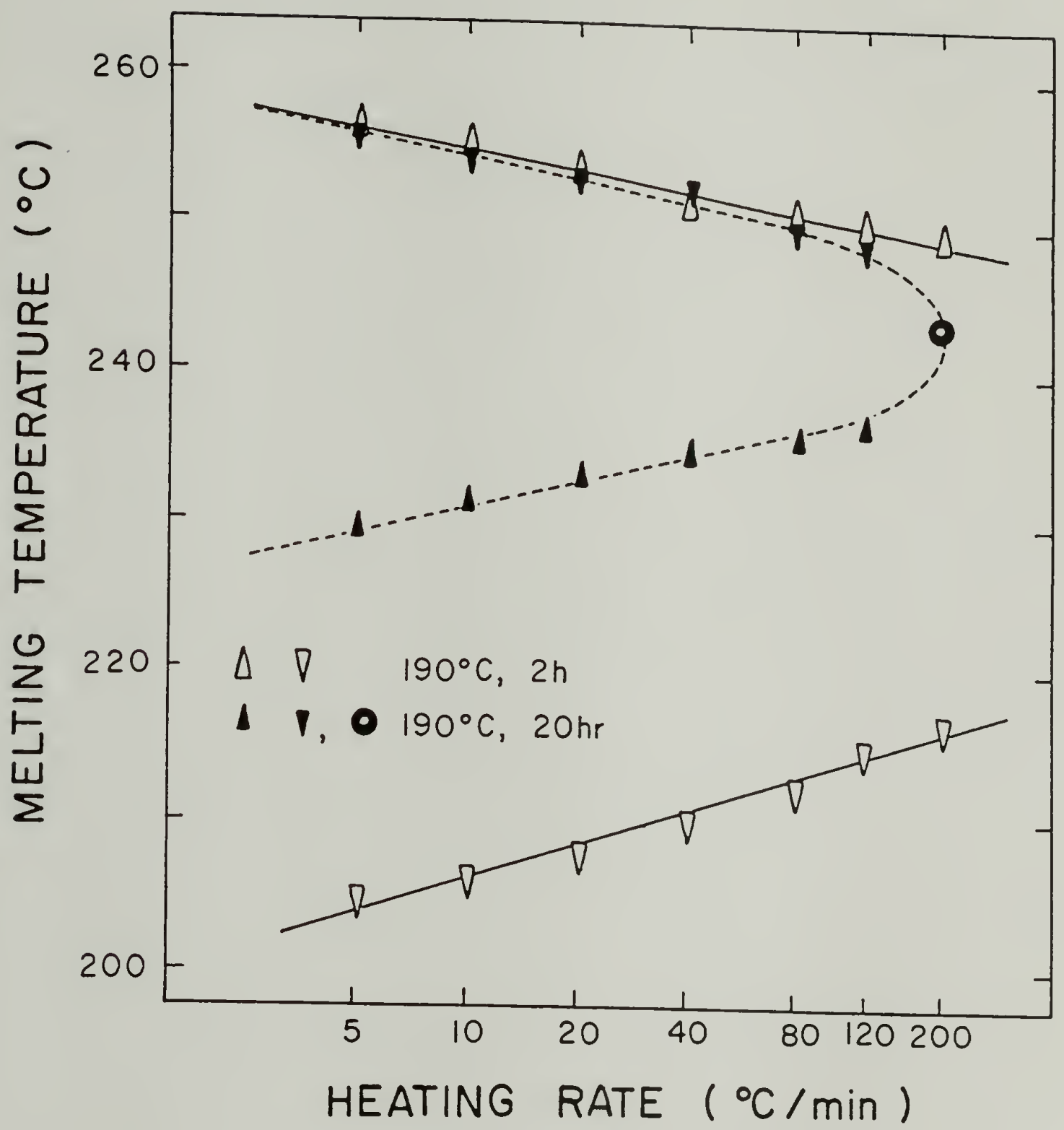

Figure 2.20. The two melting peak temperatures vs. heating rate for poly(ethylene terephthalate) cold-crystallized at 190°C.

40°C/min. As previously discussed in section 2.3.3, T_m1 is only "a portion" of melting of original crystals and the rest of the melting is compensated by recrystallization exotherm. Therefore T_m1 is considered not to represent the melting temperature of the original crystals prior to heating.

2.3.7 Small-Angle X-ray Scattering

Small-angle X-ray scattering patterns for annealed and melt-crystallized PEEK are shown in Fig. 2.21. As the annealing temperature was decreased, scattering curves become broad and shift to wide angle indicating small crystal thickness. The long periods of cold-crystallized and annealed PEEK from the glassy state were measured. One-dimensional crystalline and amorphous layers have been assumed; thus, the long period consists of one crystalline and one amorphous layer. The long period was increased with increased annealing temperature, as shown in Fig. 2.22. Little difference was observed between annealed and cold-crystallized PEEK. The crystal thickness (ℓ_c) was calculated using the long period and crystallinity from density of the sample. The long period, crystallinity and crystal thickness are listed in Table 2.2. Also, T_m1 and T_m2 observed at 20°C/min and arithmatic average of T_m1 and T_m2 or $\bar{T}_m$ are added.

In Fig. 2.23, T_m1 is plotted vs. $1/\ell_c$. The data show a linear relationship which yields T_m° of about 430°C. This T_m° may vary with the scanning rate of DSC since T_m1 superheats, as shown in Fig. 2.8 and 2.19. Two of the three data from ref. 8 are consistent with our

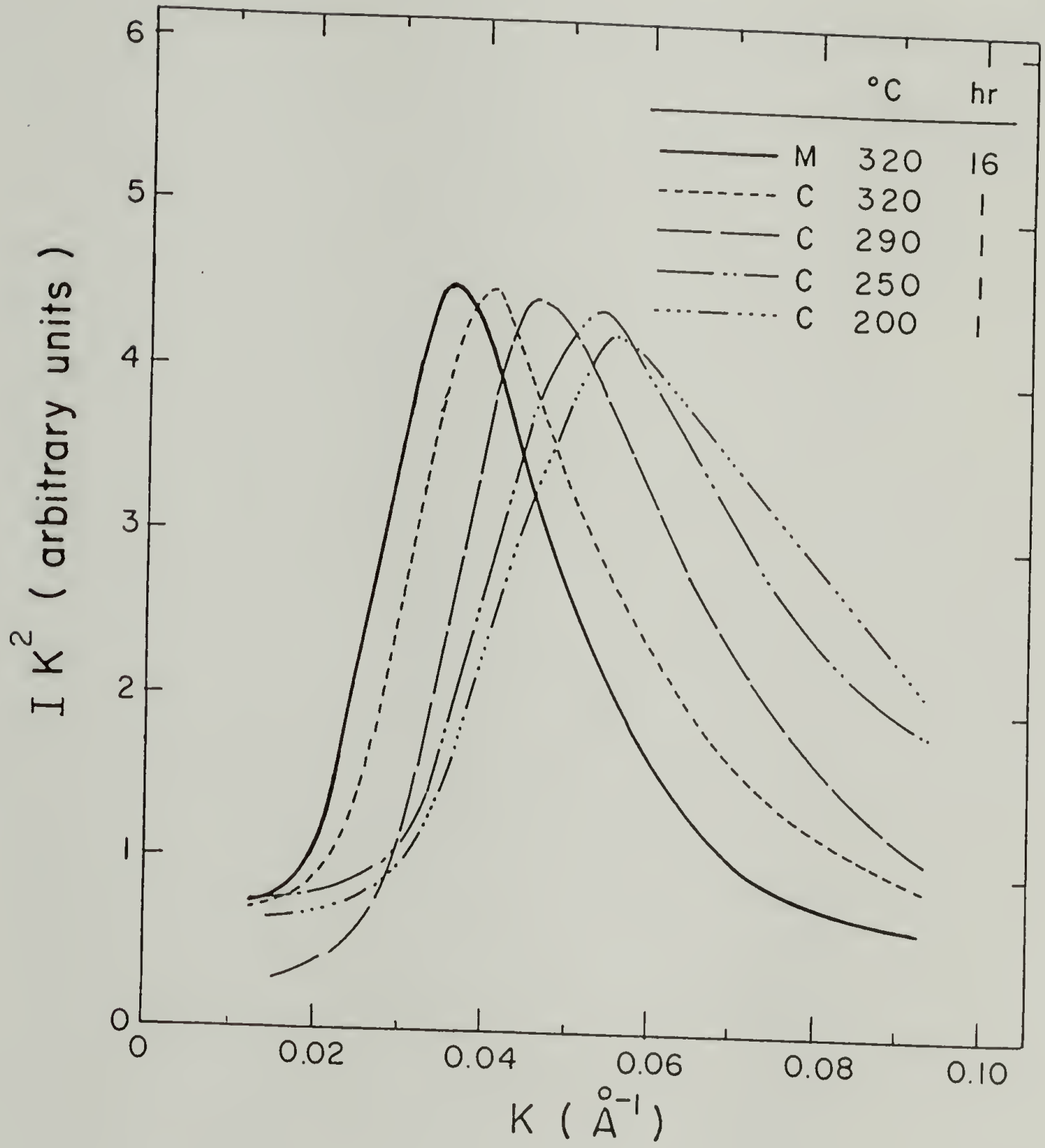

Figure 2.21. IK^2 vs. K for PEEK melt-crystallized (M) and annealed (C) at indicated temperatures. $K = 4\pi \sin\theta/\lambda$.

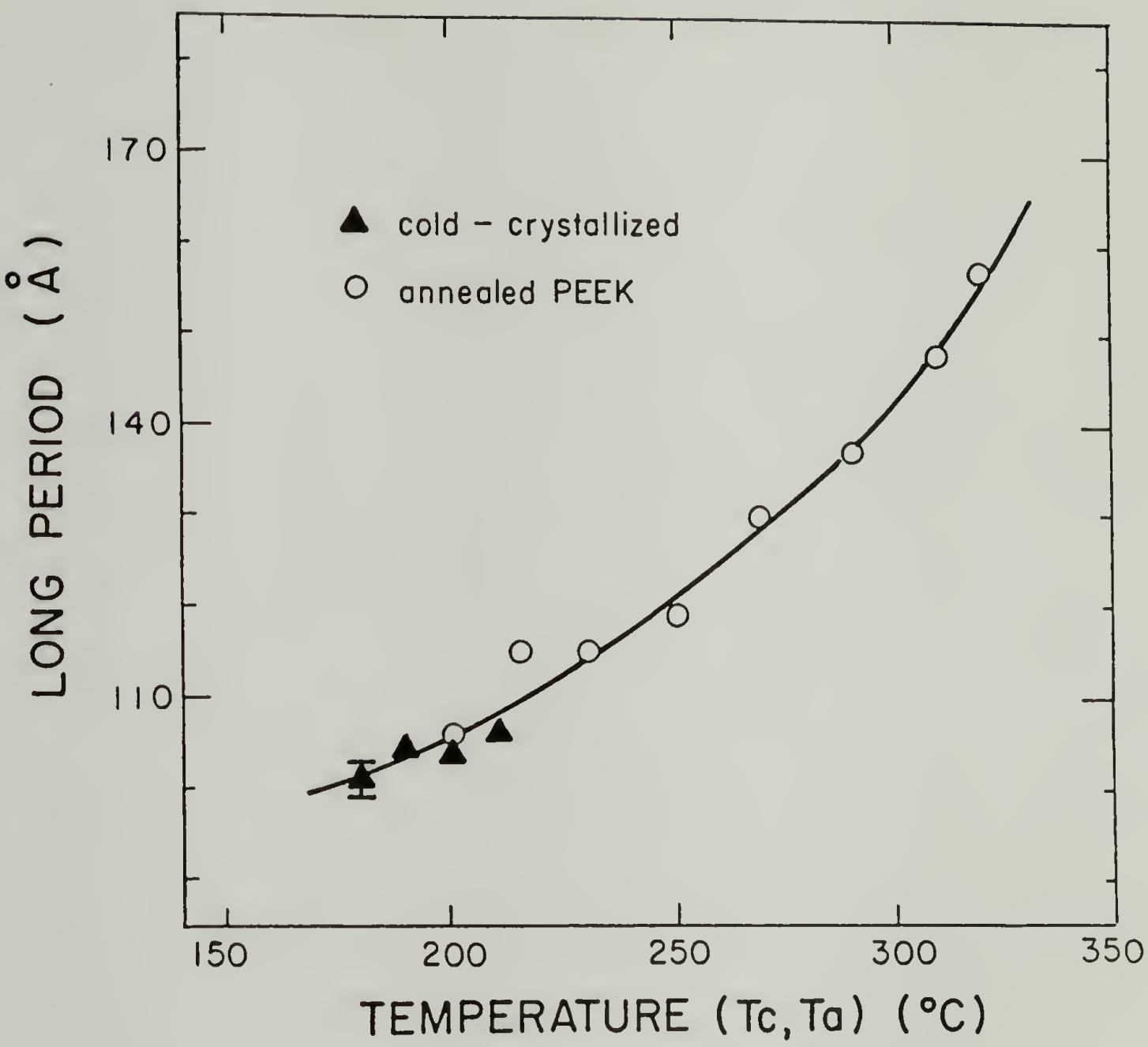

Figure 2.22. Long period vs. crystallization temperature for cold-crystallized and annealed PEEK.

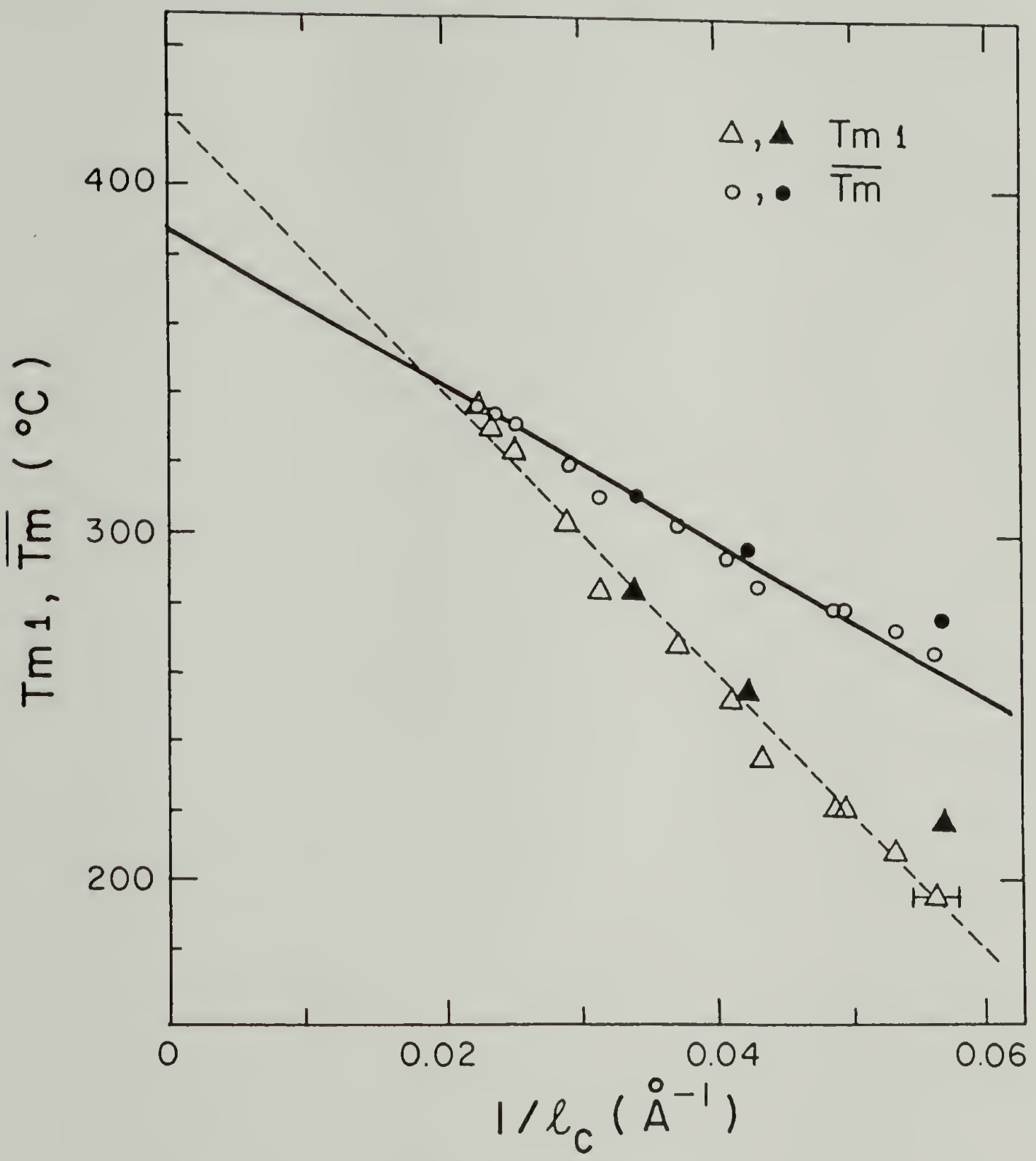

Figure 2.23. T_m^1 and $\bar{T}_m^-$ vs. 1/(crystal thickness). Solid symbols (▲, ●) data of ref. 8.

data; however, T_m^o of 395°C was reported in ref. 8. As discussed, T_m1 is not considered to represent the melting temperature of the original crystals. The average of T_m1 and T_m2, or $\bar{T}_m$, is in the vicinity of the peak temperature of the coalesced melting endotherm which is considered to represent the true melting of the original crystals. Therefore $\bar{\bar{T}}_m$ is also plotted vs. $1/\ell_c$ in Fig. 2.23. The line yields T_m^o of 384°C which is comparable with the value of 389°C obtained using a Hoffman-Weeks plot (section 2.3.4) and surface free energy of 39 erg/cm^2.

2.4 Conclusions

The double-melting behavior of PEEK has been found to be due to a crystal reorganization on heating. The low-temperature endotherm has been found to represent only a portion of the melting endotherm of original crystals. The high-temperature endotherm is the melting of crystals reorganized during a heating scan. The reorganization process is considered to occur at crystal surfaces through a partial melting followed by recrystallization. The model modified from the one proposed by Rim and Runt for poly(caprolactone) is consistent with the melting behavior of PEEK. The low and high-temperature melting peaks are considered to be the sum of four peaks: melting of original crystals, their recrystallization, remelting of recrystallized material and finally the melting of core crystalline regions.

For melt-crystallized PEEK at lower supercooling (T_c > 310°C), it is proposed that the reorganization process increases the crystal dimensions rapidly up to a limit determined by supercooling. A Hoffman-Weeks plot shows that the thermodynamic melting point of PEEK is 389°C and the lamellar thickening factor is 1.7. During the isothermal crystallization, the initial lamellae may be thickened and these lamellae are further increased in size during the heating scan. The final lamellar thickness after reorganization reaches 1.7 times the initial lamellar thickness.

It was found for PEEK annealed at high temperatures(310, 320°C) that two melting endotherms coalesce into one at high heating rates. The melting peak temperature of the coalesced endotherm is approximately in the middle of the two melting peak temperatures. Poly(ethylene terephthalate), cold-crystallized at 190°C, also showed the same behavior. The coalescent melting endotherm was considered to represent the complete melting of whole crystals without reorganization. From the crystal thickness measured by small-angle X-ray scattering, the thermodynamic melting point and surface free energy of PEEK crystal were measured to be 384°C and 39 erg/cm^2, respectively. This thermodynamic melting point is comparable with the value of 389°C from a Hoffman-Weeks plot. The heat of fusion for fully crystalline PEEK has been measured to be 39.5 cal/g at its melting point.

C H A P T E R III

EFFECTS OF THERMAL HISTORY ON CRYSTALLIZATION OF POLY(ETHER ETHER KETONE)

3.1 Introduction

Alterations in crystallization conditions are known to result in different crystal morphologies, which influence product properties. It has been found that the thermal history in the melt or solution affects the crystallization behavior of many polymers [60]. Therefore, the thermal history prior to crystallization must be treated carefully, as well as other crystallization conditions. As the melt temperature is increased, the number of nuclei decreases, therefore, overall crystallization rate decreases. Reported examples are polyethylene [61], isotactic polypropylene [62], isotactic polystyrene [63], polychlorotrifluoroethylene [64,65], nylon 6 [66], nylon 6,6 [67], poly(ethylene oxide) [68,69], polyoxymethylene [70] and poly(ethylene terephthalate) [71,72]. Unlike solution crystallization [73,74], the holding time in the melt also influences the crystallization of polymers [66,67,70]. However, contradictory results have been obtained for polyethylene [75] and poly

(decamethylene terephthalate) [76]; crystallization of the polymers were found to be independent of the previous melt temperature.

It has been noted that crystallization of PEEK in composites depends on melt temperature (melt-annealing temperature) and holding time in the melt (melt-annealing time) [77,78]. The effects of melt-annealing temperature and time on crystallization of PEEK is discussed in this chapter.

3.1.1 Explanations for Effects of Thermal History

Morgan proposed that residual minute crystalline regions persist above the nominal melting temperature of a polymer [79]. The more perfect the crystalline region is, the higher is the temperature required for melting of the region. Thus, if the melt temperature is not sufficiently high, remnants of the more highly ordered crystals may serve as nuclei for crystallization on subsequent cooling. As the melt temperature is increased the ordered regions melt leaving a true homogeneous melt. A polymer usually melts over a wide temperature range due to a distribution of crystal size and perfection, molecular weight, and sample history. Along these lines, Wunderlich has proposed that residual annealed high-molecular-weight crystals are likely to survive the observed bulk melting temperature and to self-nucleate [60]. The coined term, "self-nucleation" has been used to describe the nucleation of a polymer melt or solution by its own crystals grown previously [60,80]. Nucleation centers attributed to

annealed high-molecular-weight crystals have been observed for solution-crystallized polyethylene [74].

The effect of thermal history on crystallization have also been attributed to the persistence of small crystalline regions trapped in cavities of solid impurities, as suggested by Turnbull [81]. If the crystalline material wets the cavity walls, the crystals in the cracks melt at a higher temperature than the bulk, depending on the curvature and size of the cracks and interfacial tension. Upon cooling, when the bulk of the liquid will supercool, the persistent crystals contained in the impurity cracks will serve as nuclei for crystallization.

3.2 Experimental

3.2.1 Materials and Viscosity Measurement

Two PEEK reactor powders of different molecular weights and an amorphous PEEK film were obtained from Imperial Chemical Industries (ICI, Wilton, U.K.) and Westlake Plastics Company (Lenni, PA, U.S.A.) respectively. Melt and solution viscosities, average molecular weights, onset temperature of degradation and ash content of the samples are listed in Table 3.1. Number and weight average molecular weight and melt viscosity of the PEEK powder samples were provided by ICI. Ash content was measured by the University of Massachusetts Microanalysis Laboratory; sample weights were measured before and

Table 3.1. Viscosities, number and weight average molecular weights ($\bar{M}_n^-$ and $\bar{M}_w^-$ respectively), onset temperature of degradation and ash content of three PEEK samples.

Sample Code	Viscosity Melt[a] NSm^{-2}	Viscosity Solution[b] $dL\ g^{-1}$	$\bar{M}_n^-$ $g\ mole^{-1}$	$\bar{M}_w^-$[c] $g\ mole^{-1}$	Onset of Degradation[d] (°C)	Ash Content (%)
Powder I	380	0.94	14,100	38,600	570.3	0.4
Powder II	450	0.99	16,800	39,800	578.2	0.1
Film	--	0.70	---	---	554.1	0.4

a. at shear rate of 1000 sec^{-1} at 400°C, provided by ICI.
b. Reduced solution viscosity.
c. provided by ICI.
d. from weight loss curves.

after oxidation at 900°C under oxygen atmosphere for 3h. All the samples were vacuum-dried at 145°C overnight prior to use. PEEK powder was screened out using a mesh (#170) and the fine powder (< 80 μ) was used in this study. This allowed good thermal contact between the powder and the aluminum DSC sample pans. The reduced solution viscosities were measured at 25°C in 98% sulfuric acid at a concentration of 0.1 g/dL using an Ubbelohde type viscometer. Since dissolution and sulphonation of PEEK occur concurrently in sulphuric acid [82] the duration time before viscosity measurement was kept constant (15h).

3.2.2 Thermogravimetric Analysis

Thermo-gravimetric analysis has been conducted using a Perkin-Elmer TGS-2 under nitrogen atmosphere. Weight loss curves were obtained at a heating rate of 5°C/min and nitrogen flow rate of 50 cc/min. The temperature was calibrated with the Curie points of nickel, perkalloy and iron. The onset temperature of degradation is defined by the temperature where the tangent to the curve at its maximum negative slope intercepts the original zero-slope tangent.

3.2.3 Isothermal and Nonisothermal Crystallization

Crystallizations of PEEK with various thermal histories have been characterized with Perkin-Elmer differential scanning calorimeters (DSC-2 and 4). Isothermal crystallization experiments at 315 and 311°C were performed in a DSC after melting PEEK samples at various

temperatures (370-420°C), considerably higher than the commonly observed melting temperature (~335°C), for several time periods (10-240 min). Another set of samples was heated to various melt-annealing temperatures (370-420°C) and held for 30 min and then cooled at -10°C/min. The crystallization curves on cooling were recorded. Temperatures and heats of transition were calibrated with pure metal standards: indium, tin, lead, and zinc. Isothermal crystallization and melt temperatures were calibrated with extrapolated melting points of the standards to zero heating rate. All DSC experiments were conducted under dry nitrogen. DSC traces were normalized to 1 mg of sample as shown in the figures.

3.3 Results and Discussion

The crystallization behavior of two PEEK powders and one amorphous PEEK film has been studied using differential scanning calorimetry (DSC). Fig. 3.1 shows heating scans (80°C/min) of the three PEEK samples, as received. The first DSC trace of powder I (trace A) shows a melting peak (12.8 cal/g) at 340°C and a small cold-crystallization exotherm (-1.1 cal/g) at 174°C. In the second heating scan (trace A') of the same sample after cooling (-150°C/min) from 400°C, the peak temperature of the melting endotherm (10.4 cal/g) decreases to 334°C and the cold-crystallization exotherm disappears. This suggests that the PEEK reactor powder may have some special crystalline morphology

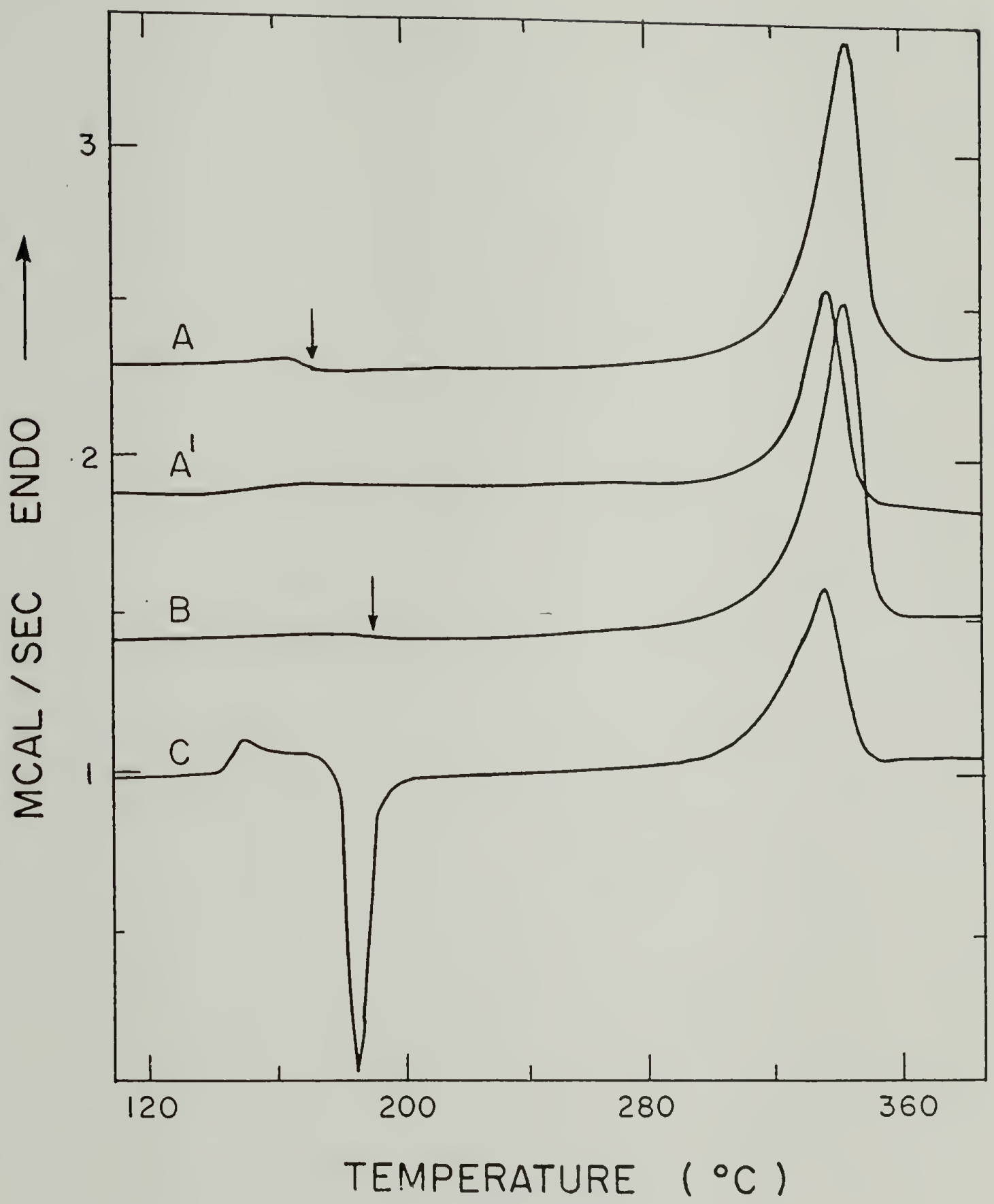

Figure 3.1. DSC traces of PEEK samples on heating (80°C/min): A, the first heating of powder I; A', the second heating of powder I; B, the first heating of powder II; C, the first heating of amorphous PEEK films. Two arrows indicate small cold-crystallization exotherms of powder I and II.

due to crystallization during polymerization [2,60]. Similarly, the first heating of powder II (trace B) shows a melting peak at 340°C and cold-crystallization peak (-0.8 cal/g) at 193°C. The first DSC trace of amorphous film (trace C) shows a melting peak at 333°C, several degrees lower than the reactor powders, and a cold-crystallization exotherm around 185°C.

3.3.1 Isothermal Crystallization

PEEK powder I was isothermally crystallized at 315°C in a DSC after melting for 10 min at various temperatures (370-410°C). Subsequent DSC traces are shown in Fig. 3.2. As the melt temperature was increased, the isothermal crystallization curves shifted to longer time and became broad. Also the peak of the curve (t_{peak}, peak crystallization time), the time when the maximum crystallization rate is observed, increased. It is notable that the crystallization curves after melting at 390 and 400°C are almost identical.

The Avrami equation has been widely used to analyze isothermal crystallizations [83,84].

$$X_c(t)/X_c(\infty) = 1 - \exp(-kt^n) \qquad (3.1)$$

$$\log[-\ln\{1-X_c(t)/X_c(\infty)\}] = n \log t + \log k \qquad (3.2)$$

where $X_c(t)$ and $X_c(\infty)$ are the degrees of crystallinity at time t and at the end of crystallization, respectively. The exponent, n, is

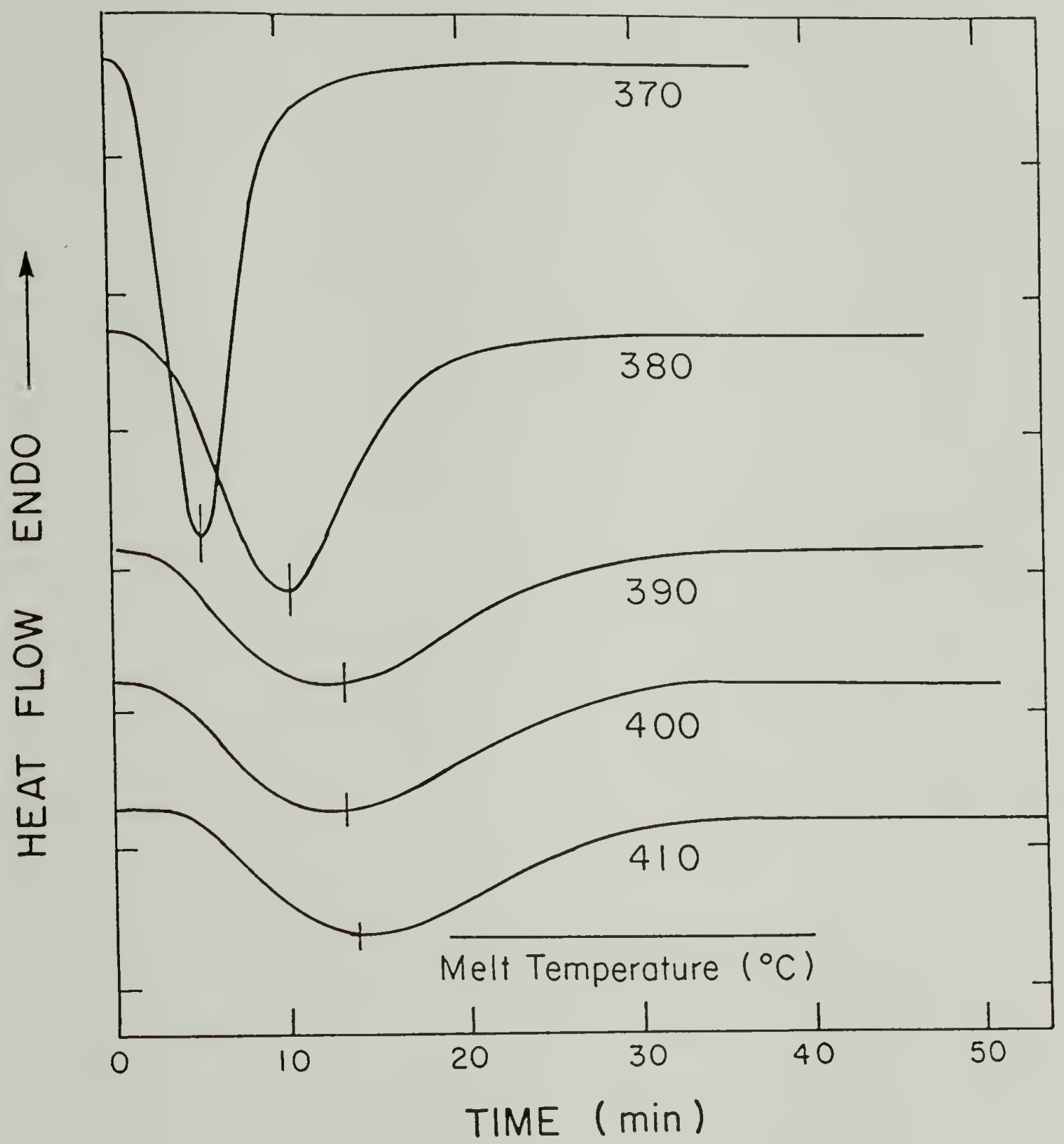

Figure 3.2. DSC isothermal crystallization curves of PEEK powder I at 315°C after melting at various temperatures (370-410°C) for 10 min. Peaks of the curves are indicated by short bars.

dependent on the type of nucleation and the crystal growth geometry; the parameter, k, is also a function of nucleation and growth.

The Avrami parameters n and k are determined from the slope and intercept, respectively, from a plot of $\log[-\ln\{1-X_c(t)/X_c(\infty)\}]$ vs. $\log(t)$, as shown in Fig. 3.3. Each curve shows an initial linear portion with subsequent leveling off at longer time. Such leveling off has been also found by Cebe and Hong for PEEK, and is thought to be due to secondary crystallization [47]. The linear portions are almost parallel, and shift to longer time with increasing prior melt temperature. It is notable that crystallization becomes independent of melt temperature for samples previously melted at or above 390°C. Comparable behavior, as has been found for many other polymers, will be discussed later. The Avrami parameters, n and k, determined from the initial linear portion in Fig. 3.3 and the peak crystallization time (t_{peak}) are listed in Table 3.2. As the melt temperature was increased, the exponent n and t_{peak} increased, but k decreased.

For spherulitic growth and athermal nucleation, i.e., all crystals start growing at the same time, the value of n is expected to be 3 [60]. In the case of thermal nucleation, i.e., nuclei are created sporadically in time and space, the exponent is expected to be 4. However, complications in the Avrami analysis often arise due to several assumptions, which do not necessarily apply to polymer crystallization, are involved in the derivation [60]. The Avrami exponent (n) showed an increase between 3 and 4 with increasing melt temperature, which may be at least partially, due to the fact that

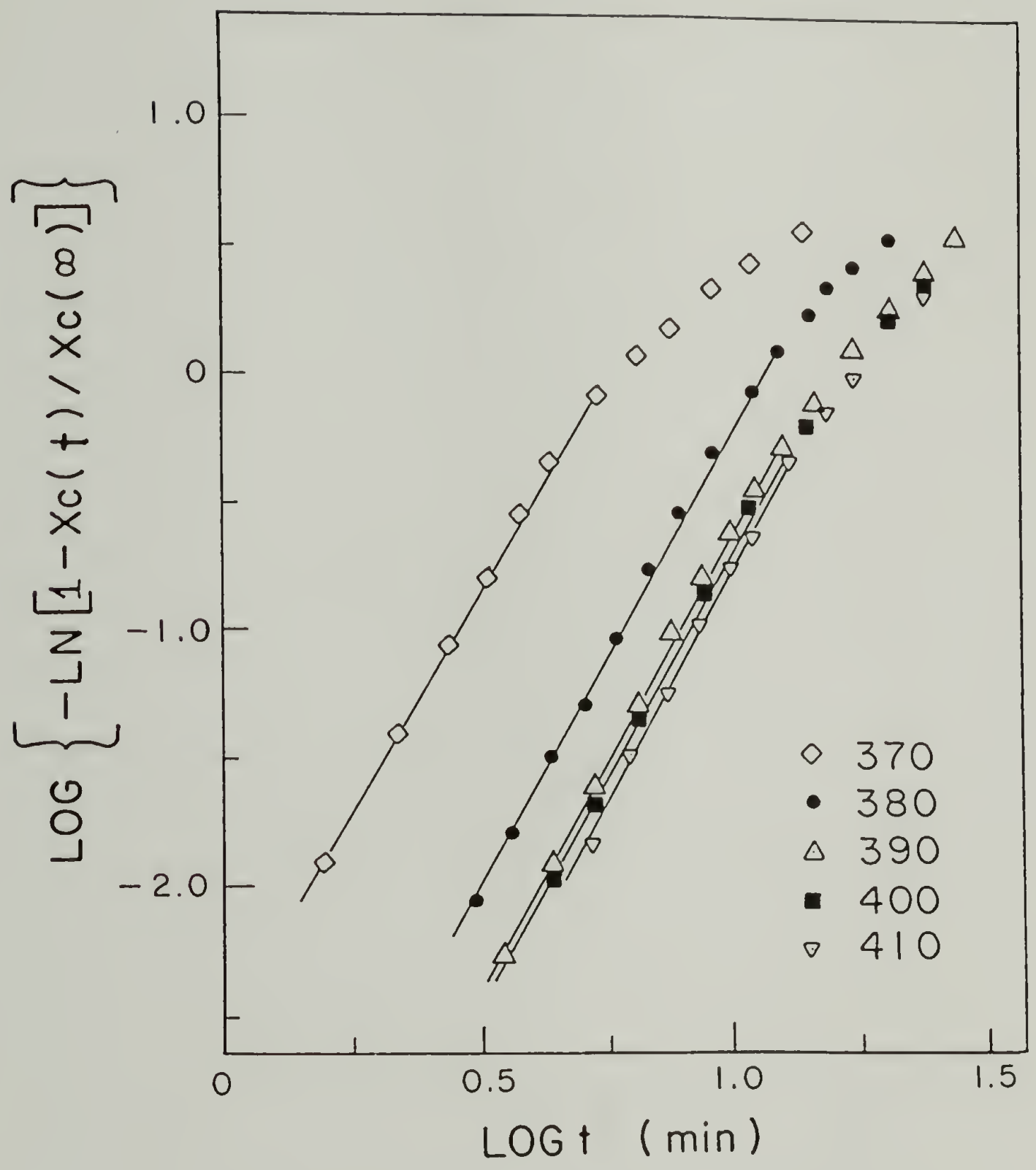

Figure 3.3. Plot of log[-ln{1-Xc(t)/Xc(∞)}] vs. log(time) for isothermal crystallization curves shown in Fig. 3.2.

Table 3.2. Avrami parameters (n and k) and peak crystallization time (t_{peak}) for isothermal crystallization at 315°C for powder I after melting at various temperatures (370-410°C) for 10 min.

Melt Temperature (°C)	n	k	t_{peak} (min)
370	3.4	2.6×10^{-3}	4.3
380	3.6	1.5×10^{-4}	10.3
390	3.6	6.7×10^{-5}	12.8
400	3.6	4.8×10^{-5}	12.9
410	3.8	2.9×10^{-5}	13.5

thermal or homogeneous nucleation becomes more predominant with increased melt temperature. Hartley, et al. found an increase in the exponent from 3 to 4 for poly(ethylene terephthalate) when the melt temperature was increased from 268 to 275 or 294°C [72]. They also found that k decreased with increasing melt temperature, which is in agreement with the data in Table 3.2. The changes in n and k for PET were attributed to thermodynamically stable, minute crystals surviving observed melting temperature [72]. It has been previously estimated by Cebe and Hong that n = 3.3, $k = 8.0 \times 10^{-5}$, and t_{peak} = 15.9 min at 315°C after melting PEEK film at 400°C for several minutes [47]. The authors believed that PEEK crystallized heterogeneously by simultaneous nucleation, possibly due to a nucleating agent. Ash (metal oxides) content of the three samples in this study have been measured to be about 0.1 - 0.4%, as shown in Table 4.1. The values for n in Table 3.2 are larger than those previously reported [47], probably because reactor powder, which has no deformation history, was studied here. Deformation of polymer chains can originate nucleation; strain-induced crystallization of PEEK has been reported [85].

The two explanations in the Introduction section are considered to account without conflict for many of the previous observations on the relation between thermal history and crystallization. The number of nuclei in various polymers have been measured as a function of melt temperature; the number of nuclei decreased with increasing prior melt temperature and eventually leveled off to a constant value (10^4 - 10^6 nuclei/g) [60,86]. The nuclei which disappeared upon melting were

attributed to self-nucleation, while those which did not disappear were attributed to the nucleation on foreign heterogeneities. The temperature at which self-nucleation disappears and reported thermodynamic melting points are compared in Table 3.3. The two temperatures are close for several polymers with one exception, polychlorotrifluoroethylene. The fact that these two temperatures are close may suggest that remnants of previous crystals survive the temperatures up to the thermodynamic melting point.

In Fig. 3.4, isothermal crystallization curves of PEEK powder I at 311°C after melt-annealing at 400°C for various times are shown. As the annealing time was increased, the crystallization curves shifted to longer time. This time dependency, little of which was observed for solution crystallization [73,74], can be explained by the high viscosity and chain entanglement in a polymer melt. It may take rather a long time even above the ordinary melting temperature, for the previous crystalline regions in the bulk or in the cracks of the foreign particles, to lose order and become a completely homogeneous melt. This is shown by the observation that as melt-annealing time at 390°C was increased, fewer PEEK spherulites developed at the initial stage upon cooling (Fig. 4.8). It was also found for carbon fiber reinforced PEEK that crystallization of PEEK depended on the melt-annealing time [77,78]. The heats of crystallization of the curves in Fig. 3.4 are similar (~9.5 cal/g). An Avrami analysis was not performed for these isothermal crystallizations at 311°C because heat

Table 3.3. Maximum temperatures for self-nucleation [60] and thermodynamic melting points of various polymers.

Polymer	Maximum temperature for self-nucleation (°C)	Thermodynamic melting point (°C)[a]
polystyrene	230[88]	235-250
poly(ethylene terephthalate)	290[72]	245-284, 290[59],340[8]
nylon 6	260[66]	214-250, 260[89],278[90]
polyethylene	138.5[86]	137-146
poly(ethylene oxide)	69, 100[86][b]	62-76
poly-1-butene form I	141[86]	126-142
poly-1-butene form II	130[86]	122-130
polychlorotrifluoroethylene	305[64]	210-222

a. from the Polymer Handbook [87], otherwise the reference is cited.
b. showed two critical temperatures.

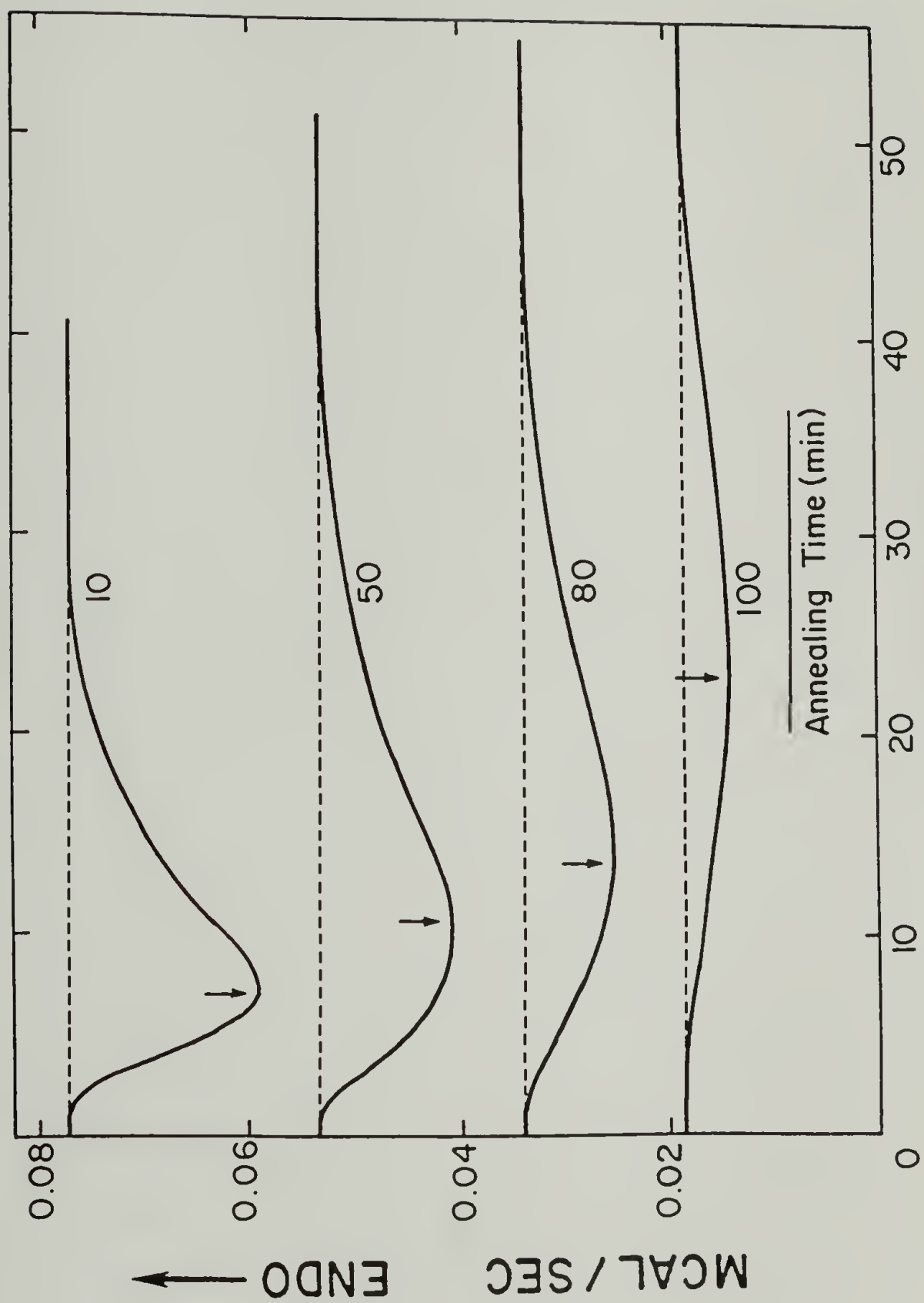

Figure 3.4. DSC isothermal crystallization curves of PEEK powder I at 311°C after melting at 400°C for various time. Peak crystallization times of the curves are indicated by arrows.

flow was often too small and it was difficult to locate the point where crystallization began.

A similar study on nylon 6 has previously been reported [91]. Isothermal crystallization curves were found to shift to longer time as either melt-annealing time or temperature was increased. Induction periods, i.e., the times before appreciable crystallization, increased with melt-annealing time and temperature. The authors found an abrupt increase in the induction periods at 280°C, which is close to the thermodynamic melting point of nylon 6, 278°C [90]. This was explained by a hypothesis that all residual crystals or ordered regions disappear at the thermodynamic melting point.

In this study on PEEK, it was found that the induction time was technically difficult to determine due to an instrumental electrical overshooting signal, which persists for as long as two minutes. Therefore, the peak of the crystallization curves have been used in Fig. 3.5. The peak crystallization time increased with increases in either melt-annealing temperature or time. At 370 or 380°C, the peak time increased slowly with melt-annealing time. However, a rapid increase in peak crystallization time is observed for melt temperatures at or above 400°C. This rapid increase cannot be explained fully by crystalline regions trapped in cavities of solid impurities. It may be due to the disappearance of the remnants of former crystals or ordered regions. Indeed, local order associated with the diphenyl ether moiety has been observed by Fourier Transform infrared spectroscopy (FTIR) for PEEK melted at 380°C, but not for

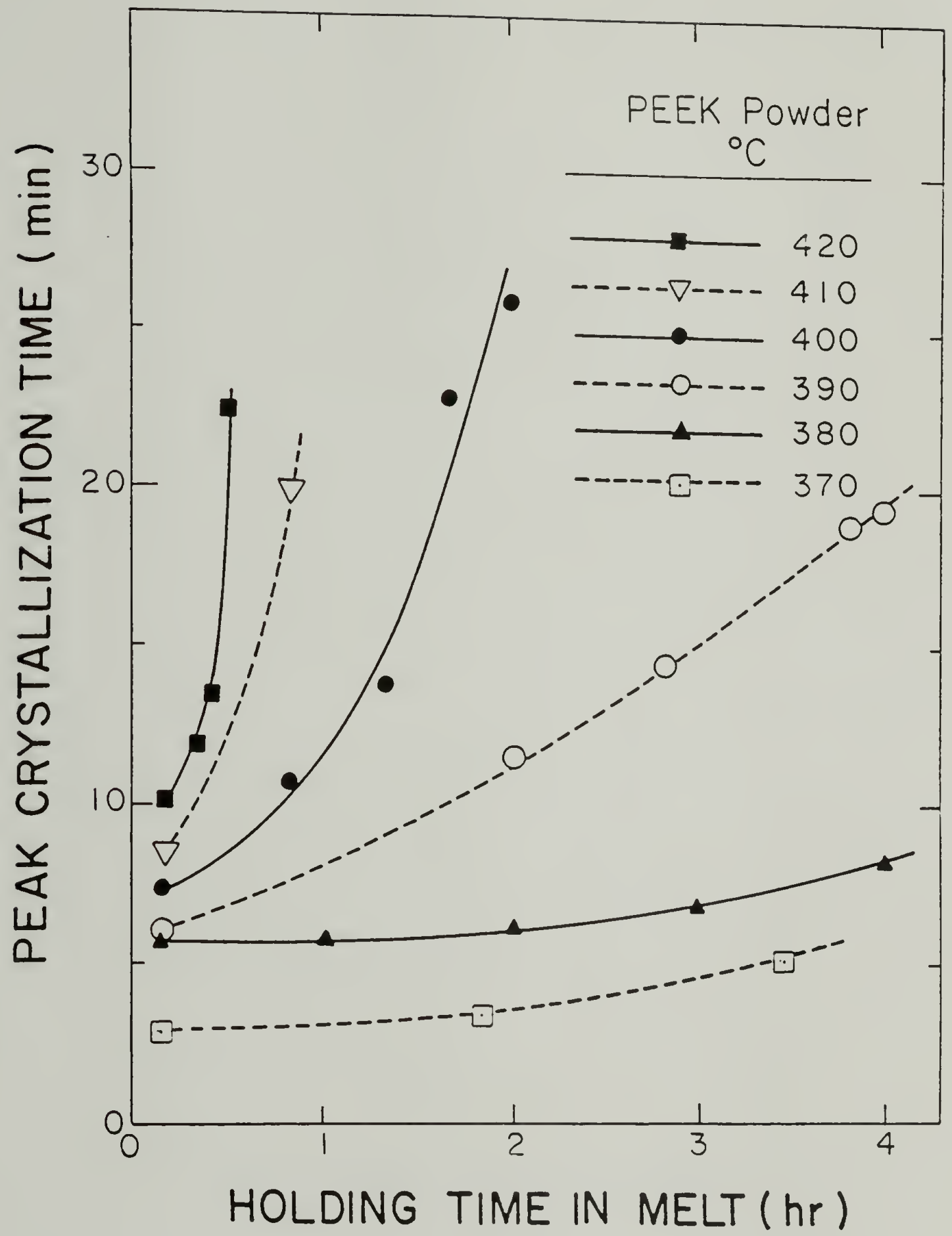

Figure 3.5. Peak crystallization times of the isothermal crystallization of powder I at 311°C after melting at various temperature (370-420°C) for various time.

PEEK melted at 400°C [32]. The authors suggested that the local order persisted up to the thermodynamic melting point of PEEK.

Fig. 3.6 shows the same plot as Fig. 3.5 for an amorphous PEEK film of lower molecular weight. A behavior similar to powder I is observed: peak crystallization time increases rapidly with time when the prior melt temperature is at or above 400°C. Therefore, the rapid increase in peak crystallization time appears to be an inherent property of PEEK. The PEEK film was found to have a little anisotropy in birefringence due to processing. Orientation of polymer molecules often creates many nuclei [85,92]. This fast nucleation and subsequent fast crystallization may explain the difference in the peak crystallization time of the film and that of powder I.

3.3.2 Nonisothermal Crystallization

PEEK powder I was cooled in a DSC after being held in the melt for 30 min at various temperatures (370-420°C). The DSC traces are shown in Fig. 3.7. As melt-annealing temperature was increased, the crystallization exotherm shifted to lower temperatures and became broader. The temperature at which the crystallization exotherm began was taken as the "onset temperature" where the supercooling is large enough for PEEK to crystallize. The onset and peak temperatures of the crystallization curves are indicated in Fig. 3.7 by short bars. As the melt-annealing temperature was increased, both the onset and peak temperatures decreased. This behavior was also observed for

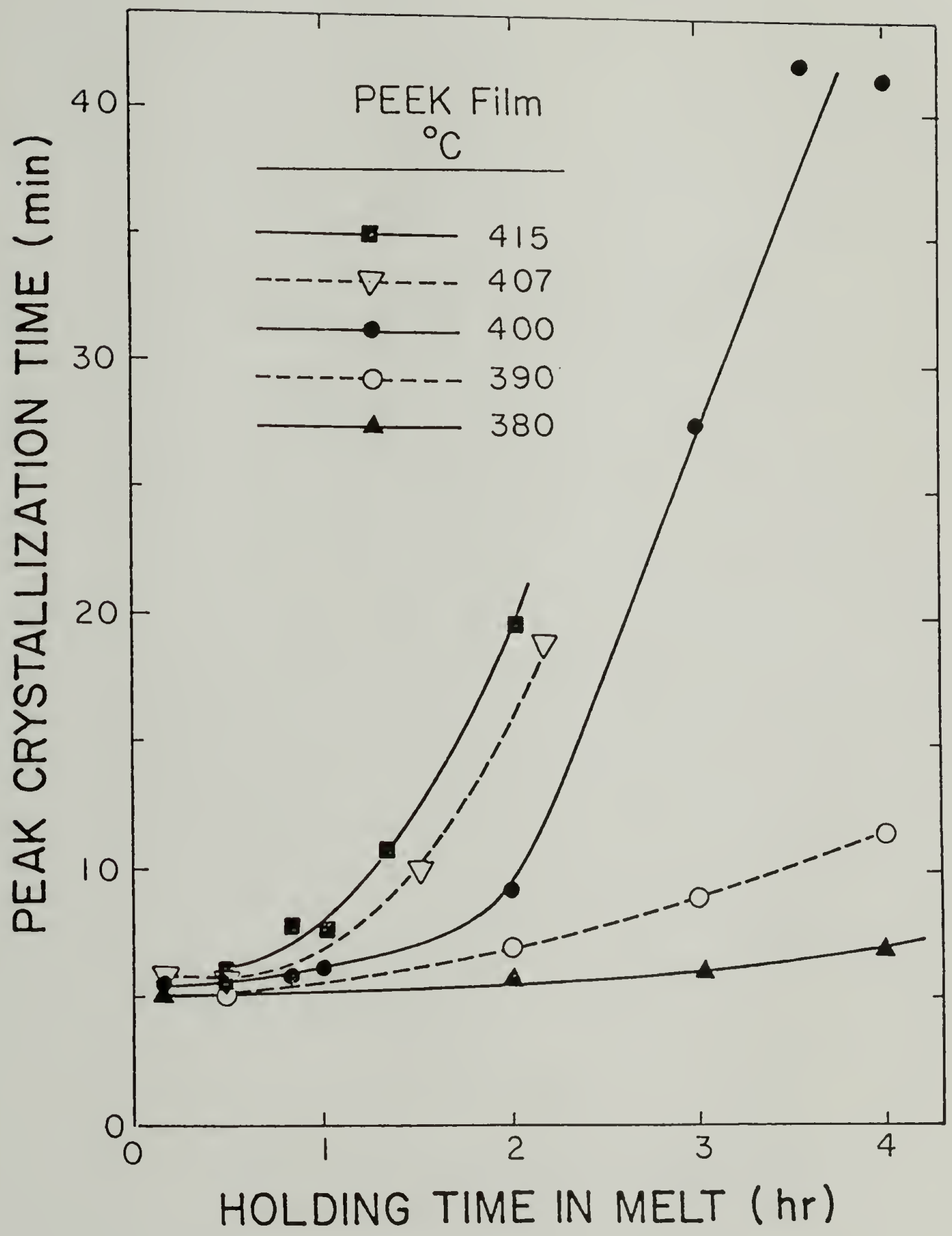

Figure 3.6. Peak crystallization times of the isothermal crystallization of films at 311°C after melting at various temperature (380-420°C) for various time.

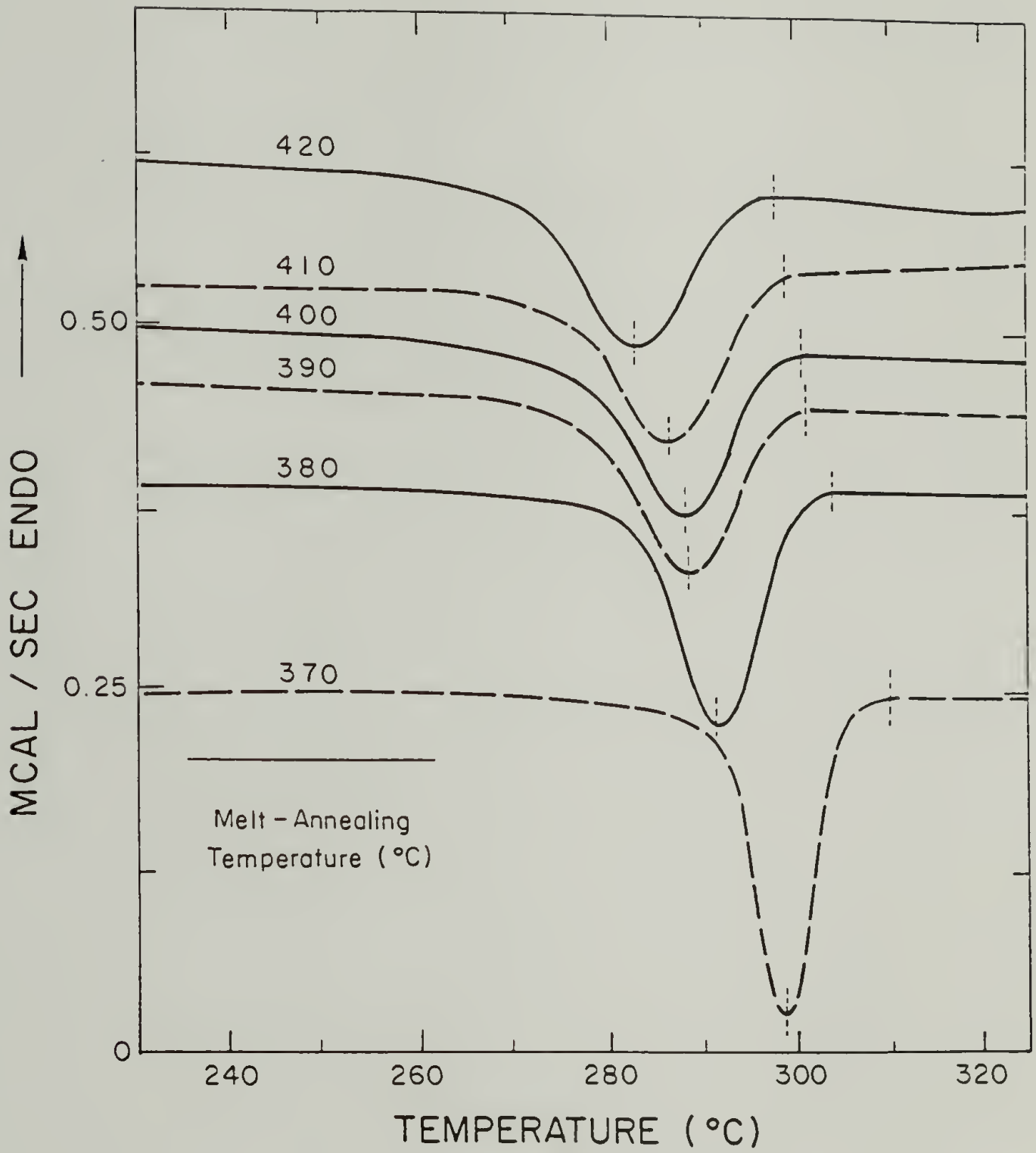

Figure 3.7. DSC cooling curves (-10°C/min) for powder I after melting at various temperatures (370-420°C) for 30 min.

another PEEK powder sample (powder II) and the mixture of powder I and II (20 wt % of powder II).

The onset and peak temperatures of the crystallization exotherms for three powder samples are listed in Table 3.4, and plotted as a function of prior melt temperature in Fig. 3.8. Both the onset and peak temperatures decreased with increasing melt temperature. When two melt-annealings were performed on a sample at different temperatures, the crystallization behavior was more dependent on the higher melt-annealing temperature. The irreversible dependence on melt-annealing temperature and time has been shown for poly(ethylene terephthalate) [71], and nylon 6 [93]. Both the onset and peak temperatures leveled off around 390°C, suggesting that the number of nuclei decreased to a constant number on approaching 390°C. This result, as well as the isothermal crystallization data (Fig. 3.3, 3.5, 3.6), indicates that the maximum self-nucleation temperature of PEEK is about 390°C which is close to the thermodynamic melting point, 384 and 389°C (Chapter II), and 395°C [8].

Powder II, which has a higher molecular weight than powder I, crystallized at lower temperatures when the melt temperature was below 375°C. Usually, polymers of higher molecular weight show slower crystallization rate due to higher viscosity [94]. However, powder II crystallized at higher temperatures when melt temperature was above 375°C. The onset and peak temperatures of powder II are less sensitive to melt temperature than powder I. The mixture of powder I (80%) and powder II (20%) (Fig. 3.8) shows the onset and peak

Table 3.4. Onset (T_{onset}) and peak temperatures (T_{peak}) and heats of crystallization (ΔH_c) on cooling (-10°C/min) of PEEK after melt-annealing for 30 min at the temperatures indicated. Heats of fusion(ΔH_f) and peak temperatures(T_m) of melting endotherms (20°C/min) for Powder I crystallized on cooling.

Melt-emp. (°C)	Powder I T_{onset} (°C)	Powder I T_{peak} (°C)	Powder I ΔH_c (cal/g)	Powder I ΔH_f (cal/g)	Powder I T_m (°C)	Powder II T_{onset} (°C)	Powder II T_{peak} (°C)	Mixture I & II[a] T_{onset} (°C)	Mixture I & II[a] T_{peak} (°C)
370	309.8	298.8	10.5	10.4	339.7	308.1	296.0	308.1	297.4
375	306.3	294.9	10.6	--	--	--	--	--	--
380	303.8	291.3	9.9	9.8	338.5	305.6	292.5	304.1	292.2
385	302.2	289.7	10.1	--	--	--	--	--	--
390	301.3	288.9	9.5	9.5	337.9	305.0	291.6	303.0	291.0
395	301.6	289.5	9.6	--	--	--	--	--	--
400	300.9	288.4	9.7	9.6	337.6	304.6	292.3	302.7	289.7
405	300.5	287.5	9.6	--	--	--	--	--	--
410	299.0	286.6	9.5	9.5	337.2	304.4	291.3	302.2	289.7
420	297.9	282.8	9.4	9.4	336.7	303.8	291.3	301.1	288.5

a. 80 wt % powder I and 20 wt % powder II were mixed.

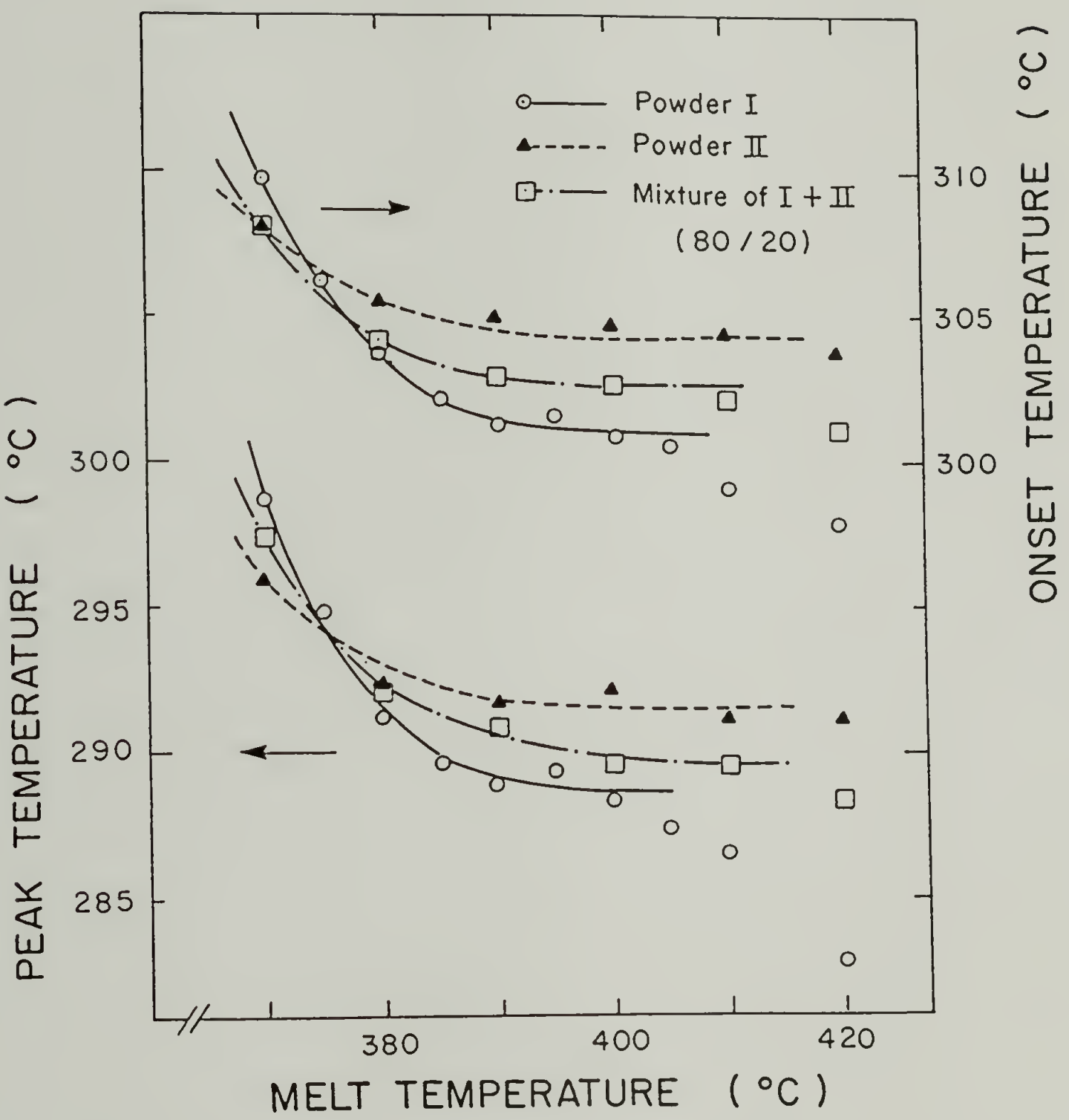

Figure 3.8. Onset and peak temperatures of DSC cooling curves for powder I and II and their mixture after melting at various temperatures (370-420°C) for 30 min.

temperatures in the middle of the two original powder samples. Since the powder particle size was less than 80 μ, powder mixing was expected to be sufficient enough to show the effects of molecular weight. Indeed, the mixture of powders became one piece of film in the aluminum sample pan after melting and crystallization. Considering the smaller portion of powder II in the mixture and the limited mixing, the crystallization of the mixture was more dependent on higher molecular weight fraction.

Table 3.4 again shows the heats of crystallization of powder I obtained on cooling. As the melt-annealing temperature was increased to 390°C, the heat of crystallization slightly decreased. When melt-annealing temperatures were 390-420°C, almost the same value of heat of crystallization was observed. This suggests that no considerable thermal reactions of PEEK molecules occurred during melt-annealing. The samples crystallized on cooling were heat-scanned at 20°C/min. As shown in Table 3.4, the heat of fusion is almost identical to the heat of crystallization on cooling. The peak temperatures of the melting endotherms decreased gradually with increased melt-annealing temperature, due to the difference in crystallization temperatures on cooling (Fig. 3.7).

The thermal stability of the polymer at the melt temperatures was also asessed. Degradation, chain-branching, and crosslinking are suspected to occur in PEEK at high melt temperatures. However, the crystallization of PEEK was found to be unaffected by exposure to 375°C for 4h under nitrogen atmosphere [95]. The heat of

crystallization after melt-annealing shown in Table 3.4 confirms this observation. Results of thermo-gravimetric analysis of PEEK under nitrogen atmosphere are shown in Fig. 3.9. The onset temperatures for weight loss of three PEEK samples are well above the melt-annealing temperatures used in this study, as listed in Table 3.1. These data are in agreement with a recent study on the thermal stability of PEEK [96], where it was found that phenol and benzoquinone were the major decomposition products. PEEK with higher molecular weight shows higher thermal stability as shown in Fig. 3.9. Little change in degradation curves was found for powder I melt-annealed at 430°C up to 2.8h.

It has been reported that the viscosity of PEEK measured in air increased with dwell time at 350-380°C, suggesting that crosslinking has occured [30]. PEEK powder I melt-annealed at 400°C up to 2.5 h under nitrogen atmosphere showed almost the same reduced viscosity (0.94 dL/g) as the original powder, within experimental error. However, PEEK powder I melt-annealed at 400°C for 4h showed an increase in reduced viscosity (to 1.3 dL/g) and ~2 % of the sample could not be dissoved in sulfuric acid, indicating that crosslinking had occurred. Crosslinking probably begins in an early stage of a melt-annealing, and may deter crystallization.

The decrease in the onset and peak temperatures of powder I after the melt-annealing above 400°C (Fig. 3.8) is not considered as a result of thermal reaction since powder II and the mixture (80 % of powder I) do not show the same behavior. As shown Table 3.4 and

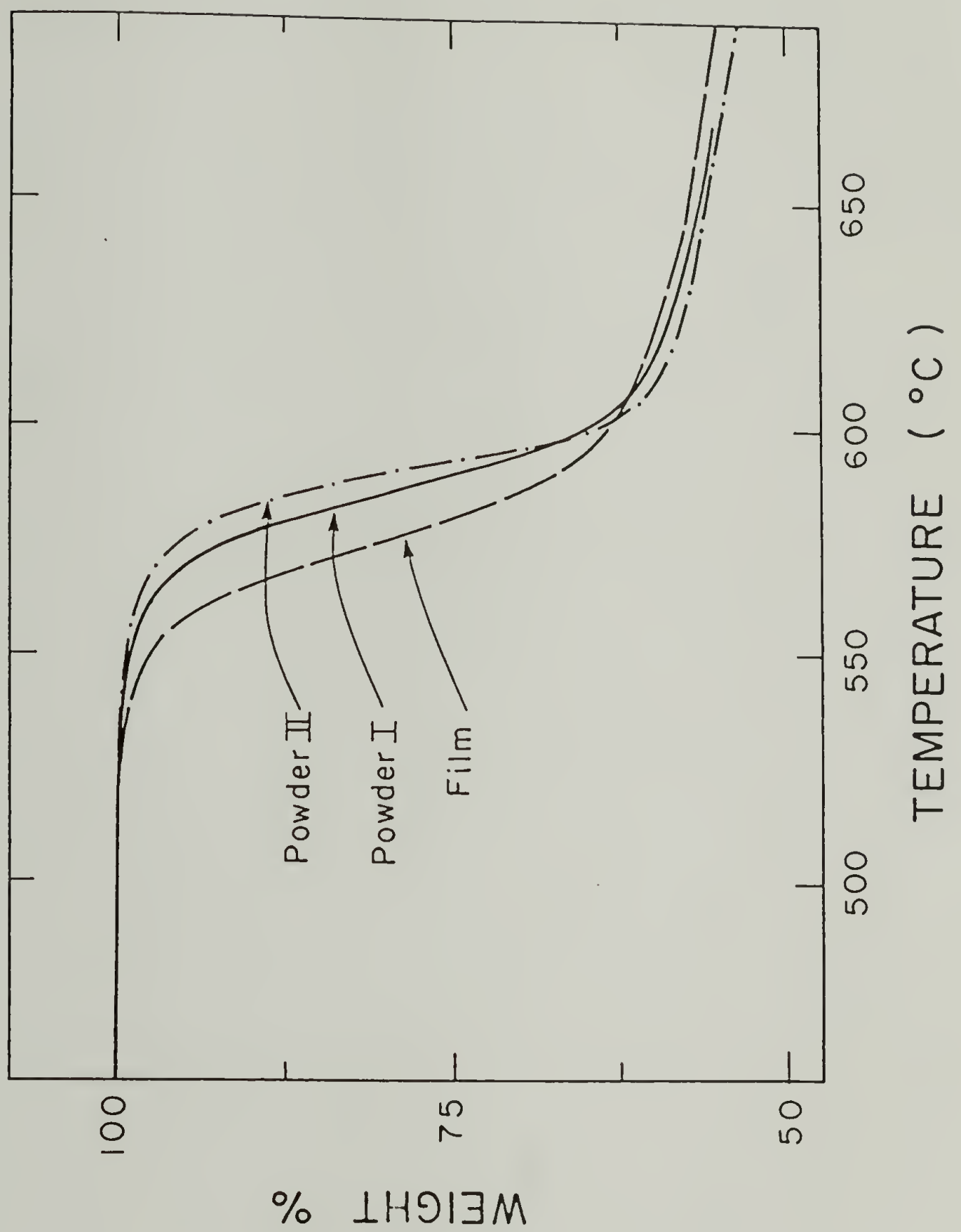

Figure 3.9. Weight loss curves for PEEK under nitrogen atmosphere. Heating rate was 5°C/min.

Fig. 3.4, the heats of crystallization do not change with melt-annealing temperature and time. This indicates minimal thermal reactions during the melt-annealings. Reactions such as decomposition, chain-branching and crosslinking may indeed occur in PEEK but too little an extent to influence the results.

3.4 Conclusions

Isothermal and nonisothermal crystallizations of PEEK samples with three different average molecular weights have been charaterized as a function of thermal history in the melt. As melt temperature was increased, isothermal crystallization exotherms shifted to longer time and crystallization curves on cooling shifted to lower temperatures. Crystallization on cooling for higher molecular weight samples was less sensitive to melt temperature. This is explained by the existence of remnants of former crystals and small crystalline regions trapped in cavities of solid impurities. Both kinds of crystalline regions can persist above the observed melting temperature and can self-nucleate if they have not been melted by the highest temperature.

As the holding time in the melt was increased, isothermal crystallization curves shifted to longer time. This is considered to be as a result of the high viscosity and chain entanglements in the melt. When PEEK was melted above 390^{o}C, the isothermal

crystallization curves showed a rapid increase in peak crystallization time with melt-annealing time. When the melt temperature was 390°C or above, the isothermal and nonisothermal crystallization behavior of PEEK has been found to be nearly independent of melt temperature. Since the thermodynamic melting point of PEEK has been estimated to be in the vicinity of 390°C (384, 389, 395°C), these different crystallization behaviors below and above 390°C are considered to support the hypothesis that the remnants of former crystals persist up to the thermodynamic melting point. Several other semi-crystalline polymers have also been found to support the hypothesis.

C H A P T E R IV

CRYSTALLIZATION OF POLY(ETHER ETHER KETONE) IN CARBON FIBER COMPOSITES

4.1 Introduction

The fiber-matrix interface plays an important role in the mechanical properties of fiber-reinforced composites. Since the stress acting on the matrix is transmitted to the fiber across the interface, an evaluation of interface structure and properties is essential for an understanding of composite properties. An early study of the interface in thermoplastic composites was published by Kardos et al. [97,98]. According to them, the mechanical properties of carbon fiber reinforced polycarbonate were improved by annealing. This was explained as due to the generation of a polycarbonate crystalline innerlayer at the fiber interface. Since the modulus of the crystalline structure is between that of the amorphous matrix and reinforcement, the crystalline interface may be a favorable medium for stress transfer. Another example of the improvement of mechanical strength using glass fibers coated with nucleating agents has been shown by Hobbs [99].

The nucleation on the carbon fiber surface has been reported for many polymers including nylon 6 [100], nylon 6,6 [101], polyethylene [102], and polypropylene [103]. Recently, poly(ether ether ketone) has been reported to crystallize on carbon fibers [104]. However, studies of interfacial structure and its effects on mechanical properties have been limited.

As discussed in Chapter III, the number of surviving nuclei in melt has been found to depend on the temperature at which the polymer was held before cooling and the time spent at that melt temperature [60]. This may be a general behavior of semicrystalline polymers [67,79,105]. A cyclic differential scanning calorimetry (DSC) experiment, much as applied to this study, has shown that the repeated melting of the same sample of nylon 6 results in a decrease of nuclei [93].

The longitudinal tensile strength (parallel to the fiber direction) of a composite is determined predominantly by the fiber strength. Conversely, the transverse tensile strength (perpendicular to the fiber direction) depends primarily on the interfacial strength between fiber and matrix [106]. Therefore the transverse tensile test has been chosen for study of the adhesion between carbon fibers and PEEK.

4.2 Experimental

4.2.1 Materials and Sample Preparation

The matrix polymer, PEEK (M_n = 14,100, M_w = 38,600) was obtained from Imperial Chemical Industry (ICI). The carbon fiber, Thornel 300 (No Finish) was obtained from Union Carbide. It was used without further treatments. PEEK powder was predried at 150°C in vacuo overnight before use. PEEK containing unidirectional carbon fibers was prepared in a hot press with a vacuum facility. Carbon fiber tows gripped at both ends were interleaved with previously-pressed amorphous PEEK films and compression molded at 390°C and 2 MPa, for 30 min in vacuo. Before compression molding two classes of samples (the SF and SS) were preheated for 30 min and two other classes (the LF and LS) were preheated for 100 min at 390°C. The compressed films were then cooled to room temperature in the press at fast (the SF and LF) or slow (the SS and LS) cooling. The preparation of four classes of samples are summarized in Table 4.1. The thickness of all composite films was about 0.22 mm.

Rectangular strips (3 x 50 mm) of the 4 classes of samples were trimmed with a paper cutter and tensile tested using an Instron Universal Testing Machine. After the DSC experiments and tensile tests, the carbon fiber content of samples was measured by dissolving out the PEEK with concentrated sulfuric acid followed by neutralization, and the washing and drying of the fibers.

Table 4.1. Compression molding condition of PEEK and PEEK with carbon fibers.

Sample[a] Code	Preheating Time[b] (min)	Cooling Rate (°C/min)
SF	30	-7
SS	30	-0.6
LF	100	-7
LS	100	-0.6

a. The first letter of sample code stands for preheating time: S(short) for 30 min and L(long) for 100 min. The second letter stands for cooling rate: F(fast) at -7 °C/min and S(slow) at -0.6°C/min.

b. At 390°C without pressure followed by compression molded at 390°C and 2 MPa for 30 min.

4.2.2 Thermal Analysis

The following DSC experiments were performed using a Perkin-Elmer DSC-2 with Thermal Analysis Data System. The LS samples of various content of carbon fiber were heated to 396°C at 10°C/min and immediately scanned on cooling. On cooling at -20°C/min exothermic crystallization curves were recorded.

The cyclic DSC experiment reported by Avramova et al. [93] has been used to measure nucleation density. Samples were heated to 395.9°C at 10°C/min, and immediately cooled rapidly to 306°C and held there for 7 min to follow PEEK crystallization. The samples were heated again to the same melt temperature and held for 20 min for the second cycle. The sample was again cooled rapidly to the same crystallization temperature, where it was again held for 7 min. For each cycle, all variables were held constant except for the melt-annealing times, which were sequentially 0, 20, 20, 50 and 20 min. The schematic diagram of this cyclic experiment is shown in Fig. 4.1. The melt annealing temperature was chosen in the range of the suggested PEEK processing temperature, 371-399°C [7]. To check that no crystallization occurred during the cooling to the crystallization temperature, the sample cooled to 306°C was immediately heat-scanned and no endotherm was observed. For each cycle, isothermal crystallization curves after the times indicated and melting peaks found on the heat-scan (10°C/min) were recorded.

CYCLE OF MELT ANNEALING -- CRYSTALLIZATION -- MELTING

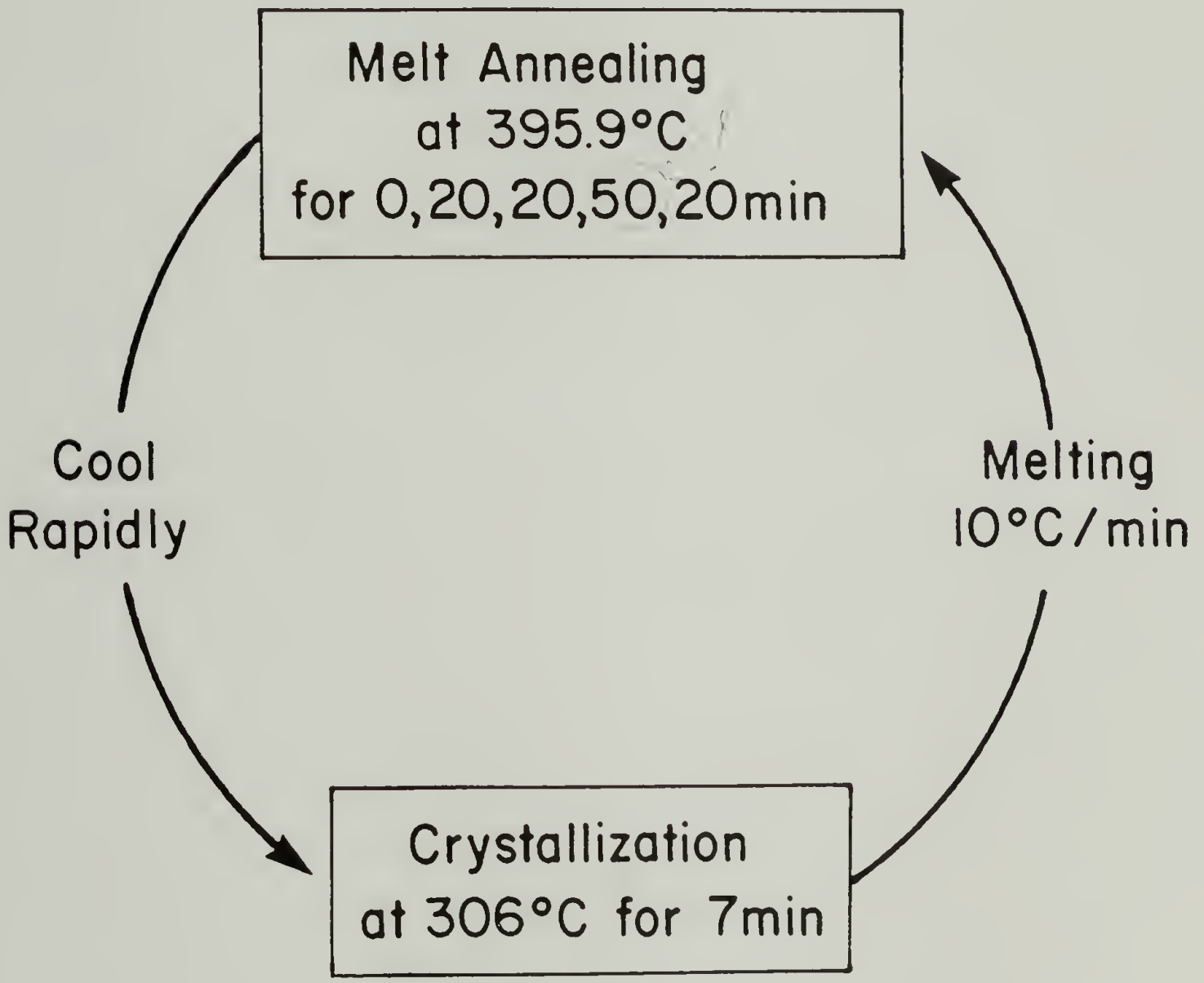

Figure 4.1. A schematic diagram of cyclic DSC experiment.

4.2.3 Optical and Electron Microscopy

PEEK films (about 20 μ thick) containing several carbon fibers were pressed (2 MPa) between microscope cover glasses for 10 min between hot plates (390°C) and in vacuo followed by rapid cooling. The samples were held at 390°C in a small furnace under nitrogen atmosphere and cooled at - 0.5°C/ min. On reaching 270°C the samples were quenched to room temperature to observe the prior morphology. Transcrystallinity on the carbon fiber surface as well as spherulites in the matrix was observed using a Leitz optical microscope with cross-polarlizers.

The tensile fracture surfaces were examined in an ETEC Auto-scan Scanning Microscope (SEM) after coating with about 200 Å thick gold layer in a Polaron E5100 SEM sputtering unit. A JEOL 100 KV transmission electron microscope was used to observe the interfacial morphology. About 500 Å thick PEEK with a single carbon fiber was cut using a diamond knife at room temperature and picked up on a cupper grid. Selected area electron diffraction (SAED) was used to investigate crystal orientation of PEEK at the interface. The diameter of SAED aperture #3 was measured to be 5.3 μ.

4.3 Results and Discussion

4.3.1 Thermal Analysis

The effect of carbon fiber on the crystallization of PEEK has been studied by differential scanning calorimetry (DSC). The curves of crystallization obtained during cooling are shown in Fig. 4.2. As the carbon fiber content was increased, the crystallization of PEEK began at lower supercooling, indicating that fibers acted as a nucleating agent.

The isothermal crystallization curves at 306°C for the neat PEEK-SF and for carbon fiber reinforced PEEK-SF are shown in Fig. 4.3 and 4.4, respectively. The minima of curves for both samples are shifted to longer time with increasing cycles. Both features suggest less bulk nucleation for longer melt-annealing times. The shift for unreinforced PEEK is more sensitive to the prior thermal history than carbon fiber reinforced PEEK. The dependency of PEEK crystallization on the holding time in melt has been reported [77]. Three crystallization curves, each following 20 min of melt-annealing, are shown in Fig. 4.3 and 4.4. The minima of the curves are shifted to longer time with increasing cycles. This further indicates that crystallization of PEEK depends not only on the previous melt-annealing time but also shows a cumulative dependency on all prior melt-annealing times.

The samples which had crystallized for 7 min were heated from the crystallization temperature to melt-annealing temperature as shown in

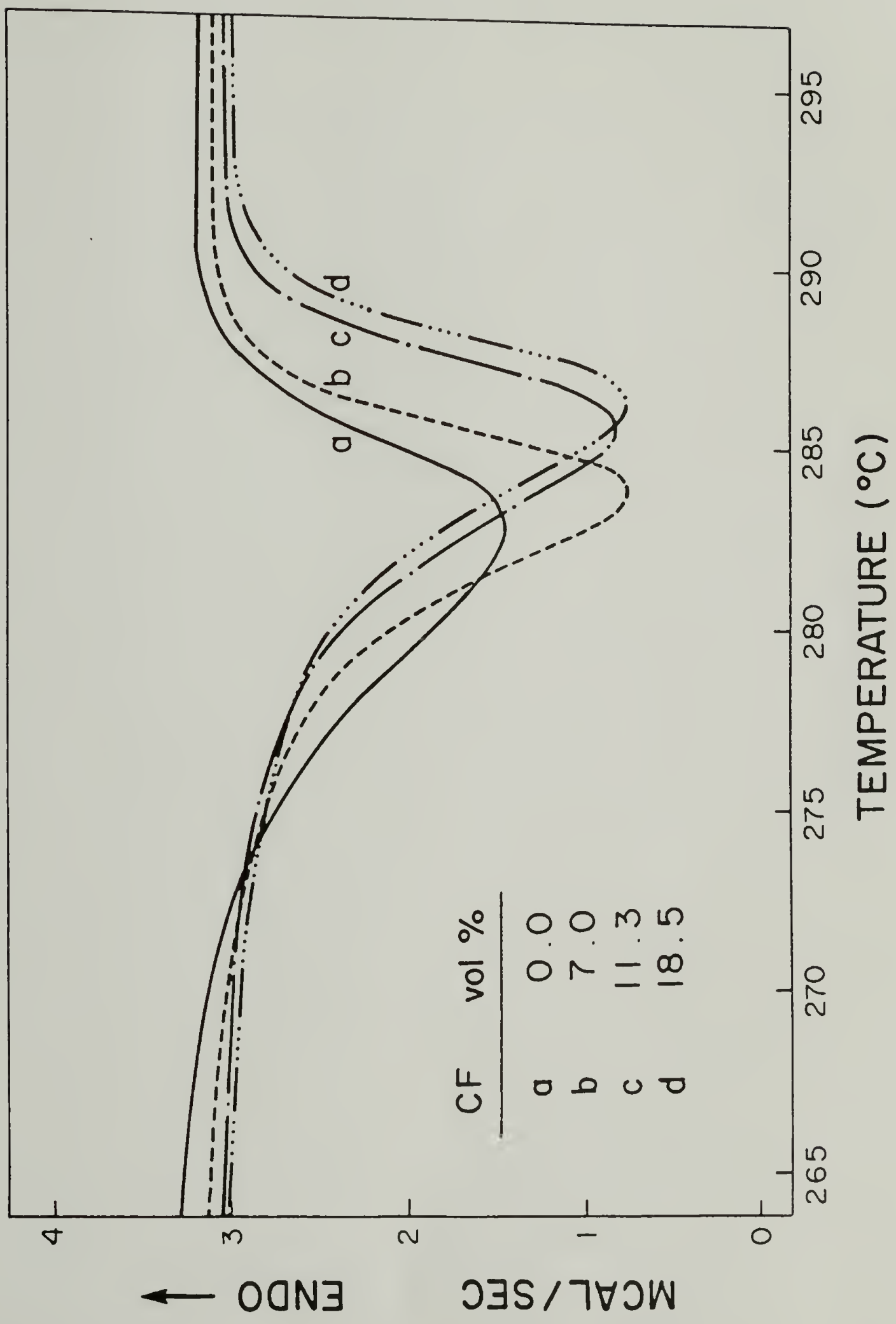

Figure 4.2. DSC crystallization curves on cooling (-20°C/min) from melt at 396°C.

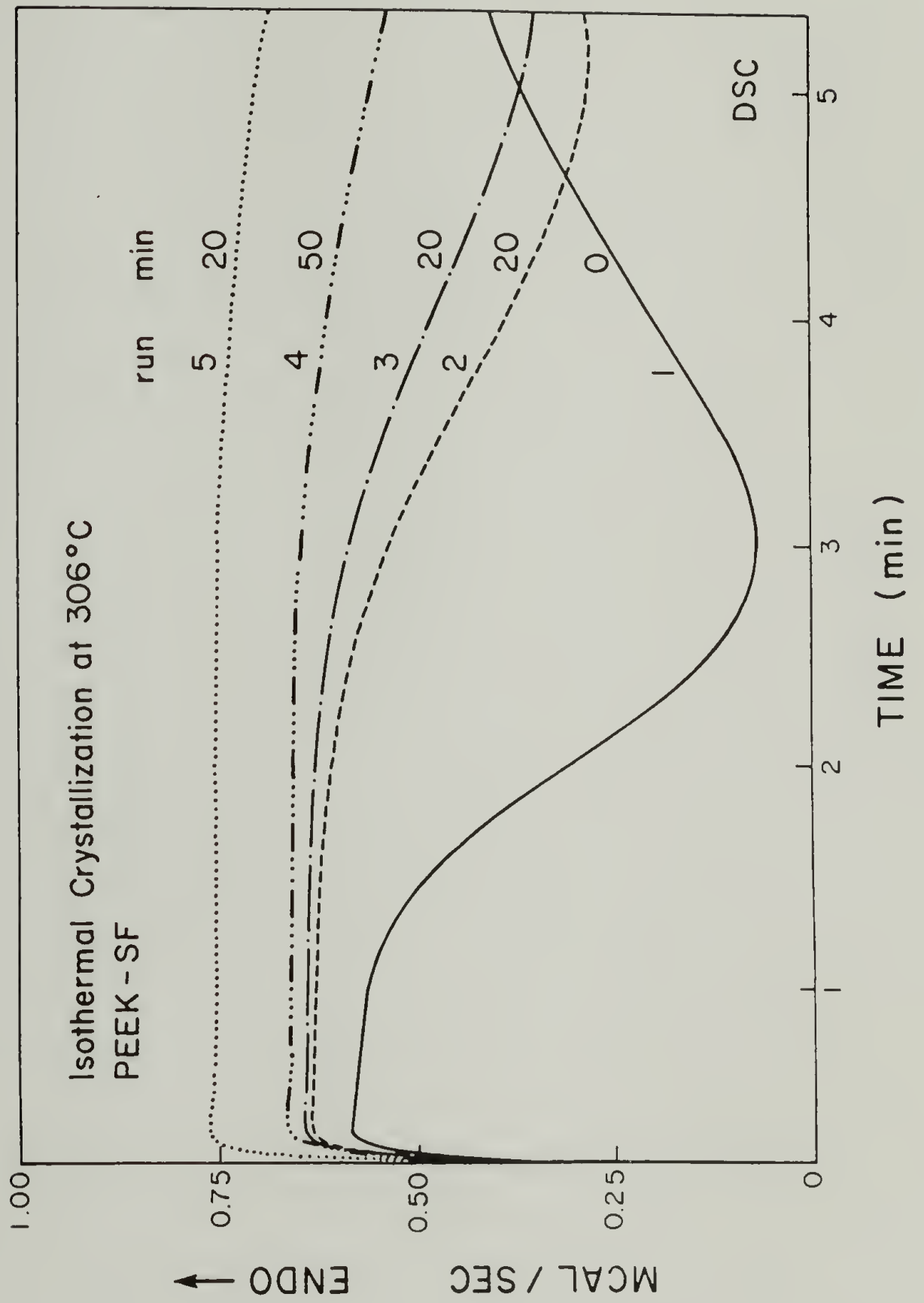

Figure 4.3. Isothermal crystallization of PEEK-SF at 306°C. Melt-annealing times in min at 395.9°C.

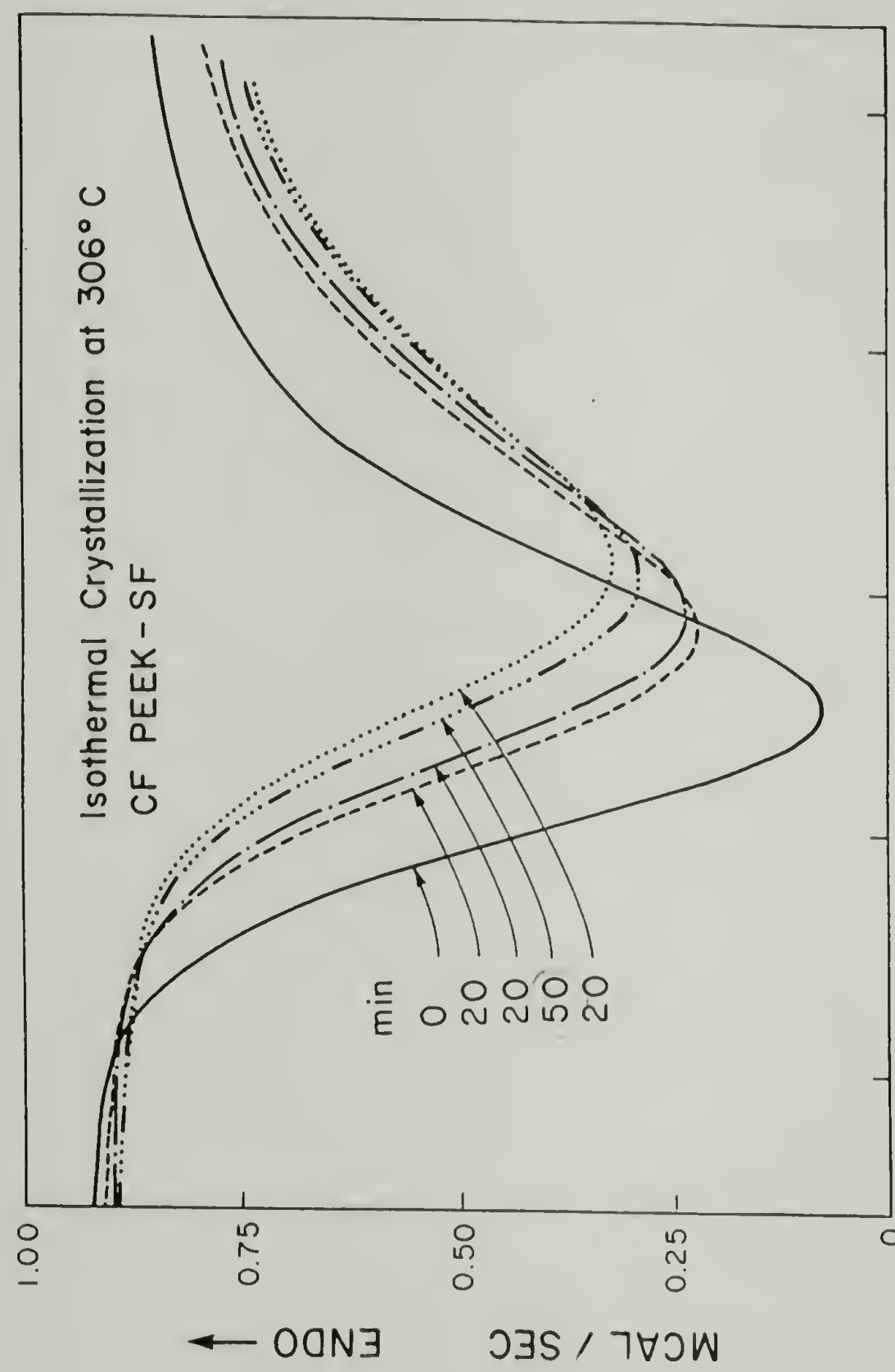

Figure 4.4. Isothermal crystallization of 15.1 vol. % carbon fiber reinforced PEEK-SF at 306°C. Melt-annealing times in min at 395.9°C.

Fig. 4.5 and 4.6. Significant difference in melting peak temperature for PEEK with and without carbon fiber was not observed. From the heat scans, the areas under melting endotherms were measured. The peak areas were converted to % crystallinity using heat of fusion given for fully crystalline PEEK, 31.1 cal/g [8] and plotted in Fig. 4.7. Without melt-annealing, the samples reach about 25% crystallinity during 7 min crystallization. The crystallinity decreased with increased holding time. The crystallization of PEEK thus shows the cumulative effect of all prior melt-annealing, as also reported for nylon 6 [93].

After the final cycle, the samples were found on cooling, to have a crystallinity similar to that of the virgin sample (31.8 and 33.4%, respectively). This suggests that no appreciable crosslinking nor degradation occurred during experimented melt-annealing. It has been reported that PEEK is thermally stable at 400°C for greater than 1h [7]. Thermal degradation has been found by thermo-gravimetric anlysis to begin at about 550°C as shown in Fig 3.9. The limited solubility of PEEK in organic solvents and sulfonation reaction that occurs in concentrated sulfuric acid make it difficult to measure the molecular weight of PEEK.

There have been explanations for effects of thermal history on crystallization as discussed in Section 3.1.1. The exact origins of nucleation sites remain uncertain for the present. The number of ordered regions decreases over long holding time at melt temperature. Relatively ordered regions in a polymer melt may act as nucleating

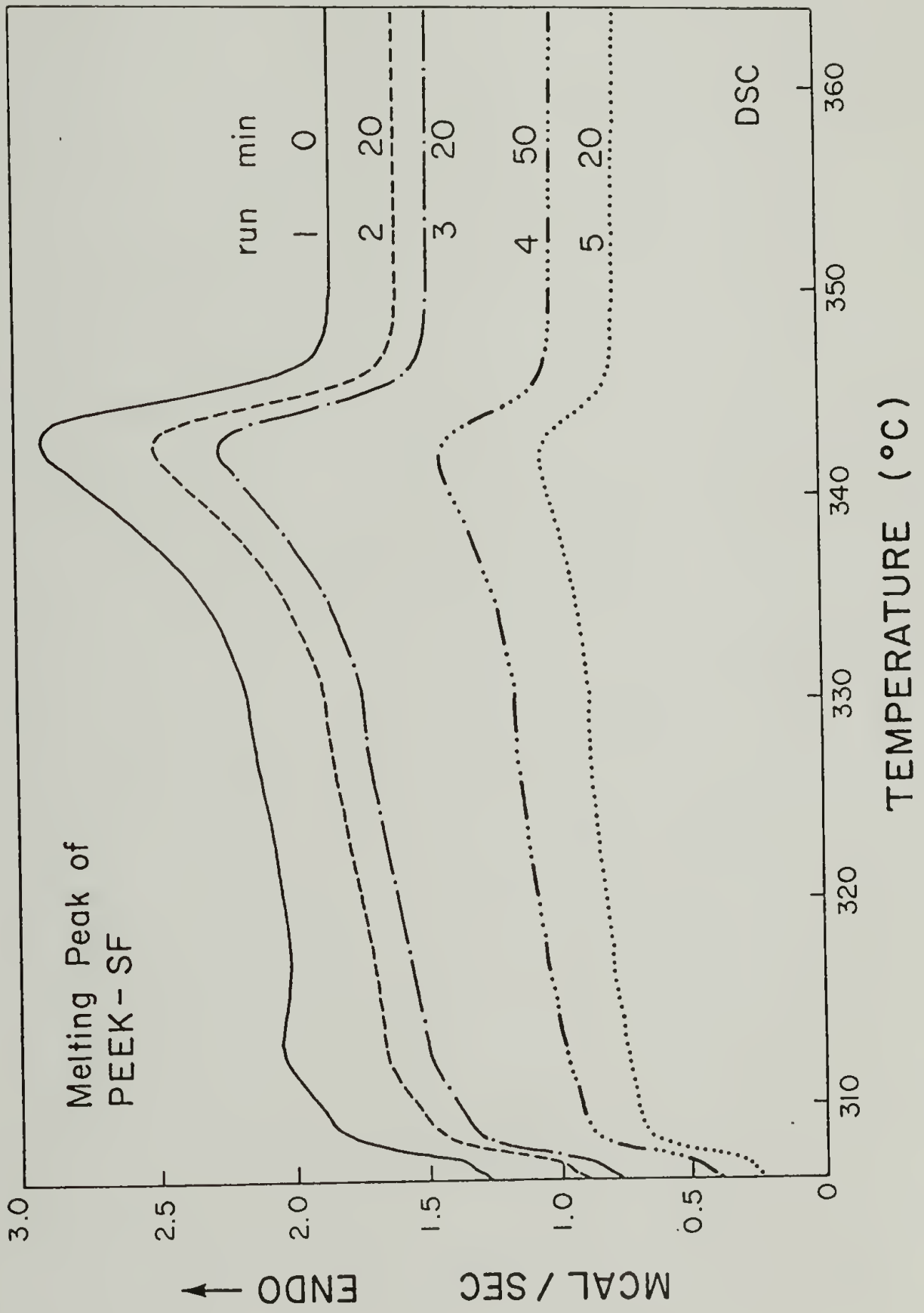

Figure 4.5. Melting traces of the PEEK-SF crystallized at 306°C for 7 min.

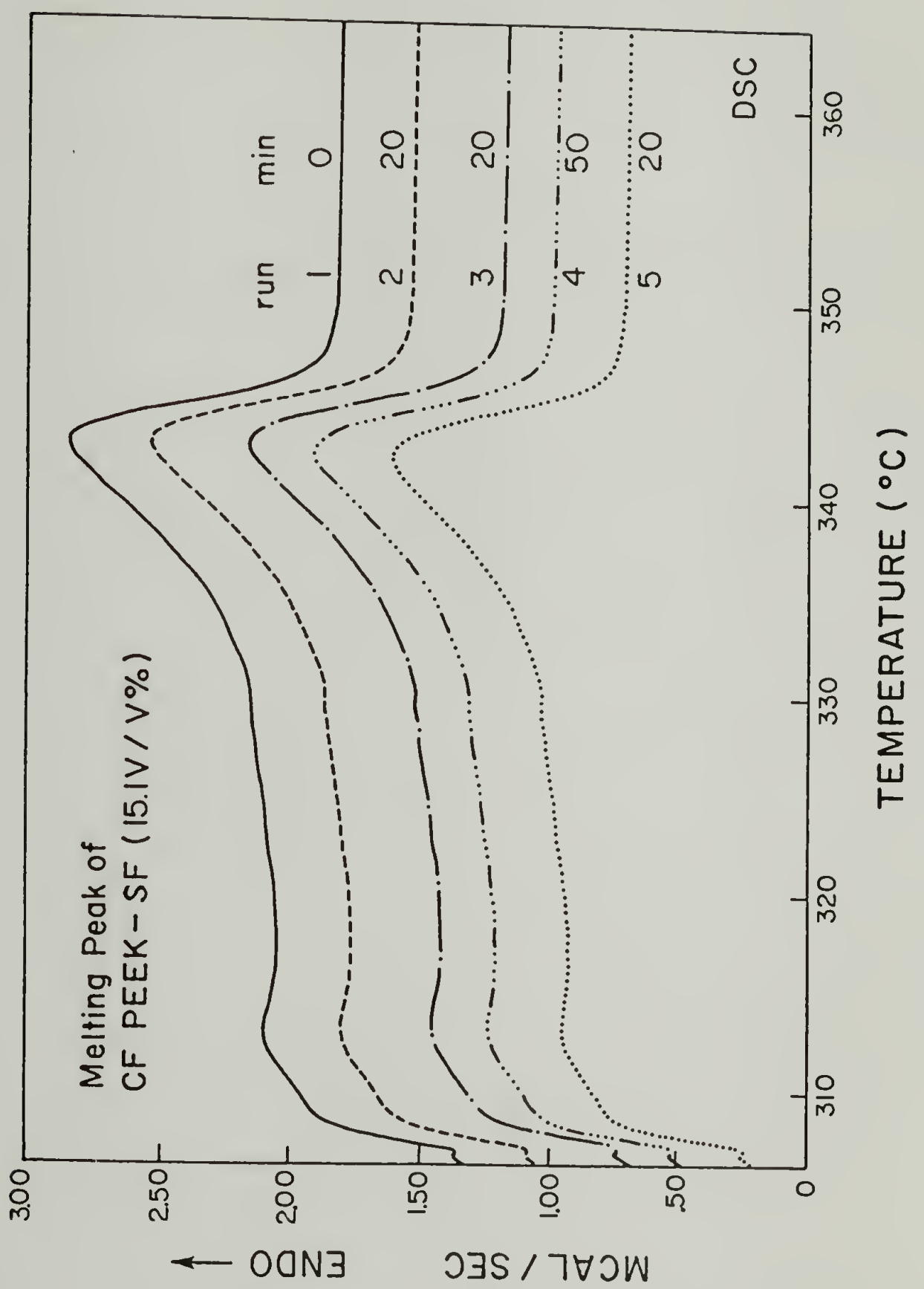

Figure 4.6. Melting traces of 15.1 vol. % carbon fiber reinforced PEEK-SF crystallized at 306°C for 7 min.

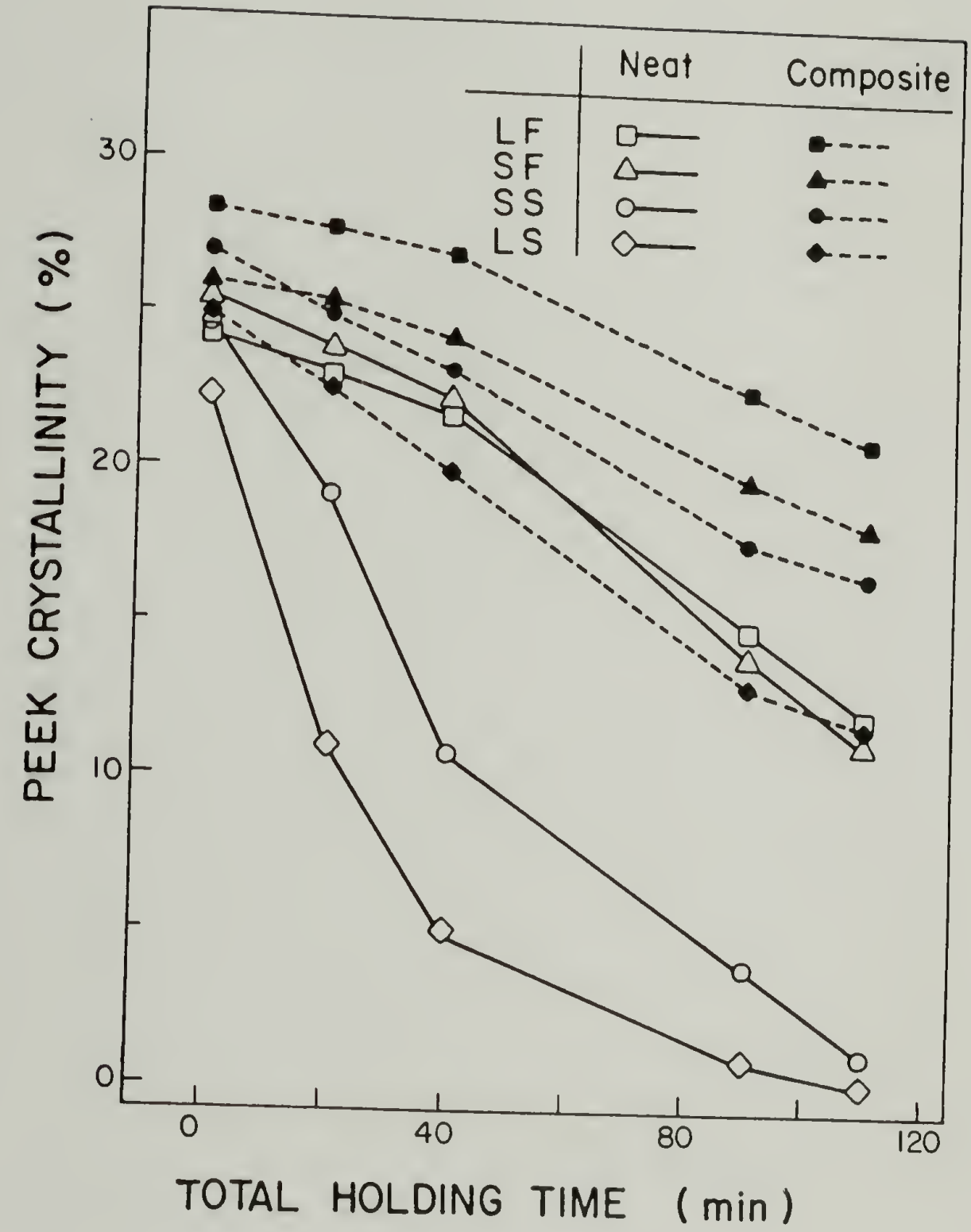

Figure 4.7. Crystallinity at 306°C in 7 min vs. total melt-annealing time at 395.9°C: (□) PEEK-LF; (△) PEEK-SF; (○) PEEK-SS; (◇) PEEK-LS; carbon fiber reinforced PEEK, (■) LF 22.1 vol. %; (▲) SF 24.6 vol. %; (●) SS 23.9 vol. %; (◆) LS 20.7 vol. %.

sites [79,105]. Indeed it has been found that PEEK retains some local order at 380°C [107].

Since the crystallization time (7 min) is not sufficient for secondary crystallization, the crystallinity developed in each cycle is considered to depend on the number of ordered regions or nuclei which have survived the previous melt-annealing. Therefore the crystallinity is proportionally dependent on the nucleation density, and the difference in nucleation density between the samples becomes more pronounced at long melt-annealing time. For the four classes of PEEK samples, the order of increasing nucleation density is found to be LS < SS < SF ~ LF. All PEEK samples with carbon fibers exhibit higher nucleation density than PEEK itself. Carbon fiber reinforced LF sample shows higher nucleation density than carbon fiber reinforced SF sample and the two samples without carbon fiber show similar nucleation density. This indicates that the contribution of carbon fiber is greater in the LF sample than in the SF sample.

The nucleation of polymer on substrates is complex and several different explanations have been offered including a consideration of surface energy of substrate [108], a possible temperature gradient [109], the matching of unit cell structures [110], and the shear stresses due to difference in thermal expansion [111].

4.3.2 Transcrystalline Region

Fig. 4.8 shows cross polar optical micrographs of PEEK crystallization in the presence of carbon fibers. For samples held in

Figure 4.8. Cross-polar optical micrographs of PEEK with carbon fibers: samples held at 390°C in hours, (1) 0.5; (2) 2; (3) 3; (4) 4 and cooled (-0.5°C/min) to 270°C, followed by quenching to room temperature.

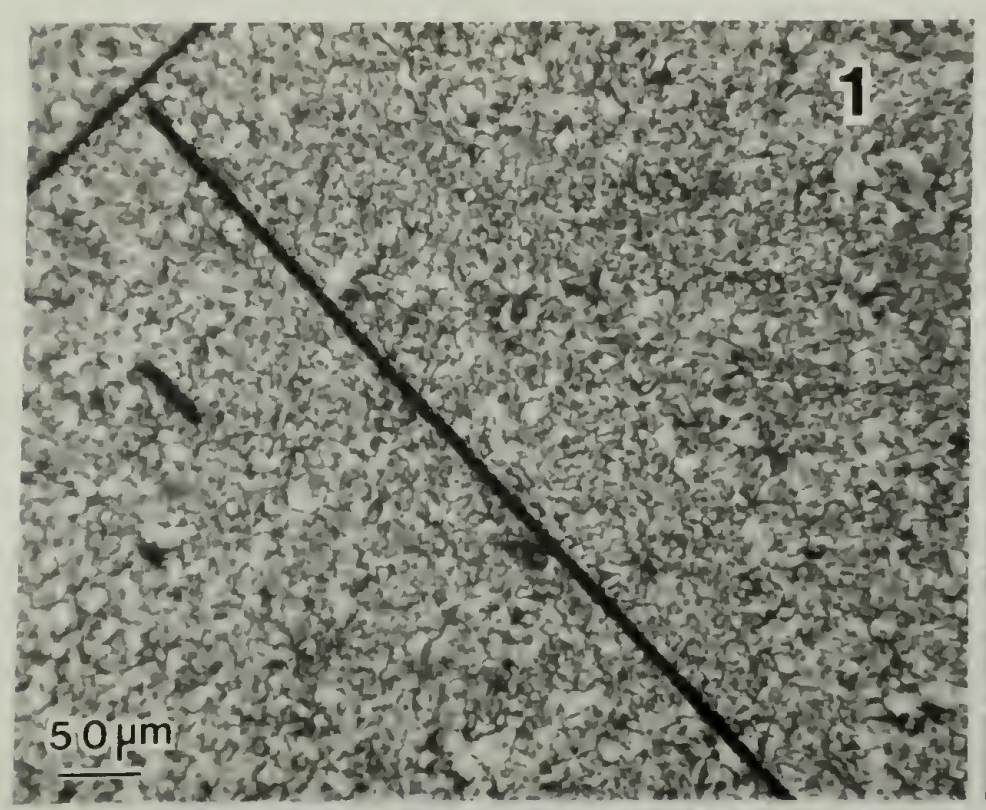
1
50 µm

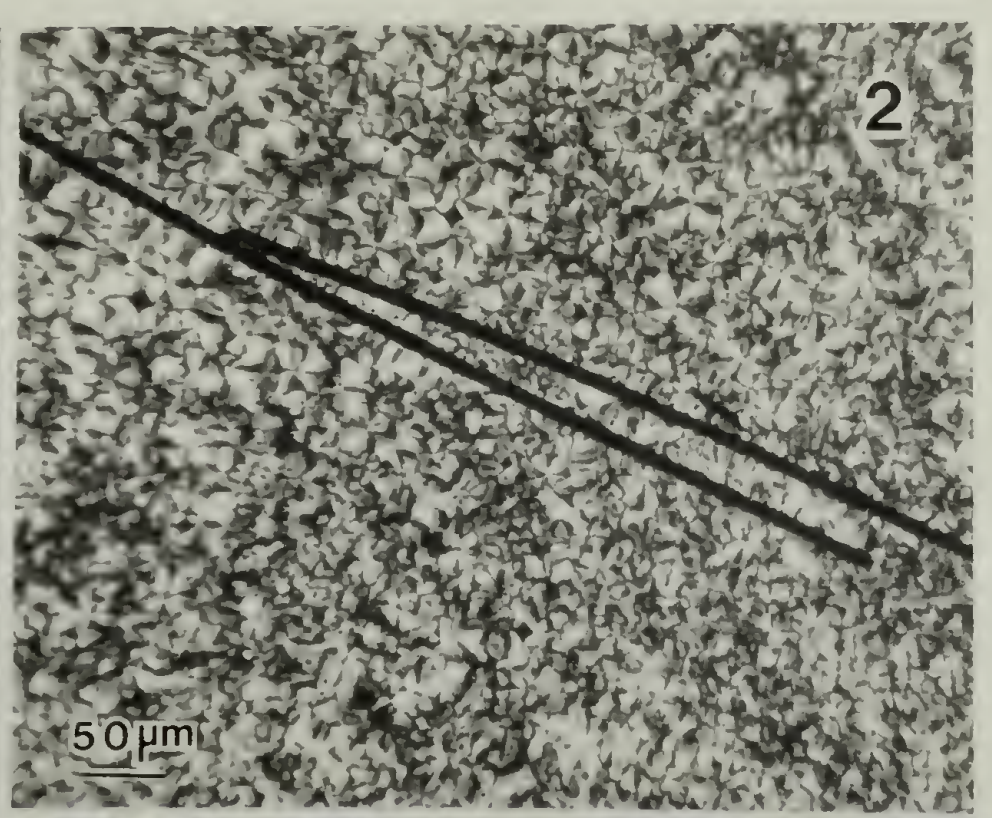
2
50 µm

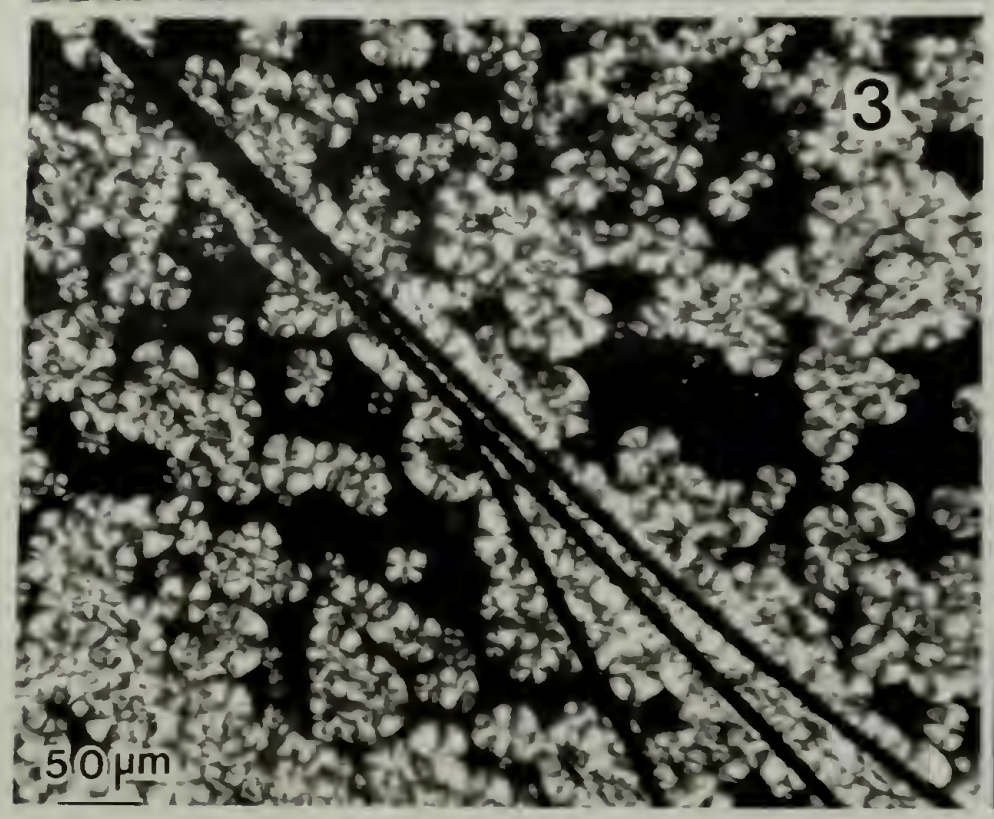
3
50 µm


4
50 µm

the melt for long time, fewer spherulites are seen in the bulk and a more distinctive transcrystalline region is developed on the carbon fiber surface. It is generally known that high density of nuclei at interface promotes unidirectional growth of spherulites because of the proximity of nucleation sites. Noticeable transcrystalline structure did not develop in sample 1 which had a thermal history similar to the SS sample. The thermal history of sample 2 is similar to that of the LS sample. Here about 5 μ thick transcrystalline region impinged with the spherulites nucleated in the matrix. The crystallization on the carbon fiber competes with crystallization in matrix. As the melt holding time was increased, the number of nuclei in the matrix decreased, favoring heterogeneous crystallization on carbon fiber. Observable transcrystallinity was not observed in the sample which had the same thermal history as the LF and SF samples. Nonetheless the heterogeneous crystallization on the carbon fiber in the LF sample is considered to be more favorable than in the SF sample as shown in Fig. 4.7. The thickness of transcrystalline region (about 30 μ) in sample 4 is almost the same as the radius of the largest spherulites in matrix, implying that carbon fiber surface and nuclei surviving in the bulk have almost the same activity.

Fig. 4.9 shows a transmission electron micrograph of microtomed PEEK with a single carbon fiber. Several well-defined spherulites are seen in the matrix. Electron diffraction pattern in Fig. 4.9 was obtained at the interface. The pattern is the same as an electron diffraction pattern along the radius of a spherulite. Therefore it is

Figure 4.9. A transmission electron micrograph of a 500 Å thick section of PEEK crystallized 324°C for 23h with a single carbon fiber. A selected area electron diffraction was from PEEK at the interface. The vertical direction in diffraction is perpendicular to the fiber surface.

Transmission Electron Micrographs of
Spherulitic PEEK with a Carbon Fiber (T-300)

considered that b-axis of PEEK crystal orients outward from carbon fiber surface as observed along the radius of a spherulite [30]. PEEK spherulites nucleated on carbon fiber surface has been observed using scanning electron microscopy after etching with an oxidizing solution [48,112,113].

4.3.3 Interfacial Bond Strength

To measure the interfacial bond strength, tensile tests were carried out in the transverse direction (perpendicular to fiber direction). The transverse tensile strength of a composite is usually less than the strength of the matrix polymer [106]. The low transverse strength of unidirectional laminates often limits the design of structures such as pipes for internal pressure [106]. The transverse tensile strengths are plotted vs. carbon fiber content in Fig. 4.10. All composites show little dependence on fiber content over the test range. The values of the SS and SF samples are comparable with each other but considerably lower than those of the LS and LF samples. The LS and LF samples show considerably higher values than the matrix, indicating that they exhibit a strong interfacial bond between carbon fiber and PEEK. The averaged values with the corresponding percent crystallinities are listed in Table 4.2. The transverse tensile properties do not appear to be sensitive to percent crystallinity. The toughness, i.e., the area under the stress-strain curve, of the LS and LF samples is about 5 times that of the SF and SS samples. This major difference is considered to be due to

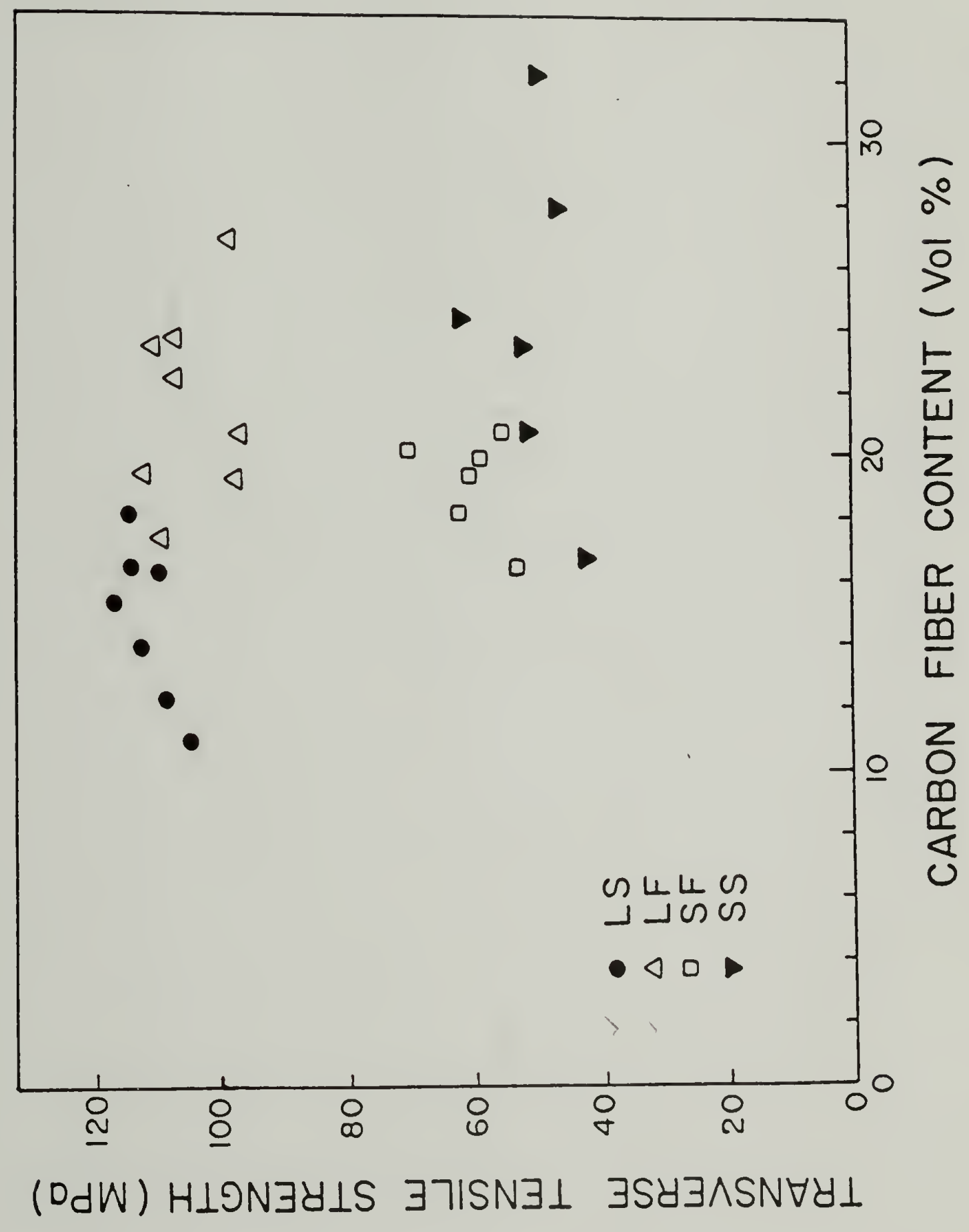

Figure 4.10. Transverse tensile strength vs. carbon fiber content.

Table 4.2. Transverse tensile properties of carbon fiber reinforced PEEK composites.[a]

Composite code	Vol.% fiber	Modulus (GPa)	Strength (MPa)	Strain-to-failure (%)	Toughness[b] (10^6 J/m^3)
LS	11-18	3.9	111	4.8	3.3
LF	17-27	4.3	106	4.4	3.3
SF	16-21	3.9	63	1.9	0.6
SS	16-32	4.0	60	1.7	0.4
SF-LF[c]	16-21	3.8	100	4.1	2.6
SS-LF[c]	16-32	4.8	91	3.0	1.8

a. Strain rate was 0.033/min.
b. Measured from the area under the stress-strain curve.
c. Reprocessed samples.

crystallization on carbon fiber. According to Keith and Padden [114] impurities which cannot crystallize diffuse away from growing crystal surfaces. Therefore if the matrix nucleation is dominant, impurities will be accumulated at the fiber-matrix interface and the interfacial bond will be weak. The interface where the PEEK matrix crystallizes predominantly by nucleation on the fiber is thus expected to produce a strong bond.

Little effect of cooling rate has been observed. This is probably because transverse tensile properties of a composite depend on the interfacial structure as well as crystalline structure of matrix. In the slowly cooled sample, crystallization on the fibers is more favorable, however, occurrence of tie chains between crystals is less favorable than in the fast cooled sample. In addition, the carbon fiber is as active as survived nuclei as found in Fig. 4.8; hence the interfacial structure primarily depends on the nucleation density of the matrix. During long preheating, nuclei in the matrix of the LS and LF samples are more extensively reduced than in the SS and SF samples. The interface in the LS and LF samples is crystallized from nucleation on the fiber surface, forming a strong bond. Some of the SF and SS samples were subsequently subjected to the thermal history of the LF sample. They showed values similar to that of the LF sample suggesting that the thermal history is the main reason for difference in transverse tensile strength. The LS and LF samples show greater strain-to-failure (4.8, 4.4%, respectively) than did the SF and SS sample (1.9, 1.7%, respectively). Strain-to-failure of commercial

carbon fiber reinforced PEEK (50-55 vol%) of ICI has been reported to be 1% [115].

The fracture surface of the samples, resulting from transverse tensile test, are shown in Fig. 4.11. In the SF and SS samples carbon fibers are nearly bare, showing poor wetting. In contrast, carbon fibers in the LF and LS samples show strong fiber-matrix adhesion, implying that failure was accompanied by matrix deformation, consistent with the corresponding mechanical properties.

4.4 Conclusions

The tendency of carbon fiber to nucleate the crystallization of PEEK has been evaluated by DSC and other techniques. As the carbon fiber content was increased the supercooling necessary for PEEK crystallization decreased. The repeated melting (at 395.9°C) of the same PEEK sample results in a decrease of the number of nuclei for crystallization. At given equivalent of thermal histories, PEEK with carbon fiber was found to have a higher nucleation density than PEEK itself.

The surface of carbon fiber and nuclei in PEEK matrix compete for crystallization growth. Reducing the number of nuclei in matrix favors PEEK crystallization on the carbon fiber. As the holding time in melt (390°C) is increased, the number of matrix spherulites formed

Figure 4.11. Scanning electron micrographs of tensile-fractured surfaces of the SF, SS, LF, and LS samples.

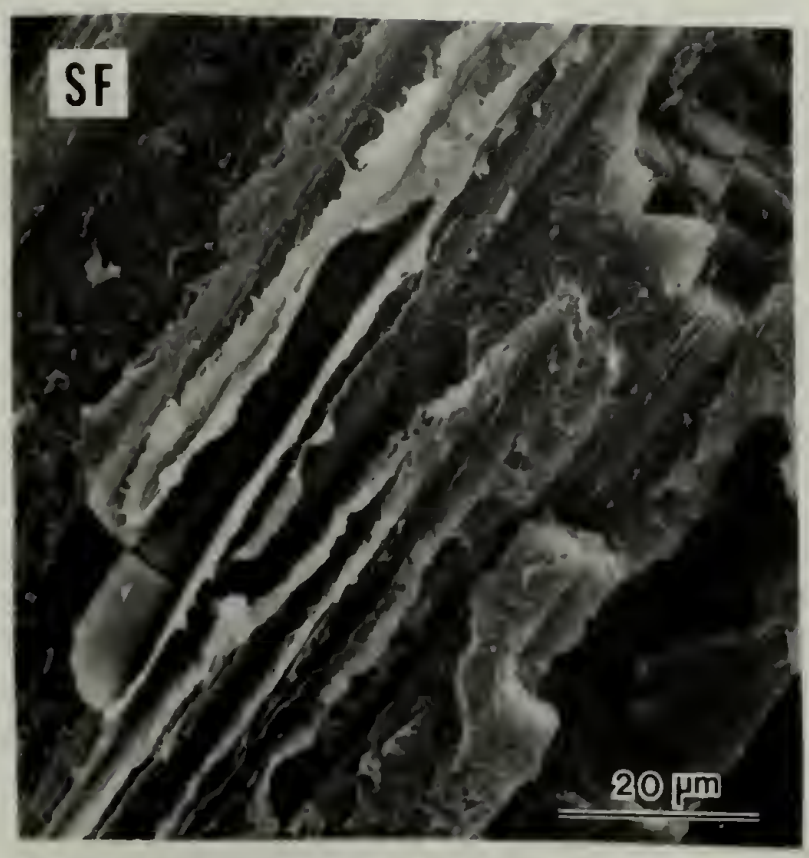
SF
20 µm


SS
20 µm

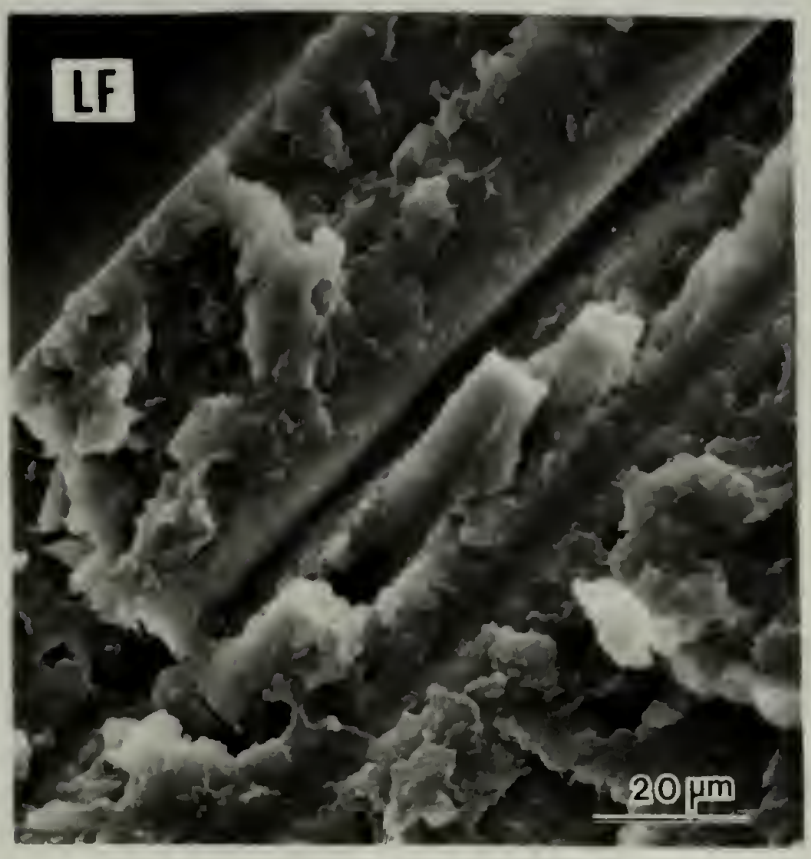
LF
20 µm

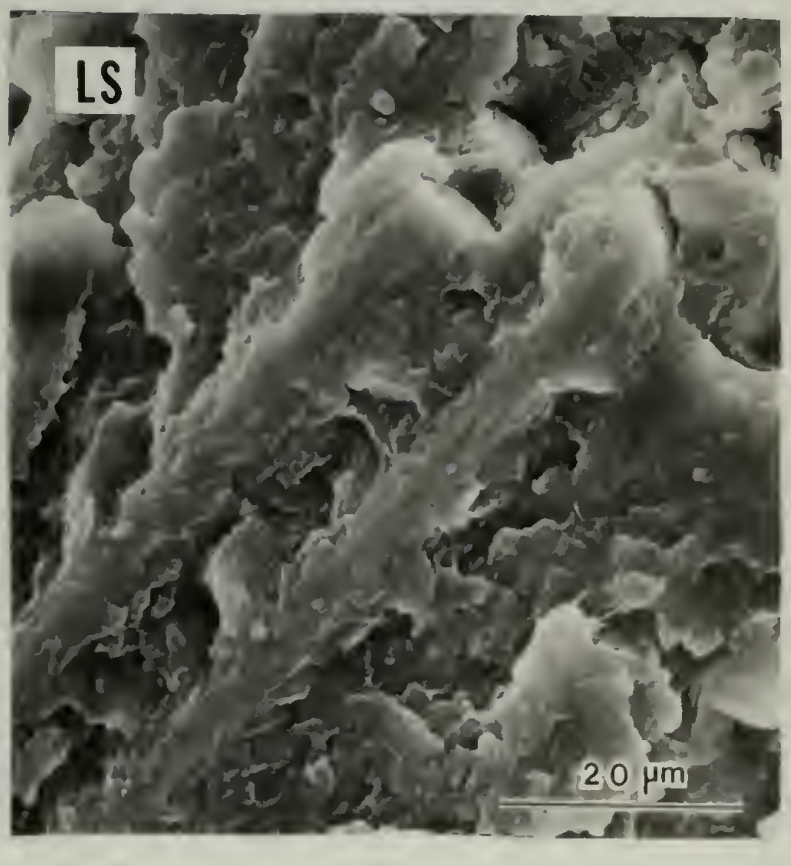
LS
20 µm

on cooling is decreased; hence a more pronounced transcrystalline region is developed.

The composites which were preheated in melt for 100 min showed much higher transverse tensile strength and strain-to-failure than those preheated for 30 min. Correspondingly the fracture surface produced in tension shows that the former samples have greater matrix adhesion to carbon fiber surface than the latter.

It is concluded that a strong interfacial bond is developed by crystallization on the carbon fiber surface. Destroying nuclei in the PEEK matrix by long preheating enhances the crystallization on the surface of the carbon fiber reinforcement.

C H A P T E R V

UNIAXIAL DRAW OF POLY(ETHER ETHER KETONE) BY SOLID-STATE EXTRUSION

5.1 Introduction

Recently there has been a considerable interest in development of polymers with high modulus. It has been realized that the greatest load-bearing capacity results from a structure of highly oriented, extended, and densely packed chains. Polymers with this structure have been developed by two basic approaches: chemical synthesis of rigid rod-like polymers and processing conventional flexible polymers in such a way that a permanent orientation of the internal structure is possible [116].

The drawing techniques can be classified into drawing from the solid state and from the melt or solution. Tensile drawing of solid polymers was used to improve the mechanical properties [117]. However, the strength and modulus obtained by conventional drawing has always been below those achieved by the newer techniques such as solid state extrusion and zone drawing and annealing [118-120].

The solid-state extrusion technique has recently been extensively used to achieve high modulus and strength [116,118-121]. High density polyethylene (HDPE) has been used preferentially because it shows one of the highest theoretical moduli (240 GPa) [116]. The high theoretical modulus of polyethylene is due to the intrinsic strength of the covalent carbon-carbon bonds and the ability to arrange the methylene chains in an extended, planar zig-zag conformation. Since PEEK chains have planar zig-zag conformations in the crystal [116,118], it is, therefore, interesting to look for improvements in mechanical properties of PEEK by drawing. Only a few drawing studies of PEEK have been reported since it is a relatively new commercial polymer [122,123].

5.2 Experimental

5.2.1 Materials

Amorphous PEEK films (0.13 mm thick) and semicrystalline PEEK rods (12.7 mm diameter) were obtained from Westlake Plastics. Reduced viscosities of 0.79 and 0.92 dL/g were measured for PEEK films and rods, respectively. The viscosity was measured at 25°C in 98% sulfuric acid at a concentration of 0.1 g/dL using an Ubbelohde-type viscometer.

5.2.2 Solid-State Extrusion

Rods were trimmed to the diameter of 9.5 mm and solid-state extruded at 310°C using stainless steel conical dies with a 20° entrance angle. Amorphous PEEK films were first crystallized at 240°C for 70h and then extruded at 154°C using the split-billet coextrusion technique [116,121]. The film (5 mm wide) was placed between polyoxymethylene (MP 165°C) split-billet halves and extruded using brass conical dies with a 20° entrance angle. All extrusion rates were 1 mm/min. Details on the solid-state extrusion technique have been previously documented [116,119,121]. Extrusion draw ratio (EDR) was measured from the displacement of lateral ink marks on the film prior to coextrusion for PEEK films. For rods, EDR was determined from the ratio of the diameters after and before extrusion. Rod samples were cut using a diamond saw (Isomet, Buehler Ltd.) and used for the following experiments.

5.2.3 Wide-Angle X-ray Diffraction

Photographs of the diffraction pattern were recorded on flat films in a Statton type (Warhus) camera. A Siemens D-500 X-ray diffractometer equipped with a pulse-height scintillation counter was used to measure the diffracted intensity. Both of these wide angle X-ray diffraction experiments were conducted in a transmission mode with Ni-filtered Cu-Kα radiation at 30 mA and 40 kV. Crystal orientation functions were calculated from scanning of the (110) and (200) crystal reflections at varying azimuthal angles [124] using the Wilchinsky

method [125]. The step size in azimuthal angle and collection time were 2 degrees and 3 min, respectively. The intensity was corrected for background.

5.2.4 Birefringence, Tensile, and Density Measurements

Orientation of the drawn PEEK film was measured by birefringence using a Zeiss polarizing microscope with a Kalkspat compensator. Birefringence was calibrated using quartz plates with calcite Eringhaus compensator exhibiting a wide range of retardations. Tensile properties of drawn and undrawn PEEK films were measured using an Instron tensile tester (model TTCM). Strain rate was 7×10^{-4}/sec and tensile moduli were measured at 0.2% strain. Moduli and strengths at break were calculated on the basis of the original cross-sectional area. The density was measured in a density column made from aqueous solutions of calcium nitrate at 23°C [37]. The sensitivity of the column was about 0.0001 g/cm^{3}mm, thus the accuracy of the density measurement was 0.05% or better.

5.2.5 Thermal Analysis

Thermal behavior was characterized with a Perkin-Elmer differential scanning calorimeter (DSC-4) calibrated with the melting transition of indium, tin, lead, and zinc. All measurements were made at a heating rate of 20°C/min in nitrogen.

5.3 Results and Discussion

5.3.1 Wide-Angle X-ray Diffraction

The X-ray scattering patterns obtained for solid-state extruded PEEK rods are shown in Fig. 5.1. As the extrusion draw ratio (EDR) was increased, the scattering patterns become narrower in azimuthal angle, indicating ever higher crystal orientation. Wide-angle X-ray diffraction studies have shown that the unit cell of PEEK crystal is orthorhombic [29,30,40,57,126,127]. From the X-ray scattering patterns in Fig. 5.1, up to 14 peaks have been identified. The observed d spacings are within 0.5% of those calculated using the unit cell dimensions reported by Rueda et al [40]. Wide-angle X-ray scattering of amorphous and semicrystalline PEEK with reflection planes are shown in Fig. 5.2. The reported values of the a, b, and c axes of the unit cell are in the ranges 7.75-7.83 Å, 5.86-5.94 Å, and 9.86-10.07 Å, respectively [29,30,40,126,127]. The unit cell contains two chains each, with two-thirds of the chain repeat unit, however, a unit cell with two repeat units has also been considered [57]. The crystal structure of PEEK is similar to that of poly(p-phenylene oxide), and the ether and carbonyl units are considered to be crystallographically equivalent [29].

The (001) reflection has been identified here at $2\theta = 9.0^{\circ}$ for highly deformed (EDR > 3) PEEK films and rods. This weak (001) reflection may be due to a slight perturbation of the 2/1 helix (planar zig-zag) of the PEEK chains in the crystal and/or due to

Figure 5.1. Wide-angle X-ray diffraction patterns of drawn PEEK rods; draw direction vertical, X-ray beam normal to film plane.

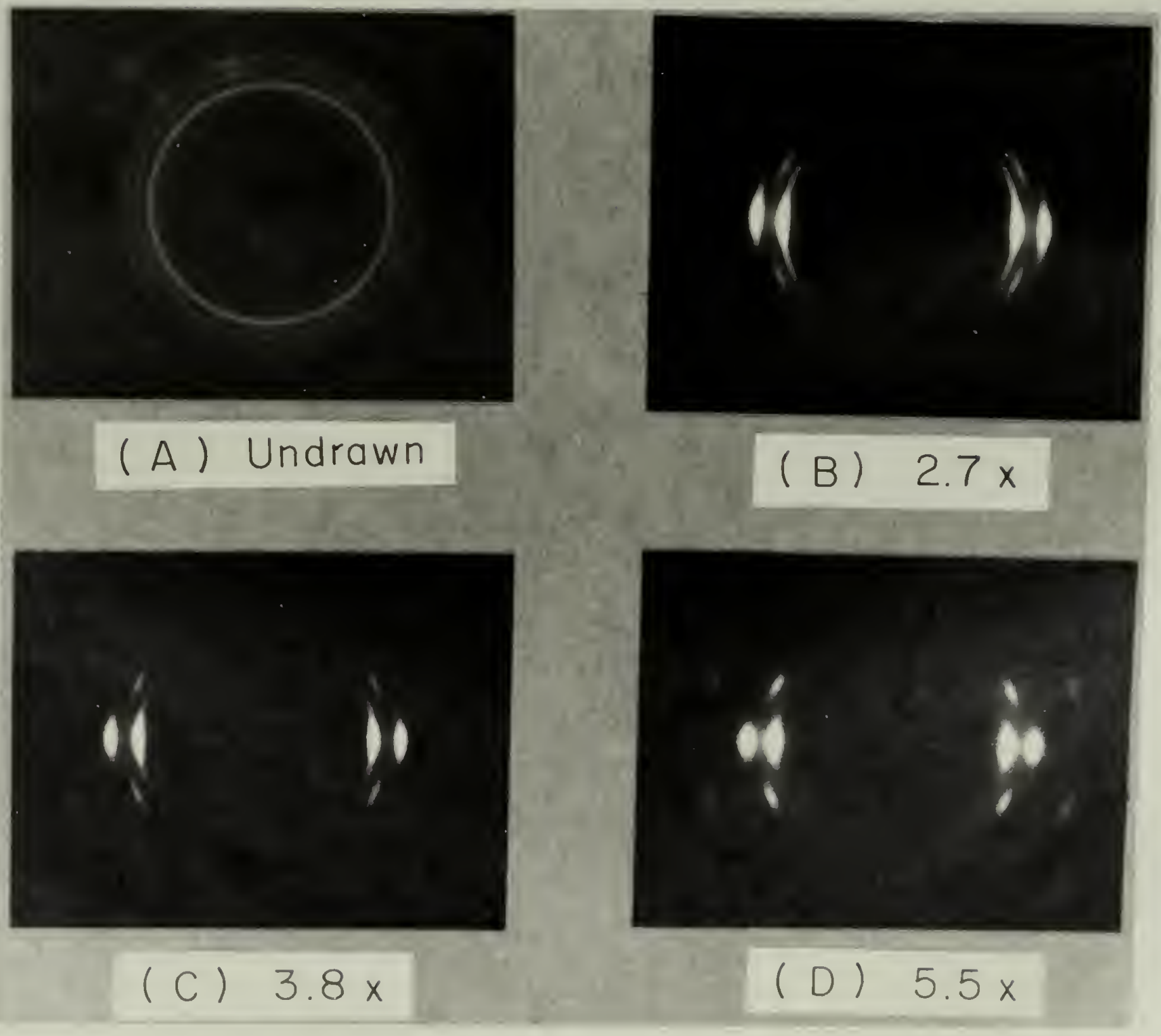
(A) Undrawn
(B) 2.7 x
(C) 3.8 x
(D) 5.5 x

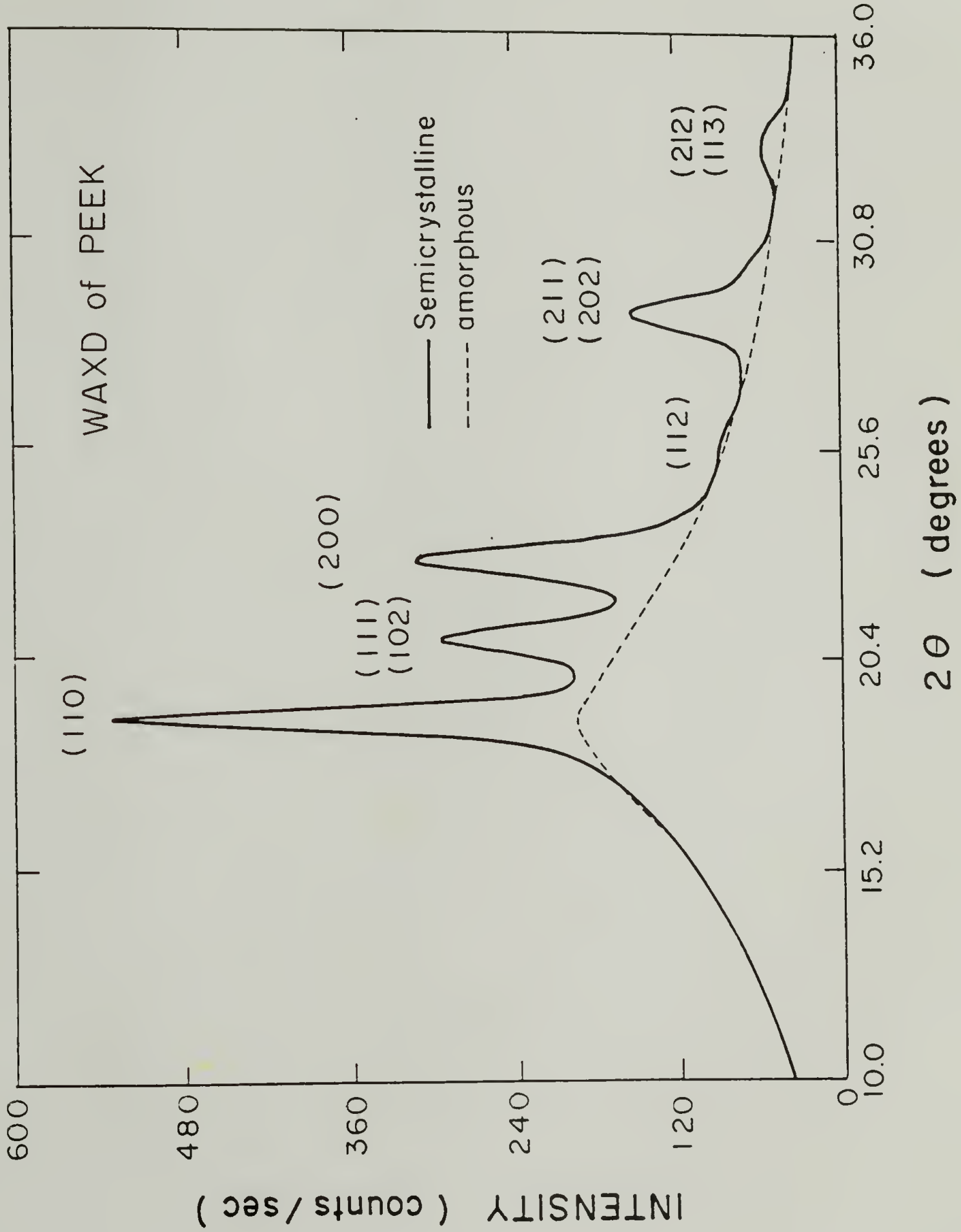

Figure 5.2. Wide-angle X-ray diffraction of undrawn semicrystalline and amorphous PEEK.

slight difference in the packing of the ether and ketone groups [128]. On tilting the sample towards the X-ray beam, meridional reflections also appeared on the fourth, fifth, and sixth lines. The (005) reflection reinforces the observation that slight perturbations from an exact two-fold helix are evident. X-ray scattering patterns in the three orthogonal directions for a solid-state coextruded PEEK film showed that the film has cylindrical symmetry about the deformation direction and thus has been uniaxially deformed.

5.3.2 Crystal Orientation Functions

The intensity along the azimuthal angles (ϕ) for the (110) and (200) reflection planes of drawn and undrawn PEEK films are shown in Fig. 5.3 and Fig. 5.4, respectively. The intensity variation was used to calculate the crystal orientation functions as shown in Fig. 5.5. The first equation in Fig. 5.5 is the Hermans-Stein orientation distribution function [124,129]. $\langle \cos^2 \phi_{j,z} \rangle$ represents the mean-square cosine (averaged over all the crystallites) of the angle between a given crystal axis, j (j = a,b,c) and the reference axis z, the uniaxial draw direction. For complete orientation with respect to the reference direction, $\langle \cos^2 \phi \rangle = 1$ and f = 1; for random orientation, $\langle \cos^2 \phi \rangle = 1/3$ and f = 0; for completely perpendicular orientation, $\langle \cos^2 \phi \rangle = 0$ and f = - 1/2.

Fig. 5.6 shows crystal orientation functions for coextruded PEEK films and for extruded rods. For both drawn samples, the orientation of the c axis (molecular chain direction) with respect to the drawing

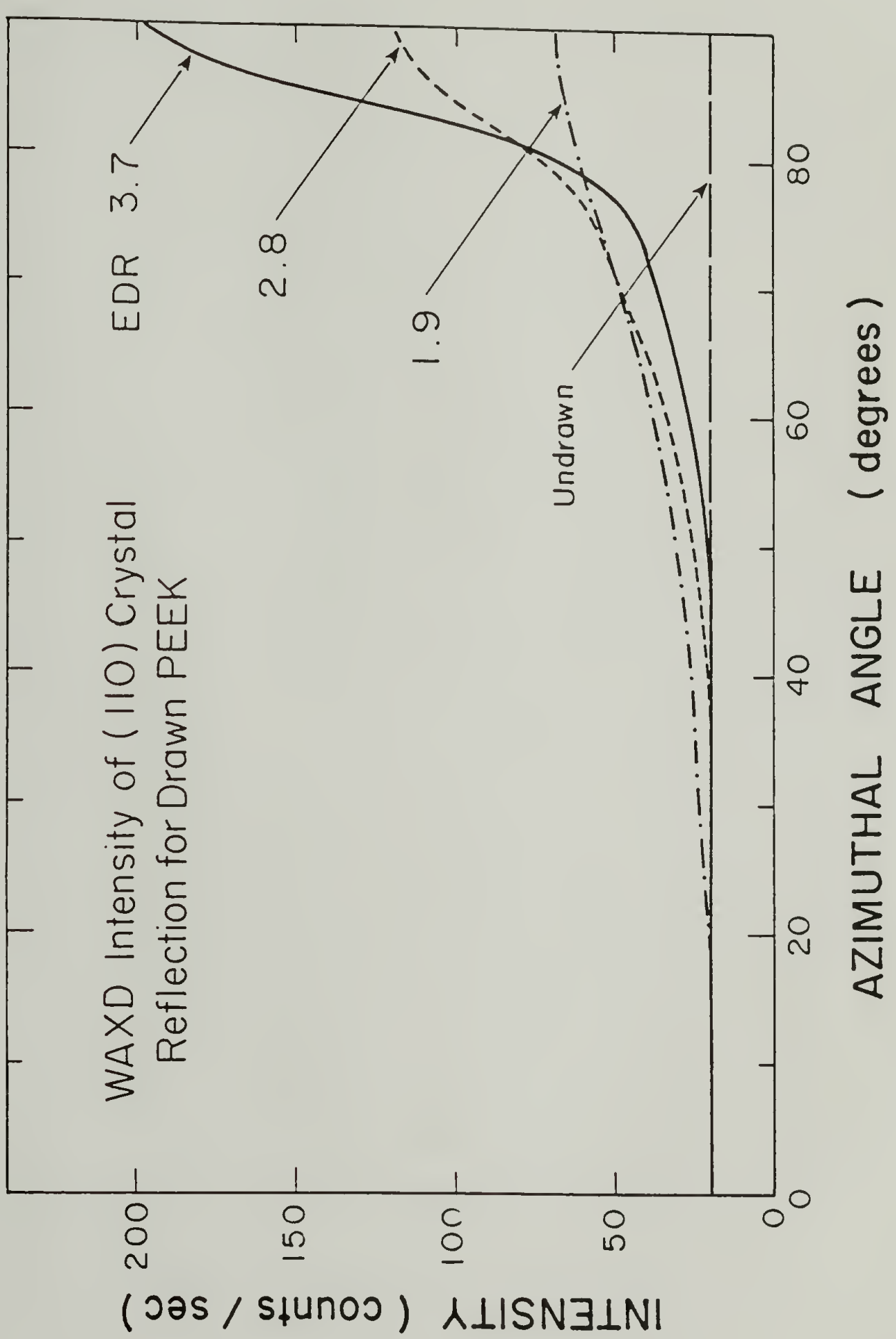

Figure 5.3. Intensity of (110) crystal reflection along the azimuthal angle for drawn and undrawn PEEK.

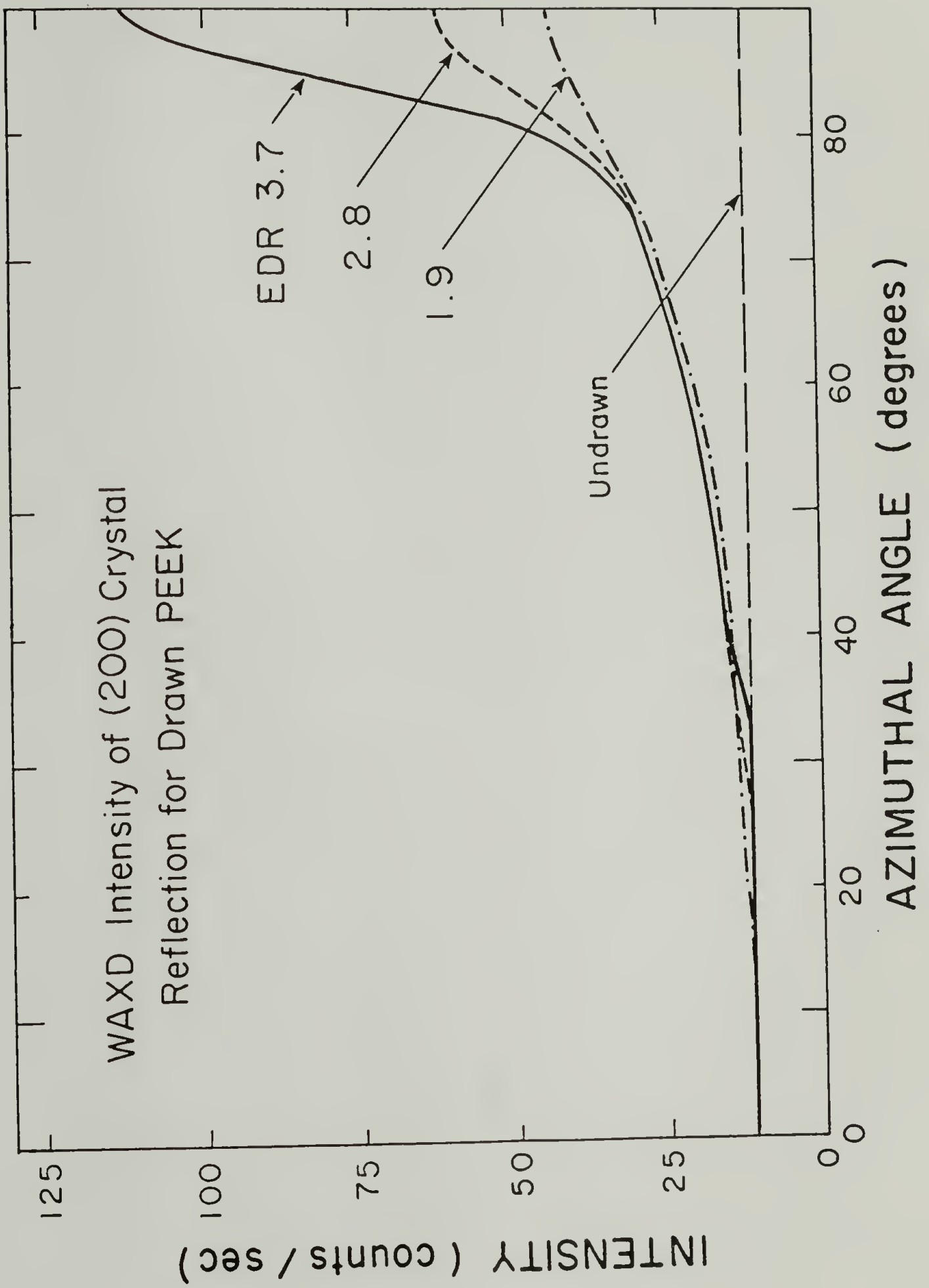

Figure 5.4. Intensity of (200) crystal reflection along the azimuthal angle for drawn and undrawn PEEK.

Crystal Orientation Functions

$$f_j = \frac{1}{2}\left(3\langle \cos^2 \phi_{j,z} \rangle - 1 \right)$$

$$\langle \cos^2 \phi_{j,z} \rangle = \frac{\int_0^{\pi/2} I(\phi) \cos^2 \phi \sin\phi \, d\phi}{\int_0^{\pi/2} I(\phi) \sin\phi \, d\phi}$$

Parameter $\langle \cos^2 \phi \rangle$	f	Orientation with respect to Z
1	1	parallel
1/3	0	random
0	-1/2	perpendicular

Figure 5.5. Crystal orientation functions.

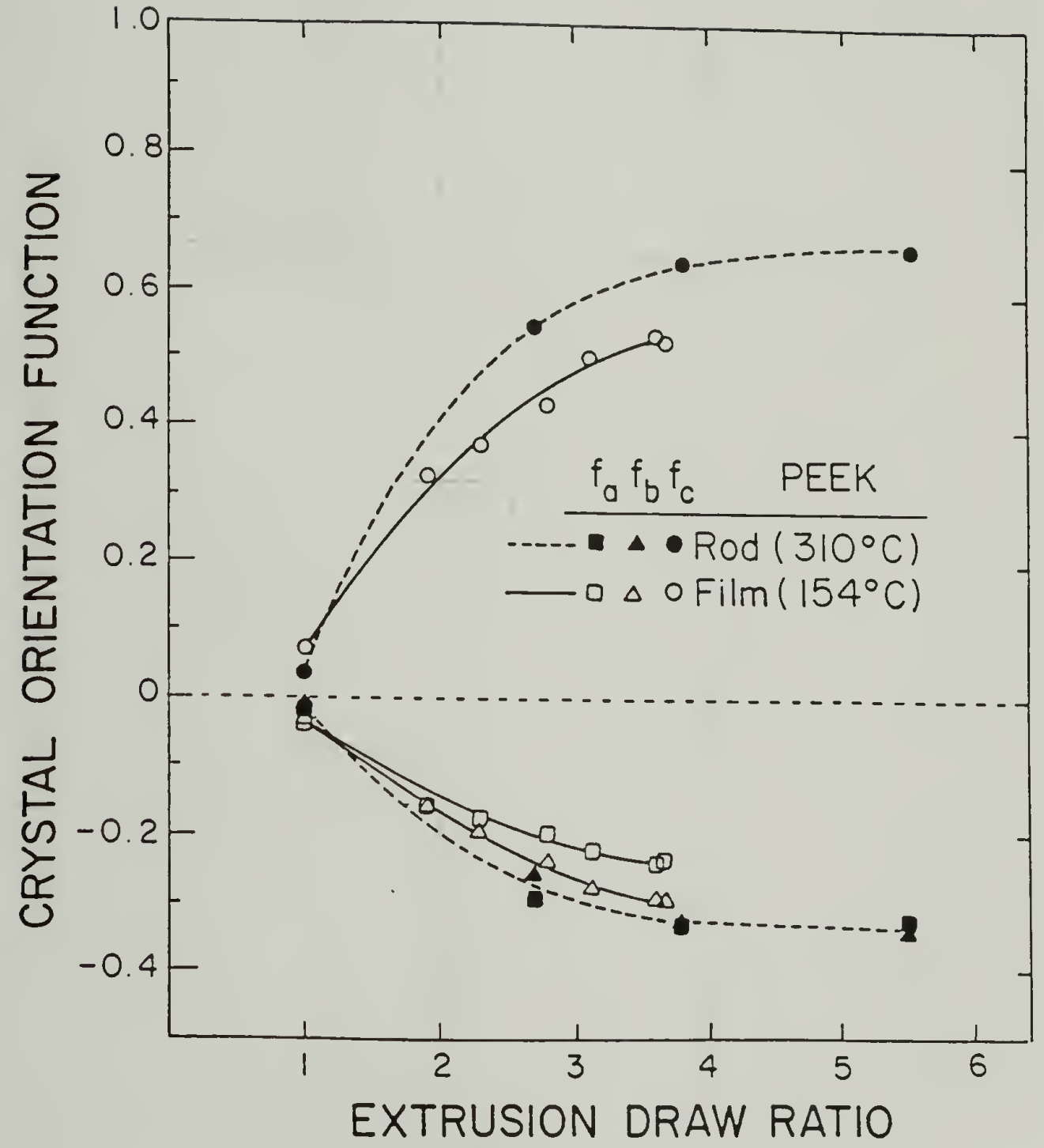

Figure 5.6. Crystal orientation functions of drawn PEEK rods and films as a function of EDR.

direction f_c increases with extrusion draw ratio (EDR), indicating that the chains in crystals orient in the drawing direction and even more with increasing EDR. Correspondingly, the a and b axes orient perpendicularly to the drawing direction. The a and b crystal axes in deformed rods orient similarly. The b axis appears to orient faster than the a-axis on drawing films. Orientation function studies of solid-state extruded polyethylene have revealed the opposite type of orientation behavior [130]. The (110) and (200) reflections for PEEK are located in the range of the amorphous halo. There is, therefore, a contribution from the deformed amorphous chains to the calculated orientation functions.

The total birefringence of drawn film was measured and plotted vs. EDR in Fig. 5.7. The birefringence was increased up to 0.30 at EDR of 3.7. The refractive indices for a, b, and c axes of PEEK crystal have been calculated to be 1.77, 1.48, and 1.97, respectively and thus the maximum birefringence of a fiber is 0.34 [30]. Birefringence values of up to 0.28 have been reported for highly oriented PEEK fibers [30]. Solid-state extruded PEEK films in this study show higher values than the reported ones, indicating the higher orientation.

The highest EDR attainable in a single step on films was found to be 3.7 at 154°C. In the case of the rods, drawing up to an EDR of 5.5 in a single step has been achieved at 310°C, but the crystal orientation tends to level off beyond EDR 3.8. This is also reflected in the thermal expansion behavior of the rods in Fig. 5.8 (from ref. 131), where similar values are shown for EDR 3.8 and 5.6. The thermal

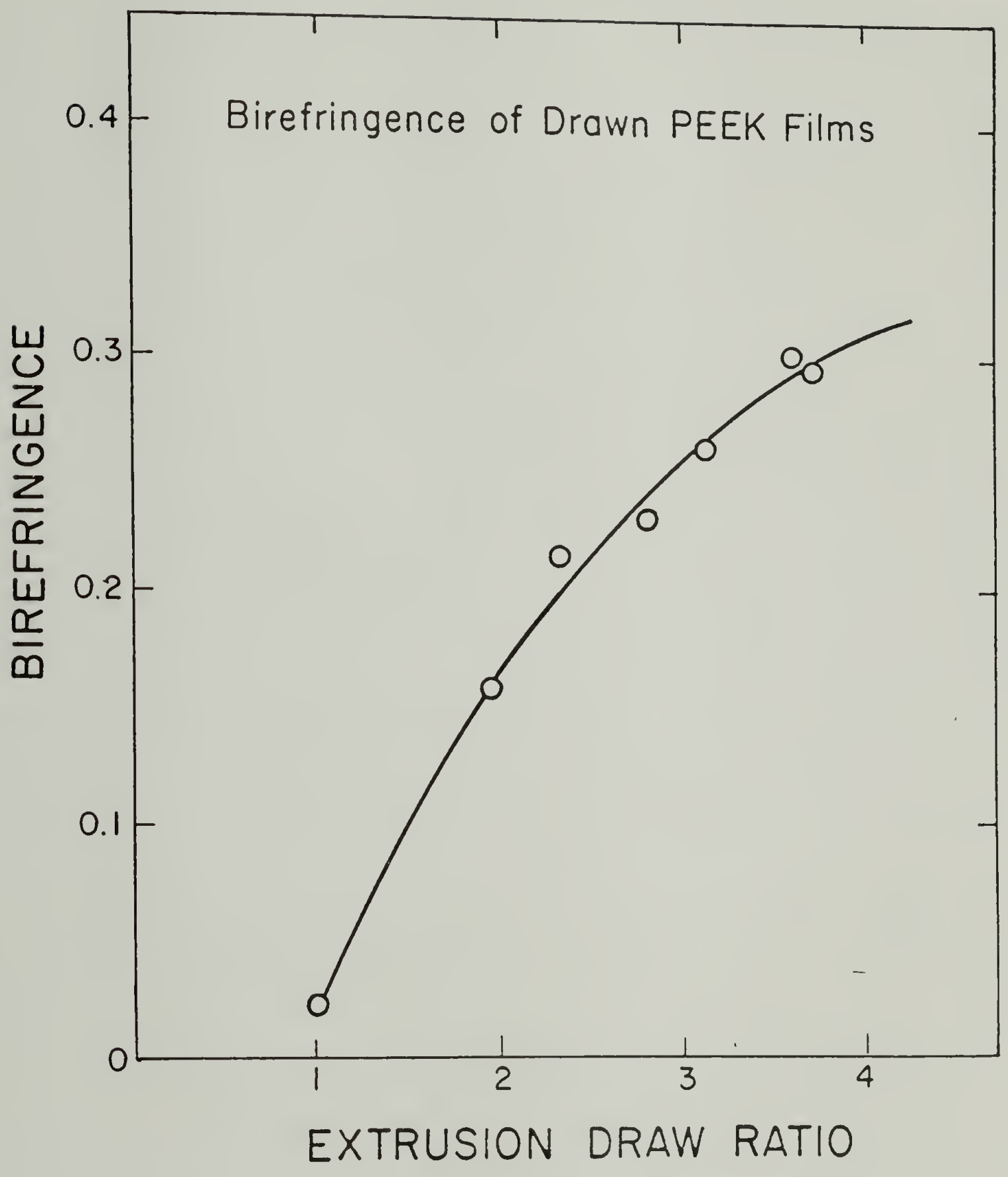

Figure 5.7. Birefringence of drawn PEEK films.

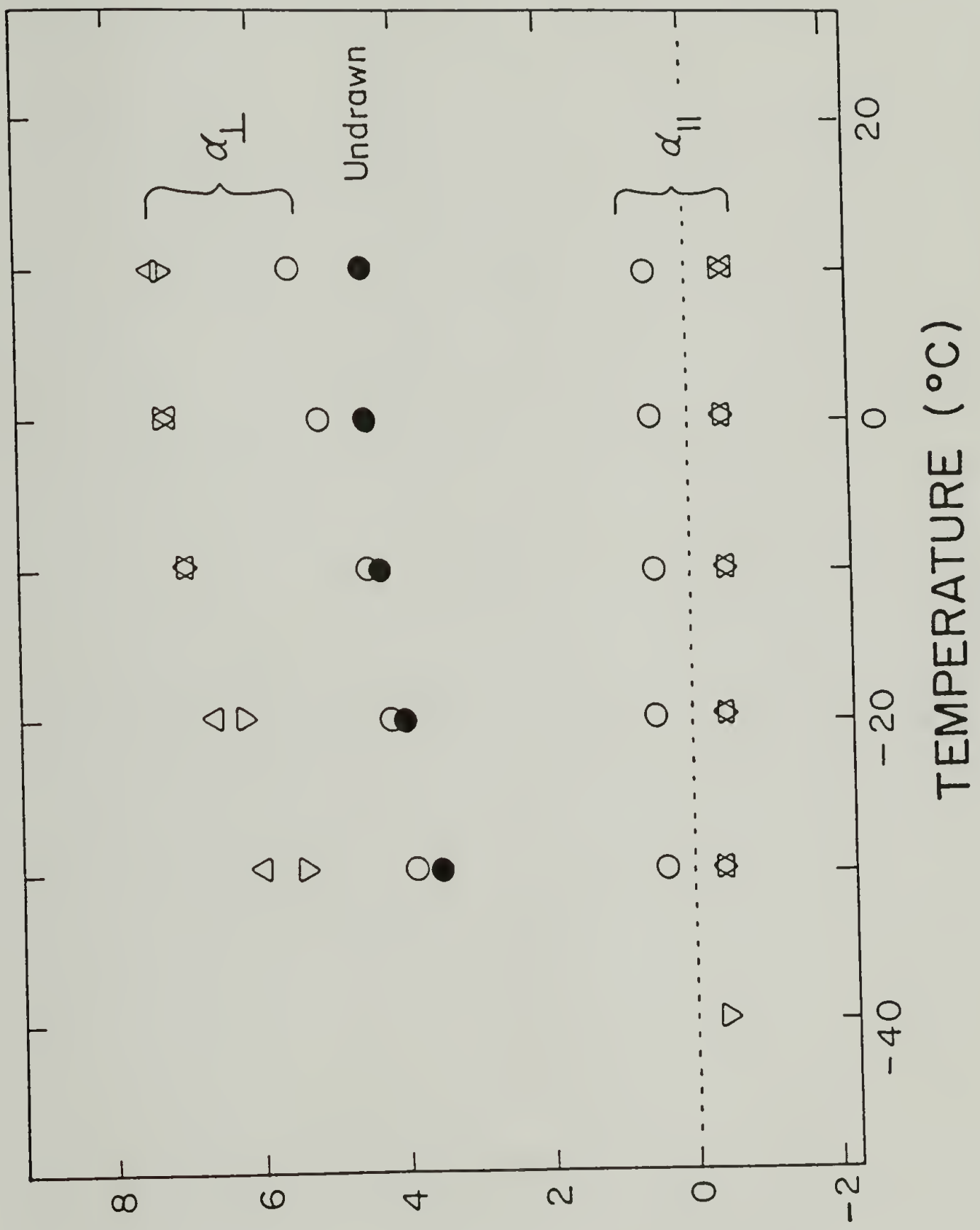

Figure 5.8. Thermal expansivity of drawn PEEK rods along (//) and perpendicular (⊥) to the draw direction as functions of temperature. (●) Undrawn, (○) EDR 2.7, (▽) EDR 3.8, (△) EDR 5.5.

expansivity of the drawn PEEK rod was measured by Lefebvre in our laboratory. The thermal expansivities of the undrawn rod and drawn rods in the transverse direction ($\alpha_{\perp}$) increased with temperature, whereas along the drawing direction ($\alpha_{//}$) they are almost constant in the range from -40 to +10°C. An interesting feature in Fig. 5.8 is the the observation of a negative longitudinal expansivity at high EDR. This is a common phenomenon in highly crystalline polymers, where crystal continuity may be developed during deformation [132,133]. The continuous intercrystalline bridges have high axial stiffness and thus will constrain the expansion of adjacent amorphous regions. This is unlikely to occur in the case of PEEK, since the crystallinity of the rod with EDR 5.5 was calculated to be 27% from the density, assuming 1.415 [40] and 1.263 g/cm^3 as the densities of crystalline and amorphous PEEK, respectively. This may indicate that highly elongated amorphous tie molecules behave in the same way as continuous crystalline bridges [134].

5.3.3 Differential Scanning Calorimetry

Fig. 5.9 shows DSC traces of the initial and drawn PEEK films. The initial crystal structure is considered to be distorted and transformed to a chain-extended crystal structure on drawing [135]. The chain-extended crystals may become larger and/or more perfect with drawing, which explains why the melting temperature increases with increasing EDR.

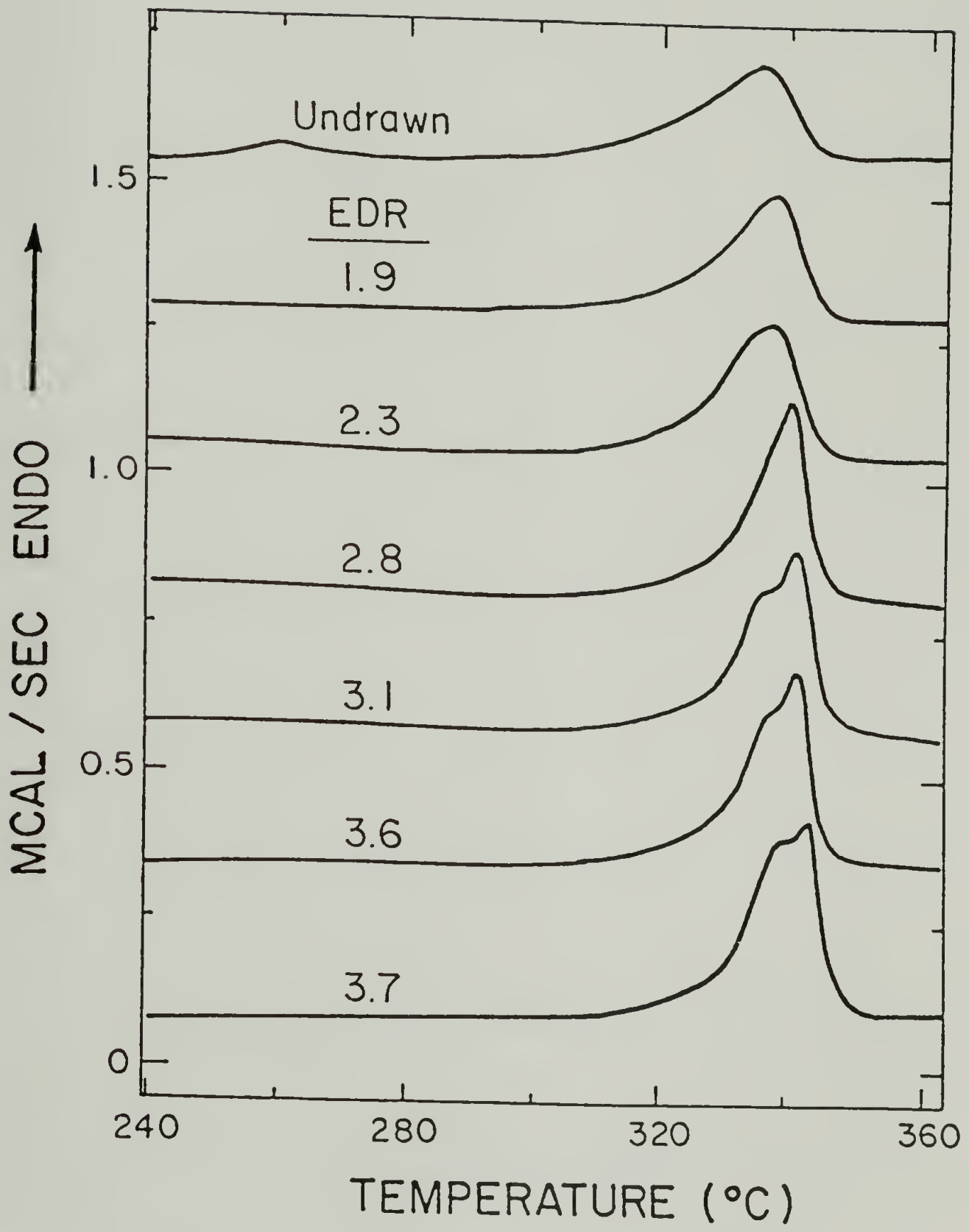

Figure 5.9. Melting endotherms of undrawn and drawn PEEK films; extrusion temperature 154°C.

As discussed in Chapter II, isothermally crystallized or annealed PEEK shows two distinct melting peaks in DSC heating-scans. The low-temperature melting peak is 10-20°C higher than the crystallization or annealing temperature. The high-temperature melting peak is almost constant (about 337°C), regardless of crystallization temperature and time. The low-temperature endotherm represents a portion of the melting of the crystals which exist in the sample prior to the DSC heating. The high-temperature endotherm is associated with the crystals which have been reorganized through partial melting and recrystallization on heating. The initial PEEK film was crystallized at 240°C and showed a low-temperature melting peak at 260°C (Fig. 5.9, Undrawn). However, no endothermic melting trace is found around 260°C in any drawn films. This provides evidence that the initially deformed crystals readily reorganize on heating. For the initial PEEK film, the glass transition temperature (T_g) was observed around 148°C. However, for drawn films the T_g was barely detectable, due to a superposed cold-crystallization exotherm which began around 150°C. With increasing EDR, the heat of the cold-crystallization increased up to 0.9 cal/g, corresponding to about 2% crystallinity assuming 39.5 cal/g (Section 2.3.5) as the heat of fusion for PEEK crystal.

Fig. 5.10 shows the DSC traces of undrawn and drawn PEEK rods. As for the drawn films (Fig. 5.9), the melting peak is shifted to higher temperature with increasing EDR. Since the extrusion temperature of the rods is well above T_g, no trace of cold-crystallization was observed.

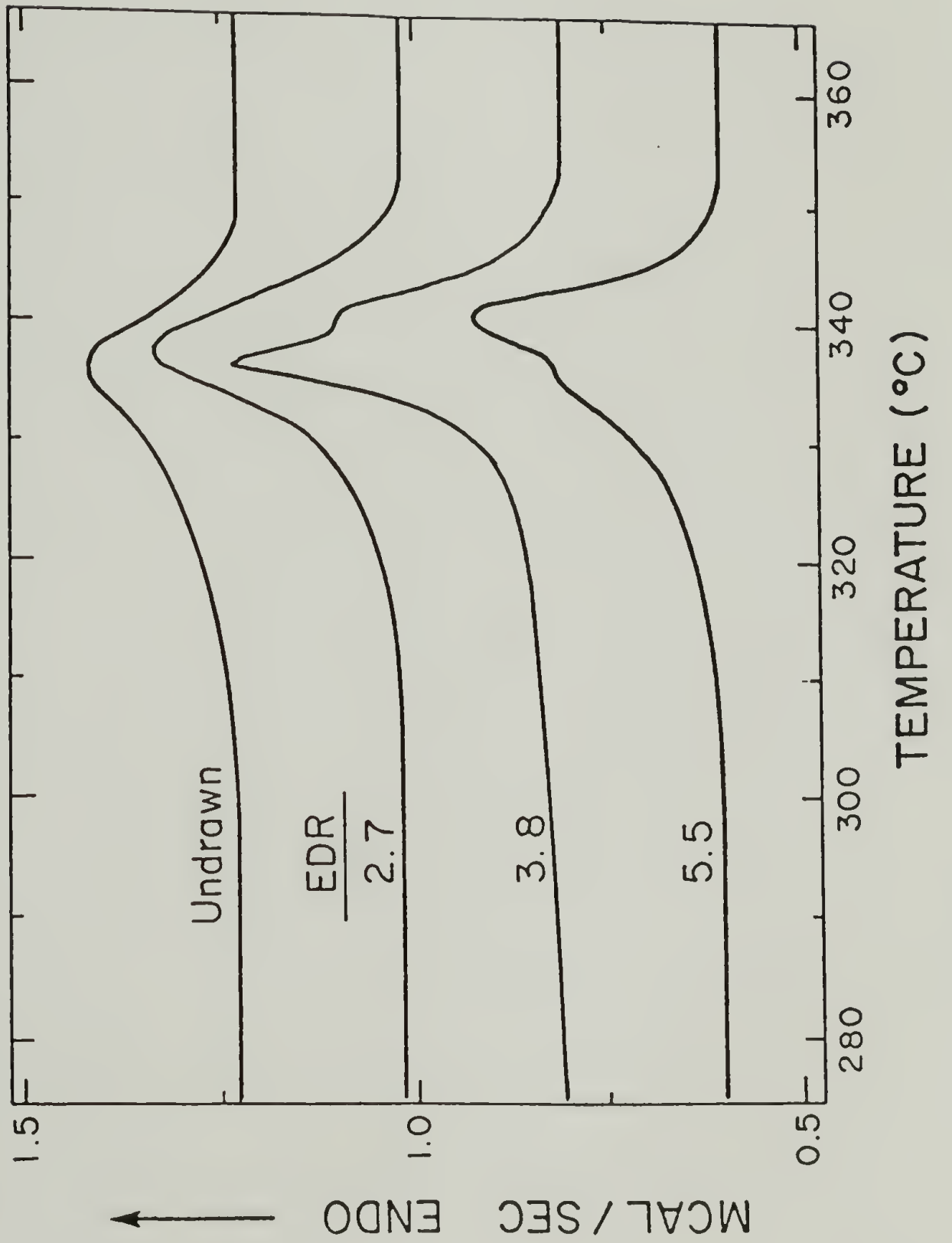

Figure 5.10. Melting endotherms of undrawn and drawn PEEK rods; extrusion temperature 310°C.

5.3.4 Density of Drawn PEEK

Fig. 5.11 shows the densities of PEEK rods and films plotted vs. EDR. Since rods are simultaneously deformed and annealed during extrusion at 310°C, the density increases with EDR. However, the temperature (154°C) at which the PEEK films were extruded is not sufficiently high to allow deformed crystals to reorganize. The observed initial decrease in density is considered to be due to the partial distortion and subsequent partial destruction of the initial crystals. At high EDR, the amorphous region is extended to pack more closely. Indeed, it has been found for polyethylene that the effective density of the crystalline region decreases while that of the noncrystalline region increases on drawing [136]. Also, formation of any extended-chain crystals will contribute to an increase in density. Therefore, a combination of these two opposing processes may generate the observed minimum in density on drawing of PEEK films. Similar behavior has been reported for high density polyethylene [137] and poly(ethylene terephthalate) [138]. In contrast to the minimum density at EDR 2.8, the heat of fusion of the melting peaks in Fig. 5.9 were measured to increase monotonously with EDR. This also suggests that the initial crystals which have been partially destructed on drawing, readily reorganize on heating.

5.3.5 Tensile Properties

Fig. 5.12 shows tensile moduli and strengths at break for PEEK films plotted vs. EDR. Both moduli and strengths increase linearly

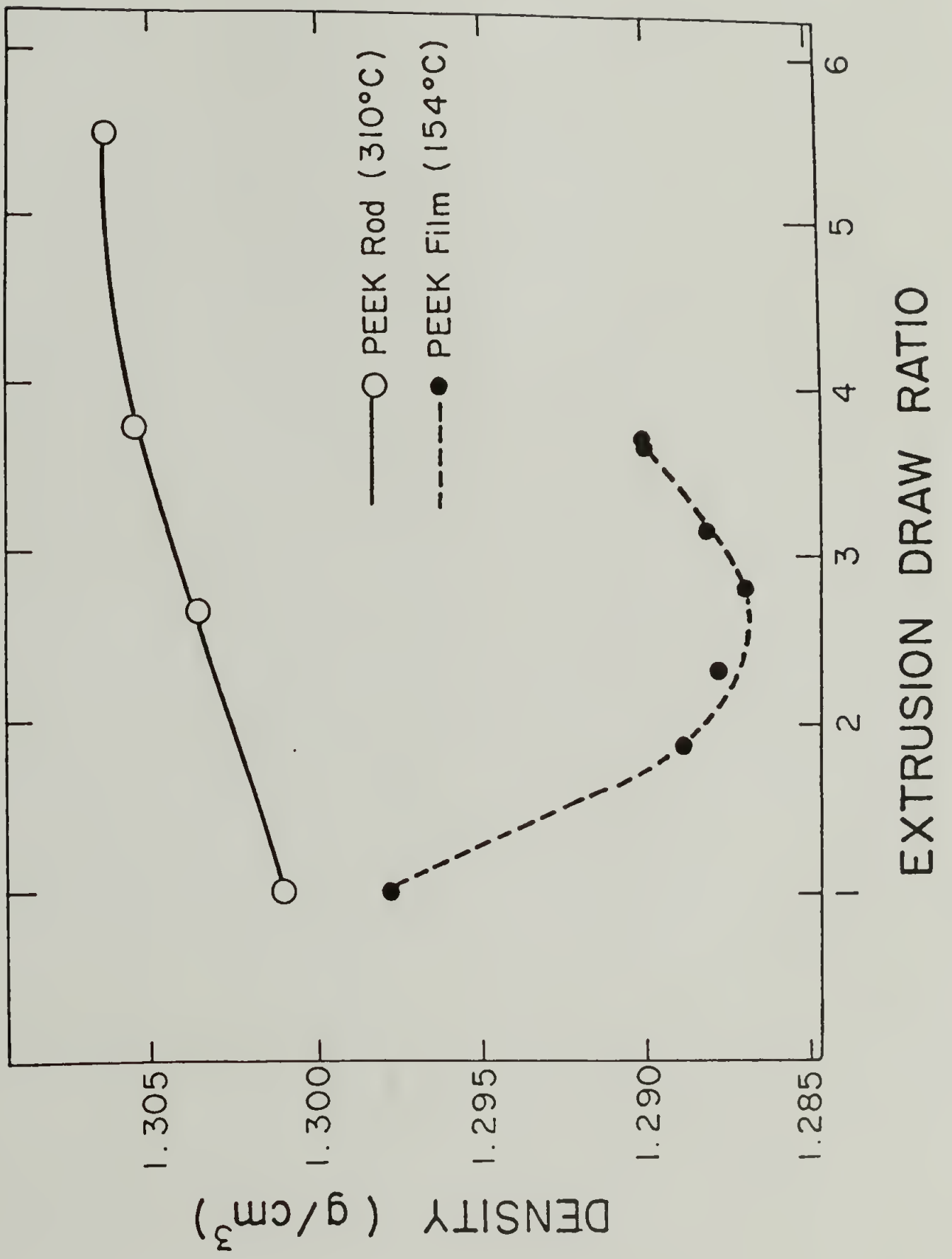

Figure 5.11. Densities of drawn PEEK rods and films as a function of EDR.

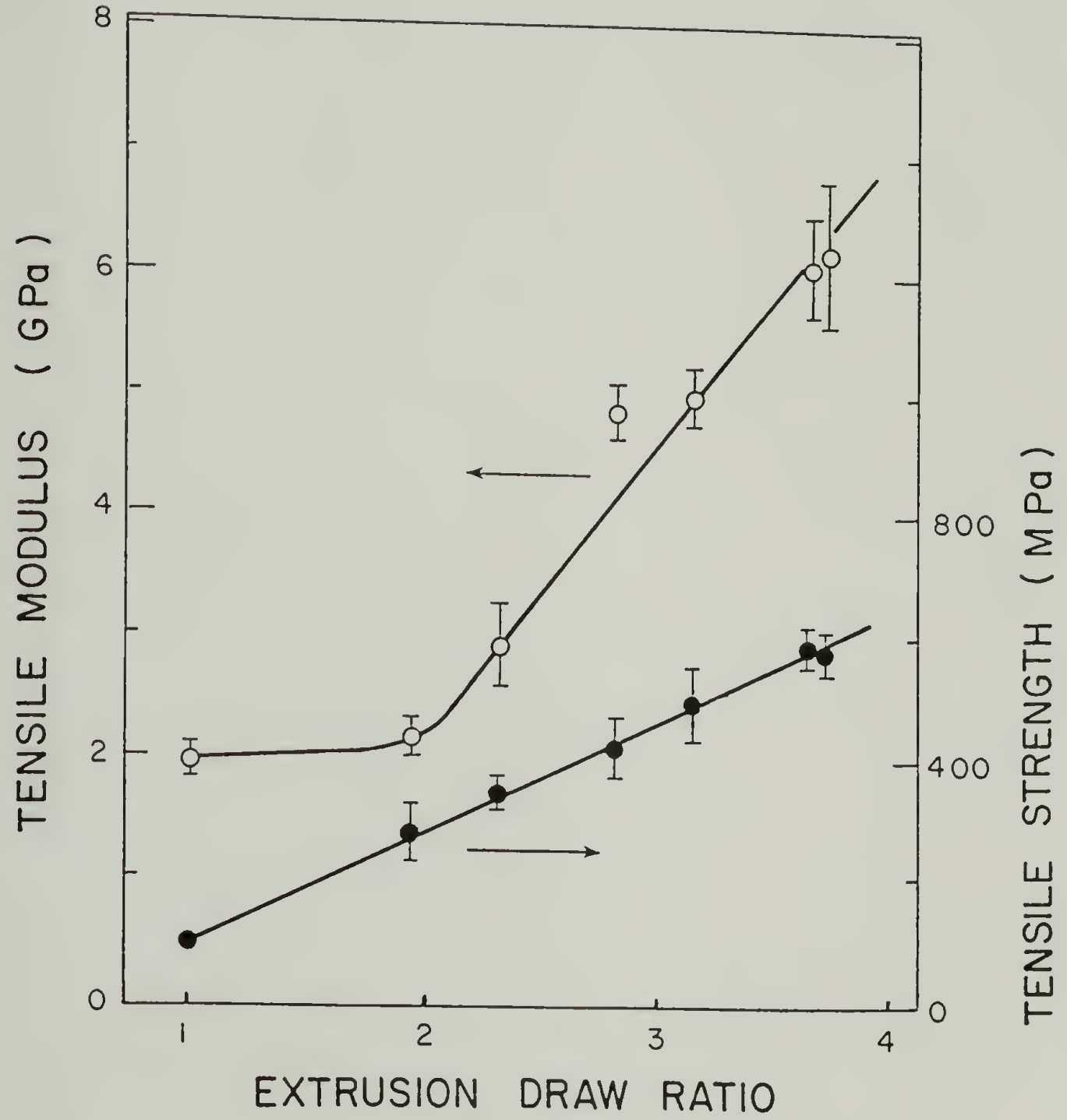

Figure 5.12. Tensile modulus and strength of drawn PEEK films as a function of EDR.

with EDR, beyond an insensitive initial region for moduli at EDR ≤ 2. Moduli up to 6.5 GPa, more than 3 times the value of the undrawn film, were obtained and are comparable with previously reported flexural moduli [122]. Tensile strengths up to 600 MPa, about 6 times the value of undrawn film, were also obtained. The dynamic modulus of 13.3 GPa was measured for zone-annealed PEEK films [123]. Drawn rods were not long enough to measure mechanical properties reproducibly.

5.4 Conclusions

PEEK has been drawn using the solid-state extrusion technique to produce highly oriented crystalline regions. The c axis orientation function, total birefringence, melting temperature, tensile modulus, and strength were increased with EDR, indicating that the PEEK chains in the crystals were oriented to the draw direction and transformed to chain-extended crystals. The crystal orientation tends to level off beyond EDR of 3.8 as reflected in the thermal expansion behavior. Total birefringence also levels off at the value of 3.0 which is comparable with the maximum birefringence of PEEK crystal along the molecular chain, 0.34.

Wide-angle X-ray diffraction patterns of drawn PEEK films and rods showed the weak (001) crystal reflection. This may indicate a slight perturbation of the planar zig-zag conformation of the PEEK chains in

the crystal and/or slight differences in the packing of the ether and ketone groups.

The tensile properties were improved on drawing. The modulus and strength were increased by 3 and 6 times, respectively. The densities of PEEK films drawn at 154°C showed a minimum at EDR of 2.8 probably due to a combination of two opposing effects: the partial destruction of the initial lamellae and the denser packing of amorphous chains on drawing.

CHAPTER VI

SUGGESTIONS FOR FUTURE WORK

The double-melting behavior of PEEK was described and explained. The present study suggests that the double-melting behavior of PEEK is associated with the surface structure of its crystal. An interesting future study would be to investigate the interfacial structure between crystalline and amorphous regions using small-angle X-ray scattering (SAXS), low-frequence Raman spectroscopy, and nuclear magnetic resonance (NMR). SAXS of PEEK at the Porod region may yield valuable information about the thickness of the diffuse interfacial boundary. Low-frequency Raman spectroscopy has recently been used to measure the thickness of configurationally disordered regions, as opposed to core crystals in a lamella. The fraction of interfacial regions can also be determined using NMR. These studies on PEEK are expected to render a general morphological characteristic of the polymers showing multiple-melting due to the reorganization.

Though the melting behavior of PEEK crystallized in the bulk state has been reported, that of PEEK crystallized in solution is an unexplored area. The relationship between melting behavior, crystallization and dissolution temperature, solvent, and concentration of PEEK would be valuable to investigate and complementary to the present work. Crystallization of PEEK in

solution on the carbon fiber surface also seems to be very useful toward understanding the role of the surface in nucleation of PEEK. The available evidence suggests that carbon fiber surfaces induce directional crystal growth of PEEK while glass fiber surfaces do not. Studies of solution-crystallization of PEEK on PEEK fibers, aramid and other reinforcement-fibers may also be interesting.

Isothermal crystallization studies of PEEK using differential scanning calorimetry (DSC) was somewhat limited because DSC is not sufficiently sensitive to follow a slow crystallization or low heat flow. Therefore, dilatometry is suggested for following the slow crystallization after long melt-annealing time or high melt-annealing temperature.

Another intriguing study would be to examine whether the crystallization characteristics of PEEK investigated in Chapter III is a general behavior of semicrystalline polymers. Though three PEEK samples of different molecular weights were investigated, crystallization experiments of PEEK with an even wider range of molecular weight are proposed. Since the effect of melt-annealing time is considered to be associated with chain entanglements, PEEK with molecular weight below the entanglement molecular weight is particularly interesting.

In Chapter IV, it was observed using the transverse tensile test that carbon fiber-reinforced PEEK composites with more crystalline interface had stronger interfacial bond strength. Some other

mechanical experiments such as dynamic mechanical testing and three-point bending are suggested. Dynamic mechanical testing is also proposed for drawn PEEK films. Since PEEK can have various morphologies, e.g., amorphous, small crystallites and well-developed spherulites, the solid-state extrusion of PEEK with a wide variation in morphology may yield additional information as to the deformation mechanism of PEEK.

REFERENCES

1. Johnson, R.N.; Farnham, A.G; Clendinning, R.A.; Hale, W.H.; Merriam, C.N. J. Polym. Sci., Chem. Ed. 1967, 5, 2375.

2. Rose, J.B. Am. Chem. Soc., Polymer Preprints 1986, 27(1), 480.

3. Kricheldorf, H.R.; Bier, G. Polymer 1984, 25, 1151.

4. Attwood, T.E.; Dawson, P.C.; Freeman, J.L.; Hoy, R.J.; Rose, J.B.; Staniland, P.A. Polymer 1981, 22, 1096.

5. Rose, J.B. Univ. of Surrey, England, Private Communication.

6. Cogswell, F.N.; Hopprich, M. Composites 1983, 14, 251.

7. Rigby, R.B. Polymer News 1984, 9, 325.

8. Blundell, D.J.; Osborn, B.N. Polymer 1983, 24, 953.

9. White, T.R. Nature 1955, 175, 895.

10. Bell, J.P.; Slade, P.E.; Dumbleton, J.H. J. Polym. Sci., Phys. Ed. 1968, 6, 1773.

11. Bell, J.P.; Dumbleton, J.H. J. Polym. Sci., Phys. Ed. 1969, 7, 1033.

12. Sweet, G.E.; Bell, J.P. J. Polym. Sci., Polym. Phys. Ed. 1972, 10, 1273.

13. Roberts, R.C. Polymer 1969, 10, 117.

14. Roberts, R.C. J. Polym. Sci., Polym. Lett. Ed. 1970, 8, 381.

15. Holdsworth, P.J.; Turner-Jones, A. Polymer 1971, 12, 195.

16. Alfonso, G.C.; Pedemonte, E.; Ponzetti, L. Polymer 1979, 20, 104.

17. Lemstra, P.J.; Kooistra, T.; Challa, G. J. Polym. Sci., Polym. Phys. Ed. 1972, 10, 823.

18. Boon, J.; Challa, G.; Van Krevelen, D.W. J. Polym. Sci., Polym. Phys. Ed. 1968, 6, 1791.

19. Mandelkern, L.; Allow, A.L. J. Polym. Sci., Polym. Lett. Ed., 1966, 4, 447.

20. Bair, H.E.; Salovey, R.; Huseby, T.W. Polymer 1967, 8, 9.

21. Jaffe, M.; Wunderlich, B. Kolloid-Z. Z. Polym. 1967, 216, 203.

22. Lovering, E.G.; Wooden, D.C. J. Polym. Sci., Polym. Phys. Ed. 1969, 7, 1639.

23. Samuels, R.J. J. Polym. Sci., Polym. Phys. Ed. 1975, 13, 1417.

24. Prest, W.M.,Jr.; Luca, D. J. J. Appl. Phys. 1975, 46, 4136.

25. Edwards, B.C. J. Polym. Sci., Polym. Phys. Ed. 1975, 13, 1387.

26. Briber, R.M.; Thomas, E.L. Polymer 1985, 26, 8.

27. Yadav, Y.S.; Jane, P.C. Polymer 1986, 27, 721.

28. Nguyen, H.X.; Ishida, H. Polymer Composites 1987, 8, 57.

29. Hay, J.N.; Kemmish, D.J.; Langford, J.I.; Rae, A.I.M. Polymer, 1984, 25(Commun.), 175.

30. Kumar, S.; Anderson, D.P.; Adams, W.W. Polymer, 1986, 27, 329.

31. Kemmish, D.J.; Hay, J.N. Polymer 1985, 26, 905.

32. Nguyen, H.X.; Ishida, H. Polymer 1986, 27, 1400.

33. Louden, J.D. Polymer 1986, 27(Commun.), 82.

34. Clark, J.N.; Herring, F.G.; Jagannathan, N.R. Polymer 1985, 26(Commun.), 329.

35. Harrison, I.R.; Runt, J. J. Polym. Sci., Polym. Phys. Ed. 1979, 17, 321.

36. Manual for model DSC-4, Perkin-Elmer Corp., Norwalk, Connecticut, U.S.A., 1984.

37. Annual Book of ASTM Standards; American Society for Testing and Materials: Philadelphia, 1979; Designation: D 1505-68.

38. Cheng, S.Z.D.; Cao, M.Y.; Wunderlich, B. Macromolecules 1986, 19, 1868.

39. Wunderlich, B. Macromolecular Physics; Academic: New York, 1980; Vol. 3.

40. Rueda, D.R.; Ania, F.; Richardson, A.; Ward, I.M.; Balta-Calleja, F.J. Polymer 1983, 24(Commun.), 258.

41. Fischer, E.W.; Fakirov, S. J. Mater. Sci. 1976, 11, 1041.

42. Groeninckx, G; Reynaers, H. J. Polym. Sci., Polym. Phys. Ed., 1980, 18, 1325.

43. Rim, P.B.; Runt, J.P. Macromolecules 1983, 16, 762.

44. Zachmann, H.G.; Peterlin, A. J. Macromol. Sci., Phys. Ed. 1969, 3, 495.

45. Arakawa, T.; Nagatoshi, F.; Arai, N. J. Polym. Sci., Polym. Lett. Ed. 1969, 7, 115.

46. Kavesh, S.; Schultz, J.M. J. Polym. Sci., Polym. Phys. Ed. 1971, 9, 85.

47. Cebe, P.; Hong, S.D. Polymer 1986, 27, 1183.

48. Olley, R.H.; Bassett, D.C.; Blundell, D.J. Polymer 1986, 27,344.

49. Hoffman, J.D.; Davis, G.T.; Lauritzen, J.I. Treatise on Solid State Chemistry; Vol 3(Hannay, N.B. Ed.), Plenum Press: New York, 1976.

50. Bassett, D.C. Principles of Polymer Morphology; Cambridge University: Cambridge, 1981.

51. Hoffman, J.D.; Weeks, J.J. J. Res. Nat. Bur. Std.(U.S.). 1962, 66A, 13.

52. Weeks, J.J. J. Res. Nat. Bur. Std.(U.S.) 1963, 67A, 441.

53. Hoffman, J.D.; Weeks, J.J. J. Chem. Phys. 1965, 42, 4301.

54. Blundell, D.J.; Beckett, D.R.; Willcocks, P.H. Polymer 1981, 22, 704.

55. Gray, A.P. Thermochimica Acta 1970, 1, 563.

56. Dawson, P.C.; Blundell, D.J. Polymer 1980, 21, 577.

57. Wakelyn, N.T. Polymer 1984, 25(Commun.), 306.

58. Wakelyn, N.T. J. Polym. Sci., Polym. Lett. Ed. 1987, 25, 25.

59. Groeninckx, G.; Reynaers, H.; Berghmans, H.; Smets, G. J. Polym. Sci., Polym. Phys. Ed. 1980, 18, 1311.

60. Wunderlich, B. Macromolecular Physics; Academic: New York, 1976; Vol. 2.

61. Rabesiaka, J.; Kovacs, A.J. J. Appl. Phys. 1961, 32, 2314.

62. Collier, J.R.; Leal, L.M. Polym. Eng. Sci. 1969, 9, 182.

63. Boon, J.; Challa, G.; Van Krevelen, D.W. J. Polym. Sci., Polym. Phys. Ed. 1968, 6, 1791.

64. Hoffman, J.D.; Weeks, J.J.; Murphy, W.M. J. Res. Nat. Bur. St. 1959, 63A, 67.

65. Price, F.P. J. Amer. Chem. Soc. 1952, 74, 311.

66. Magill, J.H. Polymer 1962, 3, 43.

67. McLaren, J.V. Polymer 1963, 4, 175.

68. Banks, W.; Sharples, A. Makromol. Chem. 1963, 67, 42.

69. Barnes, W.J.; Luetzel, W.G.; Price, F.P. J. Phys. Chem. 1961, 65, 1742.

70. Limbert, F.J.; Baer, E.J. Polym. Sci., Polym. Chem. Ed. 1963, 1, 3317.

71. Keller, A.; Lester, G.R.; Morgan, L.B. Phil. Trans. 1954, A247, 1.

72. Hartley, F.D.; Lord, F.W.; Morgan, L.B. Phil. Trans. 1954, A247, 23.

73. Keller, A.; Willmouth, F.M. J. Polym. Sci., Polym. Phys. Ed. 1970, 8, 1443.

74. Blundell, D.J.; Keller, A. J. Macromol. Sci., Phys. Ed. 1968, 2, 301.

75. Banks, W.; Gordon, M.; Sharples, A. Polymer 1963, 4, 289.

76. Sharples, A. Polymer 1962, 3, 250.

77. Shukla, J.G.; Sichina, W.J. SPE ANTEC 1984, Tech. Papers 30, 265.

78. Sichina, W.J.; Gill, P.S. SPE ANTEC 1985, Tech. Papers 31, 293.

79. Morgan, L.B. J. Appl. Chem. 1954, 4, 160.

80. Blundell, D.J.; Keller, A.; Kovacs, A.J. J. Polym. Sci., Polym. Lett. Ed. 1966, 4, 481.

81. Turnbull, D. J. Chem. Phys. 1950, 18, 198.

82. Bailly, C.; Williams, D.J.; Karasz, F.E.; MacKnight, W.J. Polymer 1987, 28, 1009.

83. Avrami, M. J. Chem. Phys. 1939, 7, 1103.

84. Avrami, M. J. Chem. Phys. 1940, 8, 212.

85. Chien, M.C.; Weiss, R.A.; Miller, A.L. SPE ANTEC 1986, Tech. Papers 32, 449.

86. Vidotto, G.; Levy, D.; Kovacs, A.J. Kolloid Z.Z. Polym. 1969, 230, 289.

87. Brandrup, J.; Immergut, E.H. Polymer Handbook; John Wiley and Sons, 2nd Ed.: New York, 1975.

88. Boon, J.; Challa, G.; Van Krevelen, D.W. J. Polym. Sci., Polym. Phys. Ed. 1968, 6, 1835.

89. Illers, K.H.; Haberkorn, H. Makromol. Chem. 1971, 142, 31.

90. Fakirov, S.; Avramova, N. J. Polym. Sci., Polym. Lett. Ed. 1982, 20, 635.

91. Fakirov, S.; Avramova, N. IUPAC 1985, Symposium on noncrystalline order in polymers, 119.

92. Binsbergen, F.L. Nature 1966, 211, 516.

93. Avramova, N.; Fakirov, S.; Avramov, I. J. Polym. Sci., Polym. Lett. Ed. 1984, 22, 311.

94. Lemstra, P.J.; Postma, J.; Challa, G. Polymer 1974, 15, 757.

95. Velisaris, C.N.; Seferis, J.C. SPE ANTEC 1985, Tech. Papers 31, 401.

96. Prime, R.B.; Seferis, J.C. J. Polym. Sci., Polym. Lett. Ed. 1986, 24, 641.

97. Kardos, J.L. J. Adhesion 1973, 5, 119.

98. Kardos, J.L.; Cheng, F.S.; Tolbert, T.L. Polym. Eng. Sci. 1973, 13, 455.

99. Hobbs, S.Y. U.S. Patent 1974, 3 812 077.

100. Bessell, T; Shortall, J.B. J. Mater. Sci. 1975, 10, 2035.

101. Frayer, P.O.; Lando, J.B. J. Polym. Sci., Polym. Lett. Ed. 1972, 10, 29.

102. Tuinstra, F.; Baer, E. J. Polym. Sci., Polym. Lett. Ed. 1970, 8, 861.

103. Hobbs, S.Y. Nature Phys. Sci. 1971, 234, 12.

104. Cogswell, F.N. 28th Natl. SAMPE Symp. 1983, 528.

105. Binsbergen, F.L. J. Polym. Sci., Polym. Symp. Ed. 1977, 59, 11.

106. Hull, D. An Introduction to Composite Materials; Cambridge University: Cambridge, 1981.

107. Nguyen, H.X.; Ishida, H. Amer. Chem. Soc., Polymer Preprint 1985, 26, 273.

108. Koutsky, J.A.; Walton, A.G.; Baer, E. J. Polym. Sci., Polym. Lett. Ed. 1967, 5, 185.

109. Eby, R.K. J. Appl. Phys. 1964, 35, 2720.

110. Chatterjee, A.M.; Price, F.P.; Newman, S. J. Polym. Sci., Polym. Phys. Ed. 1975, 13, 2369.

111. Gray, D.G. J. Polym. Sci., Polym. Lett. Ed. 1974, 12, 645.

112. Barlow, C.Y.; Fife, B.; Nield, E.; Peacock, J.A. A Fiber-Matrix Interface Study of Some Experimental PEEK/Carbon-Fibre Composites, International Conference on Composite Interfaces, Cleveland, May, 1986.

113. Crick, R; Fife B.; Nield, E.; Peacock. J.A. Examination of the Morphology of Aromatic Polymer Composites (APC-2) Using an Etching Technique, International Conference on Composite Interfaces, Cleveland, May, 1986.

114. Keith, H.D.; Padden, F.J. J. Appl. Phy. 1963, 34, 2409.

115. Belbin, G.R.; Brewster, I.; Cogswell, F.N.; Hezzell, D.J.; Swerdlow, M.S. SPE 7th PACTEC Preprint 1983, 376.

116. Zachariades, A.E.; Porter, R.S. The Strength and Stiffness of Polymers; Marcel Dekker Inc.: New York, 1983.

117. Vincent, P.I. Polymer 1968, 1, 7.

118. Chuah, H.H. Structure-Property Studies in the Deformation of Semicrystalline Polymers, Ph.D. Dissertation, University of Massachusetts, 1985.

119. Zachariades, A.E.; Mead, W.T.; Porter, R.S. Chem. Reviews 1980, 80, 251.

120. Gibson A.G.; Ward, I.M.; Cole, B.N.; Parsons, B. J. Mater. Sci. 1974, 9, 1193.

121. Zachariades, A.E.; Porter, R.S. J. Macromol. Sci., Polym. Phys. Ed. 1981, 19, 377.

122. Richardson, A.; Ania, F.; Rueda, D.R.; Ward, I.M.; Balta-Calleja, F.J. Polym. Eng. Sci. 1985, 25, 355.

123. Kunugi, T.; Mizushima, A.; Hayakawa, T. Polymer, 1986, 27(Commun.), 175.

124. Alexander, L.E. X-ray Diffraction Methods in Polymer Science; Kriegen: Huntington, NY, 1979.

125. Wilchinsky, Z.W. Advances in X-ray Analysis; Plenum Press: New York, 1963, Vol. 6, 231.

126. Fratini, A.V.; Cross, E.M.; Whitaker R.B.; Adams, W.W. Polymer 1986, 27, 861.

127. Dawson, P.C.; Blundell, D.J. Polymer 1980, 21, 577.

128. Atkins, E. Univ. of Bristol, England, Private Communication.

129. Stein, R.S. J. Polym. Sci. 1958, 31, 327.

130. Chuah, H.H.; Porter, R.S. J. Polym. Sci., Polym. Phys. Ed. 1984, 22, 1353.

131. Lee, Y.; Lefebvre, J-M.; Porter, R.S. J. Polym. Sci., Polym. Phys. Ed. in press.

132. Choy, C.L.; Chen, F.C.; Ong, E.L. Polymer 1979, 20, 1191.

133. Choy, C.L.; Ito, M.; Porter, R.S. J. Polym. Sci., Polym. Phys. Ed. 1983, 21, 1427.

134. Choy, C.L.; Chen, F.C.; Young, K. J. Polym. Sci., Polym. Phys. Ed. 1981, 19, 335.

135. Peterlin, A. J. Mater. Sci. 1971, 6, 490.

136. Adams, W.W.; Briber, R.M.; Sherman, E.S.; Porter, R.S.; Thomas, E.L. Polymer 1985, 26, 17.

137. Chuah, H.H.; DeMicheli, P.E.; Porter, R.S. J. Polym. Sci., Lett. Ed. 1983, 21, 791.

138. Pereira, J.R.C.; Porter, R.S. J. Polym. Sci., Polym. Phys. Ed. 1983, 21, 1147.

BIBLIOGRAPHY

Adams, W.W.; Briber, Robert M.; Sherman, Edward S.; Porter, Roger S.; Thomas, Edwin L., "Microstructure of High Modulus Solid State Extruded Polyethylene:2", Polymer 1985, 26, 17-26.

Alexander, Leroy E. X-ray Diffraction Methods in Polymer Science; Kriegen: Huntington, NY, 1979.

Alfonso, Giovanni C.; Pedemonte, Enrico; Ponzetti, Lorenzo, "Mechanism of Densification and Crystal Perfection of Poly(ethylene terephthalate)", Polymer 1979, 20, 104-112.

Annual Book of ASTM Standards; "Density of Plastics by the Density-Gradient Technique", American Society for Testing and Materials: Philadelphia, 1979; Designation: D 1505-68, 674-700.

Arakawa, Tamio; Nagatoshi, Fumio; Arai, Naoki, "Thermal Analysis of Lamellar Crystals of Nylon 6", J. Polym. Sci., Polym. Lett. Ed. 1969, 7, 115-120.

Atkins, E., Univ. of Bristol, England, Private Communication.

Attwood, T.E.; Dawson, P.C.; Freeman, J.L.; Hoy, R.J.; Rose, J.B.; Staniland, P.A., "Synthesis and Properties of Poly Aryl Ether Ketones", Polymer 1981, 22, 1096-1103.

Avrami, Melvin, "Kinetics of Phase Change. I. General Theory", J. Chem. Phys. 1939, 7, 1103-1112.

Avrami, Melvin, "Kinetics of Phase Change. II. Transformation-Time Relations for Random Distribution of Nuclei", J. Chem. Phys. 1940, 8, 212-224.

Avramova, N.; Fakirov, S.; Avramov, I., "Cumulative Memory Effect in Nylon 6", J. Polym. Sci., Polym. Lett. Ed. 1984, 22, 311-313.

Bailly, Cristian; Williams, David J.; Karasz, Frank E.; MacKnight, William J., "The Sodium Salts of Sulphonated Poly(aryl ether ether ketone): Preparation and Characterization", Polymer 1987, 28, 1009-1016.

Bair, H.E.; Salovey, R.; Huseby, T.W., "Melting and Annealing of Polyethylene Single Crystals", Polymer 1967, 8, 9-20.

Banks, W.; Gordon, M.; Sharples, A., "The Crystallization of Polyethylene Crystal Nuclei", Polymer 1963, 4, 289-302.

Banks, W.; Sharples, A., "The effects of Melt Temperature on Nucleation in Crystallizing Polymers", Makromol. Chem. 1963, 67, 42-48.

Barlow, C.Y.; Fife, B.; Nield, E.; Peacock, J.A., "A Fiber-Matrix Interface Study of Some Experimental PEEK/Carbon-Fibre Composites", International Conference on Composite Interfaces, Cleveland, Ohio, May, 1986.

Barnes, W.J.; Luetzel, W.G.; Price, F.P., "Crystallization of Poly(ethylene oxide) in Bulk", J. Phys. Chem. 1961, 65, 1742-1748.

Bassett, D.C. Principles of Polymer Morphology; Cambridge University: Cambridge, 1981.

Belbin, G.R.; Brewster, I.; Cogswell, F.N.; Hezzell, D.J.; Swerdlow, M.S., "Carbon Fiber Reinforced Poly(ether ether ketone): A Thermoplastic Composite for Aerospace Applications", SPE 7th PACTEC Preprint 1983, 376-385.

Bell, J.P.; Dumbleton, J.H., "Relation between Melting Behavior and Physical Structure in Polystyrene", J. Polym. Sci., Phys. Ed. 1969, 7, 1033-1057.

Bell, J.P.; Slade, P.E.; Dumbleton, J.H., "Multiple Melting in Nylon 6,6", J. Polym. Sci., Phys. Ed. 1968, 6, 1773-1781.

Bessell, T; Shortall, J.B., "The Crystallization and Interfacial Bond Strength of Nylon 6 at Carbon Fiber and Glass Fiber Surfaces", J. Mater. Sci. 1975, 10, 2035-2043.

Binsbergen, F.L., "Natural and Artificial Heterogeneous Nucleation in Polymer Crystallization", J. Polym. Sci., Polym. Symp. Ed. 1977, 59, 11-29.

Binsbergen, F.L., "Orientation-Induced Nucleation in Polymer Crystallization", Nature 1966, 211, 516.

Blundell, D.J.; Beckett, D.R.; Willcocks, P.H., "Routine Crystallinity Measurements of Polymers by DSC", Polymer 1981, 22, 704-707.

Blundell, D.J.; Keller, A., "Nature of Self-Seeding Polyethylene Crystal Nuclei", J. Macromol. Sci. 1968, B2, 301-336.

Blundell, D.J.; Keller, A.; Kovacs, A.J., "A New Self-Nucleation Phenomenon and Its Application to the Growing of Polymer Crystals from Solution", J. Polym. Sci., Polym. Lett. Ed. 1966, 4, 481-487.

Blundell, D.J.; Osborn, B.N., "The Morphology of Poly(aryl ether ether ketone)", Polymer 1983, 24, 953-958.

Boon, J.; Challa, G.; Van Krevelen, D.W., "Crystallization Kinetics of Isotactic Polystyrene. I. Spherulitic Growth Rate", J. Polym. Sci., Polym. Phys. Ed. 1968, 6, 1791-1801.

Boon, J.; Challa, G.; Van Krevelen, D.W., "Crystallization Kinetics of Isotactic Polystyrene. II. Influence of Thermal History on Number of Nuclei", J. Polym. Sci., Polym. Phys. Ed. 1968, 6, 1835-1851.

Brandrup, J.; Immergut, E.H. Polymer Handbook; John Wiley and Sons, 2nd Ed.: New York, 1975.

Briber, Robert M.; Thomas, Edwin L., "Crystallization Behavior of Random Block Copolymers of Poly(butylene terephthalate) and Poly(tetramethylene ether glycol)", Polymer 1985, 26, 8-16.

Cebe, Peggy.; Hong,Su-Don, "Crystallization Behavior of Poly(ether ether ketone)", Polymer 1986, 27, 1183-1192.

Chatterjee, A.M.; Price, F.P.; Newman, S., "Heterogeneous Nucleation of Crystallization of High Polymers from the Melt", J. Polym. Sci., Polym. Phys. Ed. 1975, 13, 2369-2383.

Cheng, Stephen Z.D.; Cao, M.Y.; Wunderlich, Bernhard, "Glass Transition and Melting Behavior of Poly(oxy-1,4-phenylene-oxy-1,4-phenylenecarbonyl-1,4-phenylene)", Macromolecules 1986, 19, 1868-1876.

Chien, M.C.; Weiss, R.A.; Miller, A.L., "Strain-Induced Crystallization of PEEK", SPE ANTEC 1986, Tech. Papers 32, 449-450.

Choy, C.L.; Chen, F.C.; Ong, E.L., "Anisotropic Thermal Expansion of Oriented Crystalline Polymers", Polymer 1979, 20, 1191-1198.

Choy, C.L.; Chen, F.C.; Young, K., "Negative Thermal Expansion in Oriented Crystalline Polymers", J. Polym. Sci., Polym. Phys. Ed. 1981, 19, 335-352.

Choy, C.L.; Ito, M.; Porter, Roger S., "Thermal Expansivity of Oriented PEEK", J. Polym. Sci., Polym. Phys. Ed. 1983, 21, 1427-1438.

Chuah, Hoe H., Structure-Property Studies in the Deformation of Semi-Crystalline Polymers, Ph.D. Dissertation, University of Massachusetts, 1985.

Chuah, Hoe H.; DeMicheli, Paul E.; Porter, Roger S., "Density Changes on Drawing by Solid-State Extrusion of High-Density Polyethylene", Polym. Sci., Lett. Ed. 1983, 21, 791-797.

Chuah, Hoe H.; Porter, Roger S., "Solid-State Extrusion of Chain-Extended Polyethylene", J. Polym. Sci., Polym. Phys. Ed. 1984, 22, 1353-1365.

Clark, J.N.; Herring, F.G.; Jagannathan, N.R., "Applications of Cross-Polarization and Magic-Angle Sample Spinning NMR Technique to Poly(aryl ether ketone)", Polymer 1985, 26(Commun.), 329-331.

Cogswell, F.N., "Microstructure and Properties of Thermoplastic Aromatic Polymer Composites", 28th Natl. SAMPE 1983, 528-534.

Cogswell, F.N.; Hopprich, M., "Environmental Resistance of Carbon Fiber-Reinforced Poly ether ether ketone", Composites 1983, 14, 251-253.

Collier, J.R.; Leal, L.M., "Effect of Melt History on Polymer Crystallization", Polym. Eng. Sci. 1969, 9, 182-189.

Crick, R; Fife B.; Nield, E.; Peacock. J.A. Examination of the Morphology of Aromatic Polymer Composites (APC-2) Using an Etching Technique, International Conference on Composite Interfaces, Cleveland, Ohio, May, 1986.

Dawson, P.C.; Blundell, D.J., "X-ray Data for Poly(aryl ether ketone)", Polymer 1980, 21, 577-578.

Eby, R.K., "Diffusion in a Polymer with Lamellar Morphology, Polyethylene", J. Appl. Phys. 1964, 35, 2720-2724.

Edwards, B.C., "The Nature of Multiple Melting Transitions in Cis-Polyisoprene", J. Polym. Sci., Polym. Phys. Ed. 1975, 13, 1387-1405.

Fakirov, S.; Avramova, N., "Applicability of the Gibbs-Thomson Equation to Nylon 6", J. Polym. Sci., Polym. Lett. Ed. 1982, 20, 635-641.

Fakirov, S.; Avramova, N., "Accumulative Erasing Effect in the Melt Memory of Nylon 6", IUPAC 1985, Symposium on noncrystalline order in polymers, 119-121.

Fischer, E.W.; Fakirov, S., "Structure Properties of Poly(ethylene terephthalate) Crystallized by Annealing in the Highly Oriented State", J. Mater. Sci. 1976, 11, 1041-1065.

Fratini, A.V.; Cross, E.M.; Whitaker R.B.; Adams, W.W., "Refinement of the Structure of PEEK Fibers in an Orthorhombic Unit Cell", Polymer 1986, 27, 861-865.

Frayer, P.O.; Lando, J.B., "Polymerization in Electric Fields of Hexamethylene Diammonium Adipate Crystallized on Graphite Fibers", J. Polym. Sci., Polym. Lett. Ed. 1972, 10, 29-34.

Gibson A.G.; Ward, I.M.; Cole, B.N.; Parsons, B., "Hydrostatic Extrusion of Linear Polyethylene", J. Mater. Sci. 1974, 9, 1193-1196.

Gray, Allan P., "Polymer Crystallinity Determinations by DSC", Thermochimica Acta 1970, 1, 563-579.

Gray, D.G., "Transcrystallization Induced by Mechanical Stress on Polypropylene Melt", J. Polym. Sci., Polym. Lett. Ed. 1974, 12, 645-650.

Groeninckx, G; Reynaers, H., "Morphology and Melting Behavior of Semicrystalline Poly(ethylene terephthalate). II. Annealed Poly(ethylene terephthalate)", J. Polym. Sci., Polym. Phys. Ed., 1980, 18, 1325-1341.

Groeninckx, G.; Reynaers, H.; Berghmans, H.; Smets, G., "Morphology and Melting Behavior of Semicrystalline Poly(ethylene terephthalate). I. Isothermally Crstallized PET", J. Polym. Sci., Polym. Phys. Ed. 1980, 18, 1311-1324.

Harrison, I.R.; Runt, J., "The Heating Rate Dependence of Polymer Melting Points", J. Polym. Sci., Polym. Phys. Ed. 1979, 17, 321-328.

Hartley, F.D.; Lord, F.W.; Morgan, L.B., "Crystallization Phenomena in Polymers III.", Phil. Trans. 1954, A247, 23-34.

Hay, J.N.; Kemmish, D.J.; Langford, J.I.; Rae, A.I.M., "The Structure of Crystalline PEEK", Polymer, 1984, 25(Commun.), 175-178.

Hobbs, Stanley Y., "Fiber Reinforced Composite Materials", U.S. Patent 1974, 3 812 077.

Hobbs, Stanley Y., "Row Nucleation of Isotactic Polypropylene on Graphite Fibers", Nature Phys. Sci. 1971, 234, 12-13.

Hoffman, J.D.; Davis, G.T.; Lauritzen, J.I., Treatise on Solid State Chemistry; Vol 3(Hannay, N.B. Ed.), Plenum Press: New York, 1976.

Hoffman, John D.; Weeks, James J., "Melting Process and the Equilibrium Melting Temperature of Polychlorotrifluoro-ethylene", J. Res. Nat. Bur. Std.(U.S.) 1962, 66A, 13-28.

Hoffman, John D.; Weeks, James J., "X-ray Study of Isothermal Thickening of Lamellae in Bulk Polyethylene at the Crystallization Temperature", J. Chem. Phys. 1965, 42, 4301-4302.

Hoffman, John D.; Weeks, James J.; Murphy, W.M., "Experimental and Theoretical Study of Kinetics of Bulk Crystallization in Poly(chlorotrifluoro ethylene)", J. Res. Nat. Bur. St. 1959, 63A, 67-98.

Holdsworth, P.J.; Turner-Jones, A., "The Melting Behavior of Heat Crystallized Poly(ethylene terephthalate)", Polymer 1971, 12, 195-208.

Hull, Derek, An Introduction to Composite Materials; Cambridge University: Cambridge, 1981.

Illers, K.H.; Haberkorn, H., "Schmelzverhalten, Struktur und Kristallinitat von 6-Polyamid", Makromol. Chem. 1971, 142, 31-65.

Jaffe, M.; Wunderlich, B., "Melting of Polyoxymethylene", Kolloid-Z. Z. Polym. 1967, 216, 203-216.

Johnson, R.N.; Farnham, A.G; Clendinning, R.A.; Hale, W.H.; Merriam, C.N., "Poly(aryl Ethers) by Nucleophilic Aromatic Substitution. I. Synthesis and Properties", J. Polym. Sci., Chem. Ed. 1967, 5, 2375-2398.

Kardos, J.L., "Regulating the Interface in Graphite/Thermoplastic Composites", J. Adhesion 1973, 5, 119-138.

Kardos, J.L.; Cheng, F.S.; Tolbert, T.L., "Tailoring the Interface in Graphite-Reinforced Polycarbonate", Polym. Eng. Sci. 1973, 13, 455-461.

Kavesh, S.; Schultz, J.M., "Lamellar and Interlamellar Structure in Melt-Crystallized Polyethylene. II.", J. Polym. Sci., Polym. Phys. Ed. 1971, 9, 85-114.

Keith, H.D.; Padden, F.J., "A Phenomenological Theory of Spherulitic Crystallization", J. Appl. Phy. 1963, 34, 2409-2421.

Keller, A.; Lester, G.R.; Morgan, L.B., "Crystallization Phenomena in Polymers I", Phil. Trans. 1954, A247, 1-13.

Keller, A.; Willmouth, F.M., "Self-Seeded Crystallization and Its Potential for Molecular Weight Characterization. I. Experiments on Broad Distributions", J. Polym. Sci., Polym. Phys. Ed. 1970, 8, 1443-1456.

Kemmish, D.J.; Hay, J.N., "The Effect of Physical Ageing on the Properties of Amorphous PEEK", Polymer 1985, 26, 905-912.

Koutsky, J.A.; Walton, A.G.; Baer, E., "Heterogenous Nucleation of Polyethylene Melts on Cleaved Surfaces of Alkali Halides", J. Polym. Sci., Polym. Lett. Ed. 1967, 5, 185-190.

Kricheldorf, Hans R.; Bier, Gerhard, "New Polymer Syntheses: II. Preparation of Aromatic Poly(ether ketone)s from Silylated Bisphenols", Polymer 1984, 25, 1151-1156.

Kumar, Satish; Anderson, David P.; Adams, W.Wade, "Crystallization and Morphology of PEEK", Polymer 1986, 27, 329-336.

Kunugi, Toshio; Mizushima, Atsushi; Hayakawa, Tomohiro, "Preparation of High-Modulus and High-Strength PEEK Film by Zone-Annealing", Polymer, 1986, 27(Commun.), 175-176.

Lee, Youngchul; Roger S. Porter, "Double-Melting Behavior of Poly(ether ether ketone)", Macromolecules 1987, 20, 1336-1341.

Lee, Youngchul; Roger S. Porter, "Crystallization of Poly(ether ether ketone) (PEEK) in Carbon fiber Composites", Polym. Eng. Sci. 1986, 26, 633-639.

Lee, Youngchul; Lefebvre, Jean-Marc; Porter, Roger S., "Uniaxial Draw of PEEK by Solid-State Extrusion", J. Polym. Sci., Polym. Phys. Ed., in press.

Lemstra, P.J.; Kooistra, T.; Challa, G., "Melting Behavior of Isotactic Polystyrene", J. Polym. Sci., Polym. Phys. Ed. 1972, 10, 823-833.

Lemstra, P.J.; Postma, J.; Challa, G., "Molecular Weight Dependence of the Spherulitic Growth Rate of Isotactic Polystyrene", Polymer 1974, 15, 757-759.

Limbert, Frank J.; Baer, Eric, "Kinetics of Nucleation and Growth of Spherulites in Homopolymers", J. Polym. Sci., Polym. Chem. Ed. 1963, 1, 3317-3331.

Louden, J.D., "Crystallinity in Poly(aryl ether ketone) Films Studied by Raman Spectroscopy", Polymer 1986, 27(Commun.), 82-84.

Lovering, Edward G.; Wooden, David C., "Transitions in Trans-1,4-Polyisoprene", J. Polym. Sci., Polym. Phys. Ed. 1969, 7, 1639-1649.

Magill, J.H., "Melting Behavior of Spherulitic Crystallization of Poly(caproamide)", Polymer 1962, 3, 43-51.

Mandelkern, L.; Allow, A.L., "The Fusion of Polyethylene Single Crystals", J. Polym. Sci., Polym. Lett. Ed., 1966, 4, 447-452.

McLaren, J.V.,"A Kinetic study of the Isothermal Spherulitic Crystallization of Polyhexamethylene adipamide", Polymer 1963, 4, 175-189.

Morgan, L.B., "Crystallization Phenomena in Fiber-Forming Polymers", J. Appl. Chem. 1954, 4, 160-172.

Nguyen, Huy X.; Ishida, Hatsuo, "Molecular Analysis of the Melting and Crystallization Behavior of PEEK", Amer. Chem. Soc., Polymer Preprint 1985, 26, 273-274.

Nguyen, Huy X.; Ishida, Hatsuo, "Molecular Analysis of the Melting Behavior of PEEK", Polymer 1986, 27, 1400-1405.

Nguyen, Huy X.; Ishida, Hatsuo, "Poly(aryl ether ether ketone) and Its Advanced Composites: A Review", Polymer Composites 1987, 8, 57-73.

Olley, R.H.; Bassett, D.C.; Blundell, D.J., "Permanganic Etching of PEEK", Polymer 1986, 27, 344-348.

Pedemonte, E.; Leva, M.; Gattiglia, E.; Turturro, A. Polymer 1985, 26, 1202

Pereira, Jose R.C.; Porter, Roger S., "Solid-State Coextrusion of PET II.", J. Polym. Sci., Polym. Phys. Ed. 1983, 21, 1147-1161.

Perkin-Elmer Corp., Manual for model DSC-4, Norwalk, Connecticut, U.S.A., 1984.

Peterlin, A., "Molecular Model of Drawing Polyethylene and Polypropylene", J. Mater. Sci. 1971, 6, 490-508.

Prest, W.M.,Jr.; Luca, D.J., "The Morphology and Thermal Response of High-Temperature-Crystallized Poly(vinylidene fluoride)", J. Appl. Phys. 1975, 46, 4136-4143.

Price, F.P., "The Development of Crystal in Polychlorotrifluoro ethylene", J. Amer. Chem. Soc. 1952, 74, 311-318.

Prime, R. Bruce ; Seferis, James C., "Thermo-Oxidative Decomposition of PEEK", J. Polym. Sci., Polym. Lett. Ed. 1986, 24, 641-644.

Rabesiaka, J.; Kovacs, A.J., "Isothermal Crystallization Kinetics of Polyethylene. II. Influence of the Sample Preparation", J. Appl. Phys. 1961, 32, 2314.

Richardson, A.; Ania, F.; Rueda, D.R.; Ward, I.M.; Balta-Calleja, F.J., "The Production and Properties of PEEK Rods Oriented by Drawing trough a Conical Die", Polym. Eng. Sci. 1985, 25, 355-361.

Rigby, Rhymer B., "Poly ether ether ketone", Polymer News 1984, 9, 325-328.

Rim, Peter B.; Runt, James P., "Melting Behavior of Crystalline/Compatible Polymer Blends: Poly(caprolactone)/Poly(Styrene-co-acrylonitrile)", Macromolecules 1983, 16, 762-768.

Roberts, R.C., "Poly(ethylene terephthalate) II-Morphological Change on Annealing", Polymer 1969, 10, 117-125.

Roberts, R.C., "The Melting Behavior of Bulk Crystallized Polymers", J. Polym. Sci., Polym. Lett. Ed. 1970, 8, 381-384.

Rose, J.B., "Discovery and Development of the Victrex Polyaryl ether sulphone, PES, and Polyaryl ether ketone, PEEK", Am. Chem. Soc., Polymer Preprints 1986, 27(1), 480-481.

Rose, J.B. Univ. of Surrey, England, Private Communication.

Rueda, D.R.; Ania, F.; Richardson, A.; Ward, I.M.; Balta-Calleja, F.J., "X-ray Diffraction Study of Die drawn PEEK", Polymer 1983, 24(Commun.), 258-260.

Samuels, Robert J., "Quantitative Structural Charaterization of the Melting Behavior of Isotactic Polypropylene", J. Polym. Sci., Polym. Phys. Ed. 1975, 13, 1417-1446.

Sharples, A., "The Formation of Nuclei in Crystallizing Polymers", Polymer 1962, 3, 250-252.

Shukla, J.G.; Sichina, W.J., "Thermal Behavior of Carbon Fiber Reinforced PEEK", SPE ANTEC 1984, Tech. Papers 30, 265-267.

Sichina, W.J.; Gill, P.S., "Charaterization of PEEK/Carbon Fiber Composites by Thermal Analysis", SPE ANTEC 1985, Tech. Papers 31, 293-295.

Stein, Richard S., "The X-ray Diffraction, Birefringence and Infrared Dichroism of Stretched Polyethylene. II. Generallized Uniaxial Crystal Orientation", J. Polym. Sci. 1958, 31, 327-334.

Sweet, G.E.; Bell, J.P., "Multiple Endothermic Melting Behavior and Physical Structure in Polymers", J. Polym. Sci., Polym. Phys. Ed. 1972, 10, 1273-1283.

Tuinstra, F.; Baer, Eric, "Epitaxial Crystallization of Polyethylene on Graphite", J. Polym. Sci., Polym. Lett. Ed. 1970, 8, 861-865.

Turnbull, D., "Kinetics of Heterogeneous Nucleation", J. Chem. Phys. 1950, 18, 198-203.

Velisaris, Chris N.; Seferis, James C., "Thermal Processing and Characterization of PEEK Matrices", SPE ANTEC 1985, Tech. Papers 31, 401-403.

Vidotto, Par G.; Levy, D.; Kovacs, A.J., "Cristallisation et Fusion des Polymeres Autoensemences", Kolloid Z.Z. Polym. 1969, 230, 289-305.

Vincent, P.I. "The Necking and Cold-Drawing of Rigid Plastics", Polymer 1960, 1, 7-19.

Wakelyn, N.T., "On the Structure of PEEK", Polymer 1984, 25(Commun.), 306-308.

Wakelyn, N.T., "Variation of Unit Cell Parameters of Poly(arylene ether ketone) Film with Annealing Temperature", J. Polym. Sci., Polym. Lett. Ed. 1987, 25, 25-28.

Weeks, J.J., "Melting Temperature and Change of Lamellar Thickness with Time for Bulk Polyethylene", J. Res. Nat. Bur. Std.(U.S.) 1963, 67A, 441-451.

White, T.R., "Melting Behavior of Crystalline Polymer Fibers", Nature 1955, 175, 895.

Wilchinsky, Zigmond W., Advances in X-ray Analysis; Plenum Press: New York, 1963, Vol. 6, 231-241.

Wunderlich, B. Macromolecular Physics; Academic: New York, 1976; Vol. 2.

Wunderlich, B. Macromolecular Physics; Academic: New York, 1980; Vol. 3.

Yadav, Y.S.; Jane, P.C., "Melting Behavior of Isotactic Polypropylene Isothermally Crystallized from the Melt", Polymer 1986, 27, 721-727.

Zachariades, Anagnostis E.; Mead, W.T.; Porter, Roger S., "Recent Developments in Ultraorientation of Polyethylene by Solid-State Extrusion", Chem. Reviews 1980, 80, 351-364.

Zachariades, Anagnostis E.; Porter, Roger S., "New Developments in Solid-State Extrusion", J. Macromol. Sci., Polym. Phys. Ed. 1981, 19, 377-385.

Zachariades, Anagnostis E.; Porter, Roger S., The Strength and Stiffness of Polymers; Marcel Dekker Inc.: New York, 1983.

Zachmann, H.G.; Peterlin, A., "Influence of the Surface Morphology on the Melting of Polymer Crystals", J. Macromol. Sci., Phys. Ed. 1969, 3, 495-517.